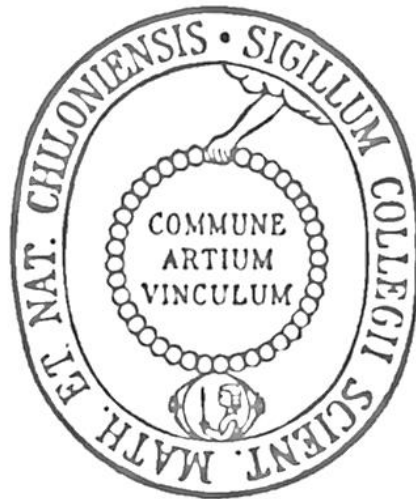


**Trehalose physicochemical characteristics as a
potential dry powder inhalation carrier for
optimized aerosol generation**



Doctoral Thesis

Submitted in fulfillment of the requirements

For the degree of

Doctor of Natural Sciences

At The

**Christian Albrecht University,
Kiel, Germany**

By

Shahir Aziz

Kiel 2015

Referee **Prof. Dr. Hartwig Steckel**

Co-Referee **Prof. Dr. Thomas Kunze**

Date of Exam **7.8.2015**

Accepted for Publication **7.8.2015**

sgd. Prof. Dr. Wolfgang J. Duschl (Dean)

Declaration

This is to certify that:

- 1) Apart from the supervisor's guidance, all the content and design of the thesis is my original own work towards the degree of Doctor of Natural Sciences.**
- 2) The Thesis has not been submitted either partially or fully for a doctoral degree to another examining body. It has not been published nor submitted for publication.**
- 3) The thesis has been prepared subject to the rules of Good Scientific Practice of the German research foundation.**

Signature

“If I have the gift of prophecy and can fathom all mysteries and all knowledge, and if I have a faith that can move mountains, but have no love, I am nothing”

1 Corinthians 13:2

Lack of a specific mark or a reference to a trademark or a patent does not imply that this work or part of it can be used or copied without copyright permission.

Abstract

The study aims to utilize trehalose particles as an inert fine carrier to improve DPI aerosolization performance, diversify the potential delivery of new drugs in DPI formulations and the feasibility of bringing high drug dose into the lungs. Inhalable fine trehalose particles were engineered by jet milling and spray drying to reach different physicochemical characteristics that were assessed and related to the evaluated aerosolization performance of the prepared formulations with model drugs. The delivery of high dose of oseltamivir phosphate (OP) antiviral drug was further improved in formulations of 25% fine trehalose particles reaching about 75% fine particle fraction (FPF) as assessed by cascade impaction. The aerosol generation of model COPD inhalable drugs was evaluated on the bases of their hydrophilic and hydrophobic nature affecting their agglomeration behavior with trehalose fine particles. Accordingly, different trehalose batches presenting different physicochemical characteristics such as particle size, morphology, surface energy, crystallinity, and hydration exhibited variation in aerosolization performance from 1% till 80% FPF as assessed by impaction. In summary, tailored DPI formulations are essential for every active pharmaceutical ingredient and particle engineering of both the carrier and the drug control the outcome of the formulation performance. Trehalose particles have shown compatibility, stability and aerosol generation effectiveness with a variety of API types and ratios. This concludes that fine trehalose particles have the potential for being an outstanding inert and safe carrier for the delivery of new and current API in DPI formulations.

Table of Contents

1. THEORETICAL BACKGROUND	1
1.1 GENERAL INTRODUCTION	2
1.2 RESPIRATORY SYSTEM	3
1.2.1 <i>Structure of the Respiratory System</i>	3
1.2.2 <i>Mechanics of breathing</i>	4
1.2.3 <i>Lung function</i>	5
1.3 RESPIRATORY DRUG DELIVERY	6
1.3.1 <i>Factors controlling lung deposition</i>	6
1.3.2 <i>Categories of oral inhalation devices</i>	7
1.3.3 <i>DPI Design</i>	8
1.3.4 <i>DPI formulations</i>	11
1.3.5 <i>Current DPI formulation approaches and performance limitations</i>	12
1.3.6 <i>Trehalose</i>	13
1.4 AIM OF WORK	14
2. METHODOLOGY	15
2.1 PARTICLE ENGINEERING AND PRODUCTION	16
2.1.1 <i>Design of experiments</i>	16
2.1.2 <i>Jet milling</i>	16
2.1.3 <i>Spray drying</i>	17
2.2 PHYSICOCHEMICAL CHARACTERIZATION	18
2.2.1 <i>Particle size distribution</i>	18
2.2.2 <i>Differential scanning calorimeter</i>	18
2.2.3 <i>Dynamic vapor sorption</i>	18
2.2.4 <i>X-Ray powder diffraction</i>	19
2.2.5 <i>Specific surface area</i>	19
2.2.6 <i>Fluidization energy</i>	19
2.2.7 <i>Thermo gravimetric analysis</i>	19
2.2.8 <i>Scanning electron microscope</i>	19
2.2.9 <i>Inverse gas chromatography</i>	20
2.3 PREPARATION OF DPI BLENDS.....	20
2.4 AEROSOLIZATION PERFORMANCE	21
2.4.1 <i>Aerosol dispersion for laser diffraction</i>	21
2.4.2 <i>Next Generation Impactor</i>	24

2.5	DRUG ASSAY	25
2.5.1	<i>UV-spectrophotometric quantification</i>	25
2.5.2	<i>Liquid Chromatography quantification</i>	25
2.5.2.1	Budesonide (BU)	25
2.5.2.2	Salbutamol Sulphate (SS)	25
2.5.2.3	Di-sodium cromoglycate (DSCG)	26
3.	CHAPTER ONE (JET MILLED TREHALOSE STUDY AND OSELTAMIVIR PHOSPHATE AEROSOLIZATION OPTIMIZATION).....	27
3.1	INTRODUCTION	28
3.2	RESULTS.....	31
3.2.1	<i>Prepared jet milled particles</i>	31
3.2.2	<i>Physicochemical characteristics</i>	32
3.2.2.1	Thermal Behavior	32
3.2.2.2	Dynamic Vapor Sorption	35
3.2.2.3	Crystalline structure.....	36
3.2.2.4	De-agglomeration behavior	36
3.2.2.5	Oseltamivir physical stability	37
3.2.3	<i>Blends and homogeneity</i>	38
3.2.4	<i>Aerosolization performance</i>	38
3.2.4.1	Laser diffraction.....	38
3.2.4.2	Cascade impaction.....	39
3.2.5	<i>Scanning electron microscopy</i>	43
3.3	DISCUSSION	45
4.	CHAPTER TWO (TREHALOSE PARTICLE ENGINEERING BY SPRAY DRYING).....	47
4.1	INTRODUCTION	48
4.2	RESULTS.....	50
4.2.1	<i>Spray dried Produced trehalose</i>	50
4.2.2	<i>X-ray powder diffraction</i>	52
4.2.3	<i>Dynamic Vapor Sorption</i>	53
4.2.4	<i>Scanning electron microscopy</i>	53
4.2.5	<i>Recrystallization of spray dried trehalose</i>	55
4.3	DISCUSSION	57
5.	CHAPTER THREE (AEROSOLIZATION PERFORMANCE OF SD VS. JM TREHALOSE FORMULATIONS)	59
5.1	INTRODUCTION	60

5.2	RESULTS.....	64
5.2.1	<i>Choice of trehalose and API qualities.....</i>	64
5.2.2	<i>Blends preparation.....</i>	67
5.2.3	<i>Aerosolization performance by NGL.....</i>	68
5.2.3.1	Hydrophobic Budesonide (BU) blends	68
5.2.3.2	Hydrophilic Salbutamol sulphate (SS) blends	72
5.2.3.3	Hygroscopic Disodium cromoglycate (DSCG) blends.....	74
5.2.4	SEM.....	78
5.2.5	Surface energy measurements	83
5.3	DISCUSSION	86
6.	CONCLUSION AND FUTURE PERSPECTIVES.....	89
7.	GERMAN ABSTRACT	92
	APPENDIX	
A.	LIST OF ABBREVIATIONS	93
B.	LIST OF FIGURES.....	95
C.	LIST OF MATERIALS.....	98
D.	LIST OF EQUIPMENT.....	99
8.	REFERENCES.....	101

1. Theoretical Background

1.1 General Introduction

The successful delivery of safe and effective active pharmaceutical ingredients (API) through the pulmonary route is dependent on; delivery device, drug formulation and the biology of the respiratory system (Forbes and Ehrhardt, 2005; Gradon and Sosnowski, 2014). The respiratory system is mainly composed of a gas exchange organ (Lungs), airway passages and a pump (chest wall) that ventilates the lungs. The major function is the gas exchange (external respiration) which is the absorption of O₂ and removal of CO₂ from the body. In addition, the respiratory system has different metabolic and endocrine functions (Barrett and Ganong, 2010; Despopoulos and Silbernagl, 2003). The Lungs contain around 300 million alveoli (thin-walled air sacs) about 0.3mm in diameter located on the terminal branches of the bronchial tree. They are surrounded by a dense network of pulmonary capillaries and have a total surface area of about 70 - 100 m² (Barrett and Ganong, 2010; Costanzo, 2006; Despopoulos and Silbernagl, 2003). Due to the large surface area of the alveolar epithelium, the short air to blood pathway and permeability to many substances, the pulmonary deposition of aerosols represents an efficient, rapid and non-invasive alternative for the delivery of many drugs (Lahnstein et al., 2008) .

For a moment we might consider inhalation therapy as a modern approach to drug delivery, but actually the historical review recorded the development of inhalation therapy starting from ancient Egyptian times about 3500 years ago (Sanders, 2007). Furthermore, a breakthrough in inhalation drug delivery development started since the early 19th century. Simple inhalation devices and aerosols containing various drugs have been used for the treatment of respiratory disorders. In addition, scientific analysis of inhalation drug delivery concepts of particles deposition in the human respiratory tract was observed and documented in 1881 by Tyndall (Heyder et al., 1986).

Inhalation therapy was considered mainly for pulmonary disease such as cystic fibrosis, asthma, chronic obstructive pulmonary diseases (COPD) and even lung cancer. The local pulmonary deposition and delivery of the administered drug facilitates a targeted treatment of respiratory diseases without the need for high dose exposures by other routes of administration and consequently reduced systemic side effects (Beck-Broichsitter et al., 2009; Minne et al., 2008; Pilcer and Amighi, 2010).

Recently, inhalation therapy has grabbed the attention for the administration of systematically API that is poorly absorbed by gastrointestinal tract or undergoes presystemic metabolic degradation such as polypeptides, proteins, steroids, genes and vaccines (Stegemann et al., 2013).

1.2 Respiratory System

1.2.1 Structure of the Respiratory System

The respiratory system includes the lungs and a series of airways that connect the lungs to the external environment. The structures of the respiratory system as illustrated in Figure 1-1 are subdivided into a conducting zone, which brings air into and out of the lungs, and a respiratory zone lined with alveoli, where gas exchange occurs. The functions of the conducting and respiratory zones and the structures lining them also differ. The conducting zone includes the nose, nasopharynx, larynx, trachea, bronchi, bronchioles, and terminal bronchioles. These structures function to bring air into and out of the respiratory zone for gas exchange and to warm, humidify, and filter the air before it reaches the critical gas exchange region. The trachea is the main conducting airway. The trachea divides into two bronchi, one leading into each lung, which divide into two smaller bronchi, which divide again. Ultimately, there are 23 such divisions into increasingly smaller airways. The conducting airways are lined with mucus-secreting and ciliated cells that function to remove inhaled particles. Although large particles usually are filtered out in the nose, small particles may enter the airways, where they are captured by mucus, which is then swept upward by the rhythmic beating of the cilia (Barrett and Ganong, 2010; Costanzo, 2006)

The respiratory zone includes the respiratory bronchioles, the alveolar ducts, and the alveolar sacs that are lined with alveoli, the main site for gas exchange. The respiratory bronchioles are transitional structures. Like the conducting airways, they have cilia and smooth muscle, but they also are considered part of the gas exchange region because alveoli occasionally bud off their walls. The alveolar ducts are completely lined with alveoli, but they contain no cilia and little smooth muscle. The alveolar ducts terminate in alveolar sacs, which also are lined with alveoli. The alveolar walls are rimmed with elastic fibers and lined with epithelial cells, called type I and type II pneumocytes (Barrett and Ganong, 2010; Costanzo, 2006)

	Name of branches	Number of tubes in branch	Particle deposition size range	
Conducting zone	Trachea	1	Impaction ($\geq 5\mu\text{m}$)	
	Bronchi	2		
		4		
	Bronchioles		8	Gravitational Sedimentation ($0.5 - 5\mu\text{m}$)
			16	
		Terminal bronchioles	32	
Respiratory zone		6×10^4	Diffusion ($\leq 0.5\mu\text{m}$)	
	Respiratory bronchioles	5×10^5		
	Alveolar ducts			
	Alveolar sacs	8×10^6		

Figure 1-1: Respiratory zones with branching hierarchy showing the particle deposition mechanism in different areas based on aerodynamic particle size (adapted from Barrett and Ganong 2010)

1.2.2 Mechanics of breathing

Pressure differences between the alveoli and the environment are the driving forces for the exchange of gases that occurs during ventilation. Alveolar pressure (P_A = intrapulmonary pressure) must be lower than the barometric pressure (P_B) during inspiration (breathing in), and higher during expiration (breathing out). If P_B is defined as zero, the alveolar pressure is negative during inspiration and positive during expiration. These pressure differences are created through coordinated movement of the diaphragm and chest (thorax) as shown in Figure 1-2, resulting in an increase in lung volume (V_{pulm}) during inspiration and a decrease during expiration. The inspiratory muscles consist of the diaphragm, scalene muscles, and external intercostal muscles. Their contraction lowers (flattens) the diaphragm, raises and expands the chest, thus expanding the lungs. Inspiration is therefore active. The external intercostal muscles and accessory respiratory muscles are activated for

deep breathing. During expiration, the diaphragm and other inspiratory muscles relax, thereby raising the diaphragm and lowering and reducing the volume of the chest and lungs. Since this action occurs primarily due to the intrinsic elastic recoil of the lungs, expiration is passive at rest and the lung collapses like a balloon and expels its air through the trachea whenever there is no force to keep it inflated. In deeper breathing, active mechanisms can also play a role in expiration: the internal intercostal muscles contract and the diaphragm is pushed upward by abdominal pressure created by the muscles of the abdominal wall (Barrett and Ganong, 2010; Despopoulos and Silbernagl, 2003)

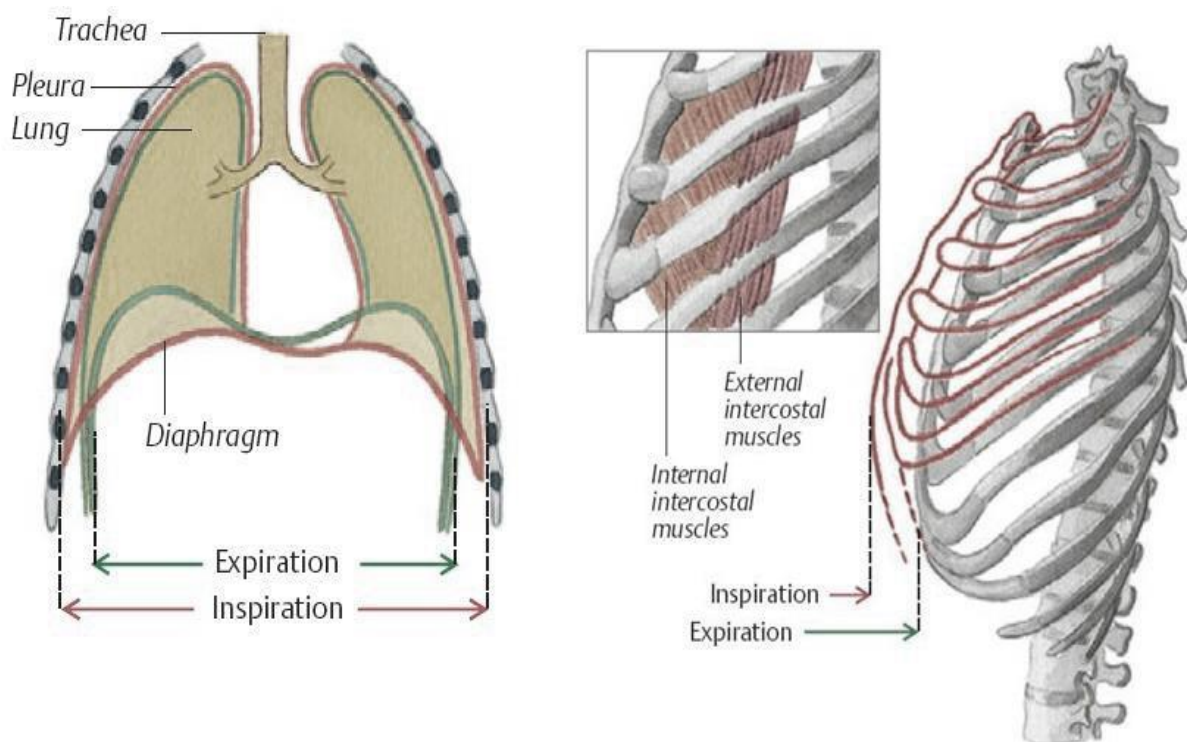


Figure 1-2: Movement of Muscles, Diaphragm and Rib Cage during inhalation and exhalation (Despopoulos and Silbernagl, 2003).

1.2.3 Lung function

At the end of normal quiet expiration, the lung–chest system returns to its intrinsic resting position. About 0.5 L of air is taken in with each breath during normal quiet respiration; this is called the resting tidal volume (V_T). Inspiration can be increased by another 3 L on forced (maximum) inspiration; this is called the inspiratory reserve volume (IRV). Likewise, expiration can be increased by about 1.2–1.7 L more on forced (maximum) expiration. This is called the expiratory reserve

volume (ERV). These reserve volumes are used during strenuous physical exercise and in other situations where normal tidal volumes are insufficient. Even after forced expiration, about 1.3 L of air remains in the lungs; this is called the residual volume (RV). Lung capacities are the sum of the individual lung volumes. The vital capacity (VC) is the maximum volume of air that can be moved in and out in a single breath. Therefore, $VC = V_T + IRV + ERV$. The average 20-year-old male has a VC of about 4.7 - 5.3 L. Normally the vital capacity decreases and residual volume increases with age. The total lung capacity (TLC) is the sum of VC and RV—on average 5.9 to 7 L. The functional residual capacity is the sum of ERV and RV. The inspiratory capacity is the sum of V_T and IRV. All numerical values of these volumes apply under body temperature–pressure saturation (BTPS) conditions (Barrett and Ganong, 2010; Despopoulos and Silbernagl, 2003).

1.3 Respiratory drug delivery

1.3.1 Factors controlling lung deposition

API particles from inspired aerosols can either be administered through the nasal or oral routes. Inspired particles deposition refers to the probability of distributing the particles among the respiratory system and becoming in contact with the inner lining. The key controllers governing lung deposition may be divided into those related to the physicochemical properties of the droplets or particles being delivered, the mechanical aspects of aerosol dispersion usually associated with the delivery device, and the physiological and anatomical considerations associated with the biology of the lungs (Florence and Siepmann, 2009; Gradon and Sosnowski, 2014; Heyder et al., 1986).

The common target for inhalation therapies is having particles that mostly able to pass the extrathoracic region and the tracheobronchial tree to deposit in the alveolar region for maximum therapeutic effect. The Particle aerodynamic size is one of the most important design variables in an aerosol formulation, along with shape, density, electrical charge and hygroscopicity. In fact, the three principal mechanisms of particle deposition in the respiratory tract rely on the size of the inhaled particles illustrated in Figure 1-3. Impaction is the inertial deposition of a particle onto an airway surface. It occurs principally at or near airway bifurcations, most commonly in extrathoracic and large conducting airways, where flow velocities are high and where

rapid changes in the direction of bulk airflow often take place, generating considerable inertial forces. The probability of impaction increases with increasing air velocity, rate of breathing, particle size ($>5 \mu\text{m}$) and density. Gravitational sedimentation is an important mechanism for deposition of particles over $0.5 \mu\text{m}$ and below $5 \mu\text{m}$ in size in the small conducting airways where the air velocity is low. Deposition due to gravity increases with enlarging particle size and longer residence times but decreases as the breathing rate increases. Submicron-sized particles (especially those less than $0.5\mu\text{m}$) acquire a random motion caused by the impact of surrounding air molecules. This Brownian motion may then result in particle deposition by diffusion, especially in small airways and alveoli, where bulk airflow is very low (Florence and Siepmann, 2009; Pilcer and Amighi, 2010; Stegemann et al., 2013).

1.3.2 Categories of oral inhalation devices

Orally inhaled drug delivery devices are divided into 3 main categories; nebulizers, pressurized metered dose inhalers (pMDI), and dry powder inhalers (DPI). Each category presents pros and cons which accordingly chosen for therapeutic needs.

Nebulizers exploit the energy produced by air-jet or ultrasonic techniques to aerosolize the active pharmaceutical ingredient (API) that is held in a liquid form. Patients use nebulizers most often in hospitals or at home, since they are less portable compared to the other types and require energy source. They are capable of delivering high API doses such as 300mg in case of antibiotics but consume more time. Furthermore they require frequent disinfection and maintenance (Geller, 2005; Pilcer and Amighi, 2010).

Metered dose inhalers are the primary choice for asthma therapy as they are small, portable, multidose and quick to use. The API is either dissolved or suspended in a liquefied propellant under pressure in a canister. On the other hand, several problems were encountered in pMDIs development, one of which is the physical stability of the API held by the propellant in the liquid form. Also the technique to coordinate the actuation and inhalation required is considered very difficult for patients to use efficiently (Dolovich and Dhand, 2011; Geller, 2005; Pilcer and Amighi, 2010).

Dry powder inhalers are available in many forms; in general they are breath actuated with no propellant, and the API is kept in a one phase dry solid state. DPIs appear to be the most promising for future use as they are portable, easy to operate and low-cost devices with improved stability of the formulation. One drawback is the inability of patients with inadequate inspiratory flow to activate the DPI (Geller, 2005; Rahimpour et al., 2014; Telko and Hickey, 2005).

1.3.3 DPI Design

In 1864, Alfred Newton has introduced the first dry powder inhaler, setting the main principle that the powder need to be pulverized and kept dry (Sanders, 2007). Later, since the invention of the Spinhaler® and its introduction on the market in 1968, the technology has significantly developed and a wide range of devices are currently available in the market or under research. Basically in a passive DPI device when breath actuated, the air flow and the inhalers' resistance cause a turbulent energy that emit the powder formulation dose to be aerosolized through a grid where the particles are dispersed and de-agglomerated releasing the API fines to reach the deep lungs as illustrated in Figure 1-3 (Islam and Cleary, 2012; Pilcer and Amighi, 2010; Telko and Hickey, 2005).

DPIs can be categorized into two main types based on the formulation packaging; single doses as that contained in capsules or multiple dose devices that contain the formulation in a foil blister or a metered reservoir, a list of some available DPI devices is shown in Figure 1-4. In contrast to the single dose inhalers, the multiple dose DPIs such as Turbuhaler and Easyhaler avoid the inconvenience of loading a capsule immediately before each use. Furthermore a metering system is often fitted and a measured dose is loaded into the air flow-path just before inhalation. On the other hand, since the API is stored within the multiple doses device, the design must ensure protection against atmospheric humidity. In view of that, most multiple dose devices are not refillable and this increases the therapeutic expense. Even though multiple dose DPIs are protected against the exposure effects of atmospheric humidity, the temperature and humidity at the time of use may affect performance including dose variation (Islam and Cleary, 2012; Pilcer and Amighi, 2010; Telko and Hickey, 2005).

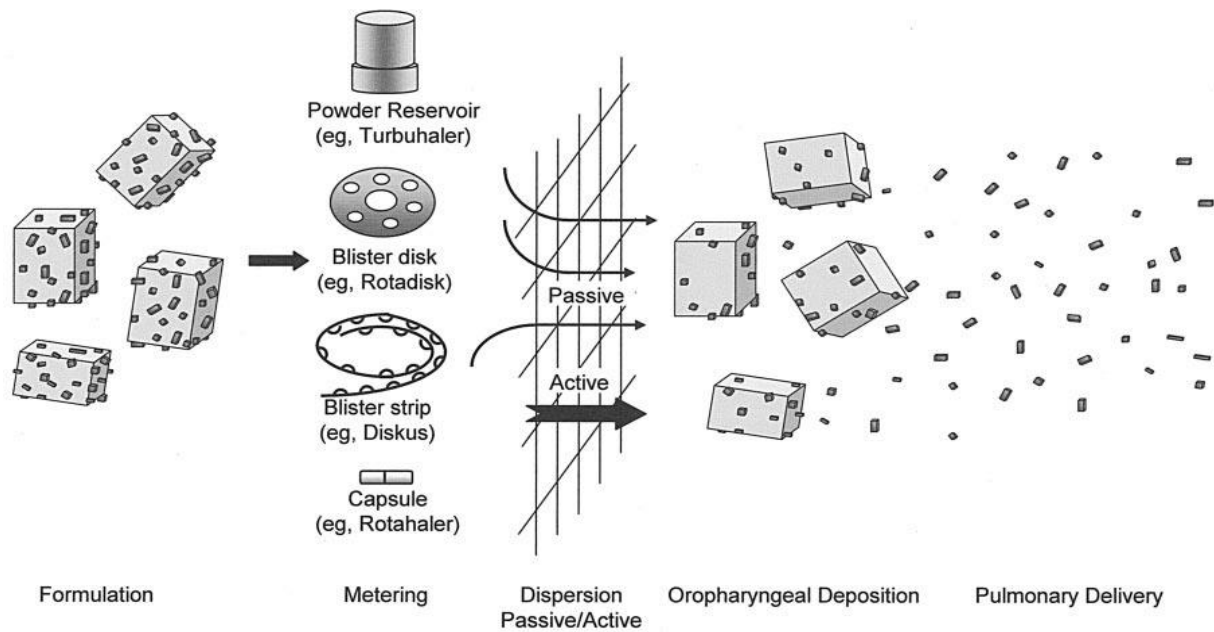


Figure 1-3: Principle mechanism of DPI design (Telko and Hickey, 2005).

Another categorization can be based on the device aerodynamic resistance or the pressure drop required for aerosolizing the formulation; it can be of high, medium or low resistance. The patients' inspiratory action is the drive to reach the required flow rate against this resistance to efficiently aerosolize and disperse the powder. Consequently, a pressure drop of a normal lung function which is about 4 kPa would lead to a flow rate of 90 to 100L/min in a model type for low resistance as the Aerolizer, flow rate of 40 to 60 in a moderate resistance inhaler such as the Easyhaler, and less than 40 L/min in high resistance inhalers such as Handihaler. Patients with severely impaired lung function and young children may not be able to sufficiently use high resistance devices due to possible incomplete dispersion and aerosolization of the DPI formulation (Gradon and Sosnowski, 2014; Islam and Cleary, 2012; Srichana et al., 1998; Tiddens et al., 2006).



Figure 1-4: List of some DPI devices available in the market; Single dose Capsule Devices; 1) Aerolizer® (low resistance), 2) HandiHaler® (high resistance), Multi-dose reservoir/cartridge; 3) Novolizer® (medium resistance), 4) Turbuhaler® (medium resistance), 5) Easyhaler® (medium Resistance), Multi-doses encapsulated in foil blisters; 6) Diskus® (low resistance).

As collected from the literature, the main characteristics for an Ideal DPI would be:

- Accurate and uniform dose delivery that is independent on the respiratory air flow.
- Optimal formulation that deliver API particles deep to the lungs with minimal retention in the device.
- Multi dose inhalers with consistent and reproducible dose delivery.
- Suitable for wide range of API either pulmonary local targeting or systemic into the blood, maintaining physicochemical stability.
- User friendly in terms of portability, economic, and feedback mechanism for dosage administration.

Unfortunately, there is no current Ideal DPI. However research is growing in two main directions; the development of DPI formulations with optimum aerosolization behavior

and the development of efficient and reliable devices. (Dolovich and Dhand, 2011; Islam and Cleary, 2012; Islam and Gladki, 2008; Telko and Hickey, 2005)

1.3.4 DPI formulations

For the API particles to reach the inner lung, they must have an aerodynamic size range of 1-5 μm . These very small particles exhibit large surface area that gives cohesive and adhesive properties hindering efficient aerosolization. Furthermore, model inhaled drugs are mainly given in μg doses which are very small amount to be inhaled alone efficiently. Accordingly, the basic approach to overcome such problems is to formulate the fine drug with a coarser carrier (about 95% w/w) to facilitate the flowability and dispersion (Tee et al., 2000; Andrade et al., 2013).

Traditionally, lactose monohydrate is the main choice as a carrier. It is mass produced from natural sources with acceptable low toxicity. In addition, lactose is a relatively simple disaccharide with a range of grades commercially available based on the particle size distribution (Traini et al., 2006; Andrade et al., 2013).

As particle size distribution affects a drug's deposition in the lungs, separation of the small solid particles used in dry powder inhalers is the most important performance characteristic for effective aerosol generation. To separate particles, the specific force of interaction must be overcome. There are four major forces of interaction between particles: mechanical interlocking due to surface asperities, capillary forces from the presence of water, electrostatic forces arising from the insulating nature of the material and van der Waals forces from the fundamental electromagnetic nature of matter (Gradon and Sosnowski, 2014; Pilcer and Amighi, 2010). The major forces of interaction present a barrier to the particles' flow and dispersion (Florence and Siepmann, 2009). Van der Waals forces are derived from the energy of interaction between two molecules, the shorter the distance between particles the higher the attractive forces and the higher the agglomeration. Since the separation distance plays a key role in the strength of van der Waals forces, it can be controlled by surface shape (e.g.: surface roughing) and use of fine spacer particulates (e.g.: fine lactose excipient) (Kou et al., 2012). Electrostatic forces must be considered for poor conductors as pharmaceutical products. Furthermore, two adjacent solid surfaces give rise to contact potential and in turn electrostatic attractive forces that increase powder aggregation. Capillary forces increase in relationship to

the relative humidity (RH) of the ambient air. At greater than 65% RH, water condenses in the space between adjacent particles. This leads to liquid bridges causing attractive forces due to the surface tension of the water. In addition, surface asperities might increase the potential for mechanical interlocking of particles, which will influence the aggregation state and ease of dispersion of particles (Florence and Siepmann, 2009).

The aerodynamic characteristics of the dose emitted from a dry powder inhaler (DPI) are determined by the degree of de-aggregation of the dose inside the inhaler during the inhalation maneuver (Nadarassan et al., 2010). In such preparations, the inspiratory force of the patient must overcome the adhesion forces between drug and carrier particles to aerosolize particles (Thi et al., 2008).

1.3.5 Current DPI formulation approaches and performance limitations

As stated earlier, physicochemical properties control the particle interactions which in turn determine the aerodynamic behavior of the DPI formulation. Optimizing the particles (size, morphology and structure) can be done through the choice of the production method. Particles can be engineered by spray drying (SD), spray freeze drying (SFD), supercritical fluid technologies (SCF), and even directly pulverized by a jet mill. Each production method has its advantages and drawbacks, depending mainly on the type of API being processed (Ashurst et al., 2000; Gradon and Sosnowski, 2014; Pilcer and Amighi, 2010). Furthermore, selected API particles were able to stand alone in carrier free formulations, showing positive results that even reached the market as budesonide in Pulmicort[®]. In this case, micron sized budesonide particles were agglomerated into spheres to reach the required flow properties and de-agglomeration behavior upon aerosolization. However, alternative carriers other than lactose are required to be able to widen the range of API that can be administered as DPI and achieve better aerosolization performance. Why lactose cannot be used with all types of API? Clinically, lactose can be delivered to diabetic and lactose intolerant patients without causing problems. However, considering its physicochemical properties, lactose is a reducing sugar that can interact with functional groups of APIs such as formoterol, budesonide, proteins and peptides (Pilcer and Amighi, 2010; Rahimpour et al., 2014; Steckel and Bolzen, 2004).

Intensive studies have been conducted on alternative sugars as potential excipients for DPI such as D-mannitol, glucose monohydrate, trehalose dihydrate, erythritol, dextrose, maltose, sorbitol, maltitol, and xylitol. They were employed as the main coarse carriers with a particle size range of about 30 – 200 μm and as ternary fine additives to enhance aerosolization performance (Pilcer and Amighi, 2010; Rahimpour et al., 2014; Steckel and Bolzen, 2004; Tee et al., 2000).

The performance of DPI is assessed in-vitro by impaction methods mainly, showing the fine particle fraction (FPF %) aerosolized that can reach the inner lung. Currently available inhalers from market and under research from literature give FPF range of 9% to 80% as collected by (Islam and Cleary, 2012). This shows the need of unconventional formulation designs improving aerosolization performance specifically for each API intended for pulmonary delivery.

1.3.6 Trehalose

Trehalose dihydrate is a disaccharide sugar that is commonly found in most life forms except mammals. It is produced as a cellular stress response factor due to its bio protective functions (Jain and Roy, 2009). It has been studied for its bio protection property specifically for dehydrated biological drugs such as proteins and peptides (Schebor et al., 2010). One of many studies, trehalose had an outstanding protective and stabilizing functions for spray dried immunoglobulin and their dry storage (Maury et al., 2005). On the other hand, attempts took place to utilize trehalose particles in improving DPI aerosolization performance. It is generally recognized as safe (GRAS) by the FDA as it has no potential to injure the lungs and easily cleared by metabolism (Pilcer and Amighi, 2010; Rahimpour et al., 2014). Unlike lactose, trehalose is a non-reducing sugar that does not cause degradation to specific molecules by Maillard reaction (Jain and Roy, 2009). Accordingly, trehalose has the edge of physical stability and compatibility with a wider formulation types. With particle engineering, prepared nano-porous micro-particles of trehalose showed positive results delivering protein drugs by DPI (Ogáin et al., 2011). Moreover, trehalose showed remarkable aerosolization performance as a carrier in DPI formulations in some studies with model pulmonary drugs; albuterol sulfate, ipratropium bromide monohydrate, disodium cromoglycate, and fluticasone propionate (Cline and Dalby, 2002; Mansour et al., 2010).

1.4 Aim of work

The study aims to utilize trehalose particles as an inert fine carrier to improve DPI aerosolization performance, diversify the potential delivery of new drugs in DPI formulations and the feasibility of bringing high drug dose into the lungs.

In a previous study to deliver oseltamivir phosphate (OP) antiviral drug as a DPI, trehalose formulations showed superior aerosolization performance over other formulations of lactose, mannitol, and glucose carriers. Hence the first chapter aims to characterize fine jet milled trehalose and to use it for optimized aerosolization of OP in dry powder inhalation formulations targeting enhanced therapeutics. Another aim was to evaluate the feasibility of bringing high drug doses into the lungs using trehalose as a fine carrier in low and medium resistance inhaler devices.

As discussed previously, particle engineering plays an important role in physicochemical properties that directly affect the aerosolization performance. Hereafter, chapter two focuses on the production of trehalose spherical particles in an inhalation grade size with smooth surface aiming to investigate the effects of surface engineered spray dried trehalose.

Aerosolization behavior is the main factor that decides whether a prepared DPI formula is accepted or not. Subsequently, the third chapter illustrates the aerosolization behavior of fine spray dried and fine jet milled trehalose carrier based DPI formulations with low dose model pulmonary drugs. It correlates the aerosolization performance to the carrier particle morphology, size, and surface energy produced under different factors.

2. Methodology

2.1 Particle engineering and production

2.1.1 Design of experiments

Two designs of experiments were carried out for studying the inlet feed variables on the trehalose particle size produced by jet milling and spray drying as discussed later. The designs were conducted and evaluated by Modde[®] DOE software.

2.1.2 Jet milling

As described in reviews, jet milling is the most useful and traditional technique for particle size reduction, although there is no control over the produced particle crystalline morphology (Malcolmson and Embleton, 1998; Pilcer and Amighi, 2010). The technique was considered and described for micro-particle production from over 10 years (Nykamp et al., 2002; Vatsaraj et al., 2003). Different APIs and trehalose batches were micronized by a fluid energy jet mill Jet-O-Mizer (Figure 2-1). To reach different target particle sizes it was controlled by two variables; grinding pressures (5 - 10 Bar) and number of runs (1 - 2 runs). 10 gram sample of each powder was added into the feed. The particles are pushed into the milling chamber by high pressure pushing nozzle where the pusher nozzle was set one bar higher than the grinding nozzle.

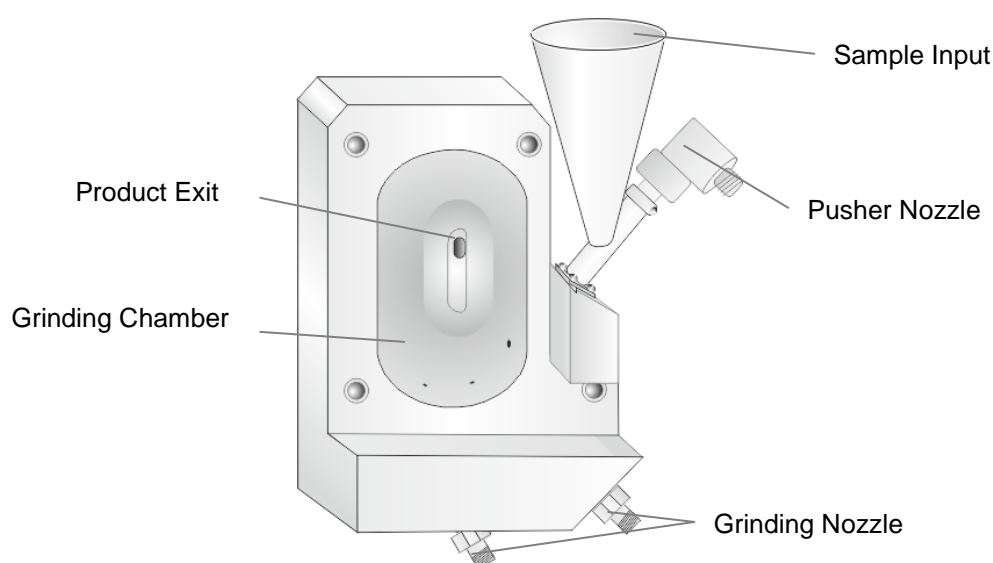


Figure 2-1: Jet mill schematic diagram

2.1.3 Spray drying

Particle engineering is a very sophisticated field of science; spray drying is a well-established method for the production of dry powder engineered particles with controlled morphology (size, shape, structure and surface energy). The product characteristics can be modified by the process and formulation parameters as described by many studies (Gradon and Sosnowski, 2014; Nandiyanto and Okuyama, 2011; Vehring, 2008).

All solutions prepared were spray dried with a Büchi B-290 Mini spray dryer. A nozzle tip of 0.7mm and nozzle screw cap of diameter 1.5mm were used. When spray drying aqueous solutions, the spray dryer was operated in the open mode, whereby the drying gas (compressed air) passes through the drying chamber and then is exhausted. When spray drying organic solutions as dichloromethane, the Büchi B-290 was operated in the closed mode, whereby the drying gas (nitrogen) is recycled to the drying chamber after precooling in a preheat exchanger and solvent condensation in a refrigerator unit (B-295 inert loop); in all cases the aspirator setting was 100%.

For trehalose solutions, they were prepared in bi-distilled water in the concentrations of; 5, 10, 15, 20, 25, 30, 40 % (w/v). The inlet temperature setting range was: 75, 85, 95 and 105 °C. The pump rate setting was tested at 10, 15 and 20%. The gas flow rate was set on the gas rotameter indicator at 30mm (500 NI/h), 40mm (670 NI/h) and 50mm (840 NI/h).

Each of salbutamol sulphate and di-sodium cromoglycate was spray dried as 5% (w/v) solution from bi-distilled water. The inlet temperature was 145°C, pump rate was 10% and gas flow set at 45mm (750 NI/h).

Budesonide was spray dried as 5% (w/v) solution in dichloromethane. The inlet temperature was 45°C, pump rate was 1% and gas flow set at 50mm (840 NI/h).

2.2 Physicochemical characterization

2.2.1 Particle size distribution

For geometric particle size distribution analysis, a powder sample after micronization or spray drying was dispersed in a RODOS module at 3 bars (Sympatec GmbH, Clausthal-Zellerfeld, Germany). Fraunhofer theory was used to calculate the particle size distribution (PSD) from the scattered laser light as described by de Boer (de Boer, Gjaltema et al. 2002). The measurements were performed in triplicates and data acquisition and calculations made with Helos-Sympatec Window X5 software.

2.2.2 Differential scanning calorimeter

Thermal properties of the different micronized and spray dried trehalose were investigated using a differential scanning calorimeter (Diamond DSC, Perkin Elmer, USA). Approximately 6-9mg of sample was accurately weighed into an aluminum pan and sealed with a lid into which one vent hole is pierced. The sample and reference (an identical pierced lid sealed pan, but empty) were heated at a rate of 10°C/min or 100°C/min from -10°C to 240°C. The calorimeter head was flushed with nitrogen gas at 20 ml·min⁻³ during all measurements. For a further insight on the glass transition properties of spray dried trehalose, modulated DSC (mDSC) was performed using a step scan method each of 3° from -20°C to 120°C, at rate of 5°C/min. MDSC gives an enhanced interpretation and detection of glass transition for complex thermal events (Gill et al., 2010). Perkin Elmer – Pyris software was used for capture and analysis of data.

2.2.3 Dynamic vapor sorption

The moisture sorption characteristics of trehalose particles were assessed by DVS (DVS-HT, surface measurement systems Ltd., London, UK). Approximately 40mg of each sample was weighed into the sample cell and subjected to two 0–90% relative humidity sorption cycles, over 10% RH increments.

2.2.4 X-Ray powder diffraction

The crystalline structure of trehalose was analyzed before and after micronization and spray drying by X-ray diffraction. Samples were analyzed by X-ray diffractometer with a rotating anode (Stoe and Cie GmbH, Darmstadt, Germany) with a Cu-K α source operated at 40 kV and 30mA.

2.2.5 Specific surface area

The specific surface area of the micronized trehalose particles were measured with the gas sorption analyzer (NOVA 2200, Quantachrome Corporation, USA). An eleven-point BET nitrogen adsorption isotherm analysis at 77 K was performed in triplicate after degassing the samples overnight under vacuum at room temperature.

2.2.6 Fluidization energy

The fluidization energy of the micronized trehalose was measured under aerated conditions by an FT4 Powder Rheometer (Freeman Technology, UK). For each run, 25mL of sample powder was analyzed in a 30mm bore borosilicate glass cylinder. The powders were evaluated using an automated aeration program that runs a sequence of tests at increasing levels of air velocity through the powder sample (0–10mms⁻¹), with a conditioning cycle before each test cycle. The fluidization energy is determined when the flow energy plateau at increasing air flow velocities (Cordts and Steckel, 2012).

2.2.7 Thermo gravimetric analysis

Moisture content of trehalose dihydrate as obtained and finest micronized trehalose were measured by thermo-gravimetric analysis (TGA - TAC7/DX – Perkin Elmer, USA). Measurements are performed using 1–2mg of sample in an alumina crucible from 30°C to 220° C at 10°C min⁻¹ heating rate under a nitrogen atmosphere.

2.2.8 Scanning electron microscope

Pure powders and blend morphologies were investigated using scanning electron microscopy (SEM, Carl Zeiss Microscopy GmbH). Samples were mounted on carbon sticky tabs and examined at different magnification power.

2.2.9 Inverse gas chromatography

Inverse gas chromatography was used to determine the surface dispersive energies of powders. For all measurements, approximately 300-600mg was packed into a pre-silanized glass column (300mm×3mm internal diameter). Weights of each sample used for packing was chosen according to previous trials and errors for optimum iGC reading. By vertical tapping for at least 10 minutes using an iGC column packer, progress was visually monitored and tapping continued until no cracks, hollows or channels in the body of the powder bed were visible. Both ends of the columns were loosely stoppered with silanized glass wool. Prior to the measurements, pre-treatment was carried out for 2 h at 303K to remove impurities adsorbed on the surface. Helium with a gas flow rate of 10 sccm (standard cubic centimeter per minute) was used to carry different probes, and the retention times were detected with a flame ionization detector (FID). Dead volume calculations were based on the elution time of methane which was used at a concentration of 0.04 (p/p°) (where p denotes the partial pressure and p° the saturation vapor pressure). The dispersive surface energies were determined by the pulse-varying probe method. Five alkane probes (Elutant) (GC grade hexane, heptane, octane, nonane and decane) were used to determine the dispersive surface energy (γ^D). Surface energy measurements at infinite dilution were performed in triplicate. The selection of conditioning time and temperature was based on preliminary experiments utilizing the method adopted from (Swaminathan et al., 2006).

2.3 Preparation of DPI blends

Targeting a high dose formulation, OP was mixed with different grade trehalose in the ratio of 3:1. On the other hand, as a standard of low dose formulations; SS, BU, and DSCG were each prepared in ratio 1: 5 formulations with different trehalose batches. All the binary DPI formulations were prepared first by geometric mixing and sieving followed by blending in a 30 cm³ stainless vessel using a turbula mixer at 42rpm for 10 min. Geometric mixing of the Carrier with API was performed to give equal distribution of the unequal amounts prior to blending. The powder of the lesser amount (i.e.; API) is mixed with similar amount of carrier. Then continued mixing with the remaining powder (i.e.: Carrier) in a similar additive manner. Afterwards the blending is repeated under same conditions and then passed

through final 355 μ m sized sieve for breaking down large agglomerates. Following blending and sieving, the drug homogeneity of all the formulations was assessed. 3 samples top, middle and bottom were taken from each formulation dissolved in an appropriate solvent and drug concentration assessed using a spectrophotometer or HPLC assay. The whole preparation was done in an environmental controlled chamber at relative humidity (RH) around 40% and temperature below 25°C.

2.4 Aerosolization performance

2.4.1 Aerosol dispersion for laser diffraction

For each of the selected micronized trehalose samples and the OP-formulations prepared, the PSD determined by laser diffraction utilizing two configurations: RODOS module and INHALER module. A Sympatec Helos (Sympatec GmbH, Clausthal-Zellerfeld, Germany) was used with an R2 lens. The INHALER module includes the Inhaler, throat and a pre-separator that is similarly assembled as the NGI and connected to a vacuum pump (Assembly shown in Figure 2-4). The pre-separator is coated with a solution of Brij35:Ethanol:Glycerol at weight ratio of 15:51:34, respectively, to prevent powder particles from bouncing.

De-agglomeration behavior of different micronized trehalose samples were assessed based on the comparison between PSD at a cutoff point of 5 μ m when fully de-agglomerated by RODOS module at 3 bars and when partially de-agglomerated as aerosolized into the INHALER module at different air flow rates (20L/min – 100L/min). Aerosolization into the INHALER module was performed without an inhaler as a control, using an application device called “Rack” instead of the inhalation device to eliminate the influence of the inhaler and gives a laminar flow for the particles. Hence, this would measure the aerosolization performance depending only on the physical nature of the powder particles. Briefly, the “Rack” consists of a stainless steel tube with an inner diameter of 5mm and a total length of 170 mm shown in Figure 2-2. For the delivery of the powder into the air stream, powder was weighed into the cavity and released into the stainless steel tubing and entrained by the air by rotating the inner part of the applicator, and then the powder was discharged.

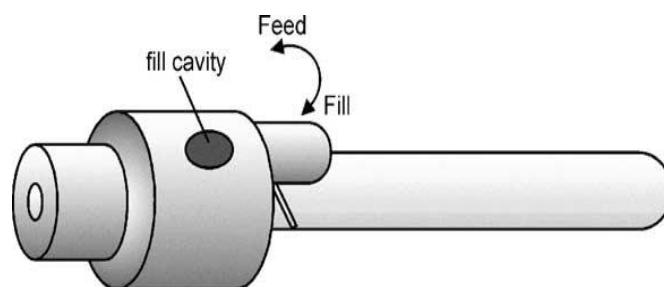


Figure 2-2: Application system "Rack" (Steckel and Bolzen 2004)

For measuring the deagglomeration behavior of oseltamivir phosphate formulations prepared (OP/TR), the capsule is discharged into the INHALER laser diffraction module by the Unihaler (Figure 2-3) at 36 mbar which gives a flow of 57L/min. Then, the particle size distribution behind the throat was calculated and compared to PSD at a cutoff point of $5\mu\text{m}$ when blends were fully de-agglomerated by RODOS module at 3 bars. All measurements were done in triplets and averages were calculated and presented using Sympatec Windox 5 software.

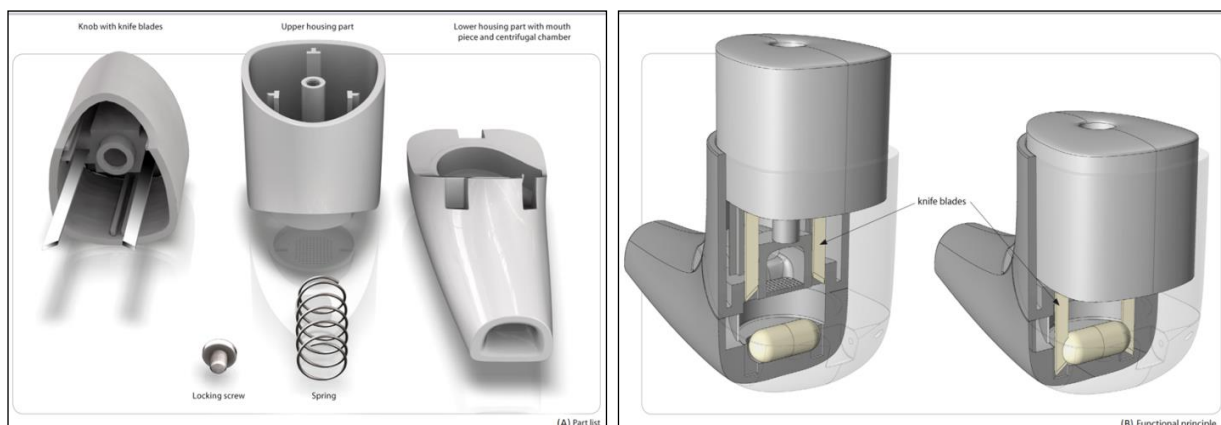


Figure 2-3: (A) Different parts of the Unihaler, (B) Assembly and functional principle of the Unihaler.

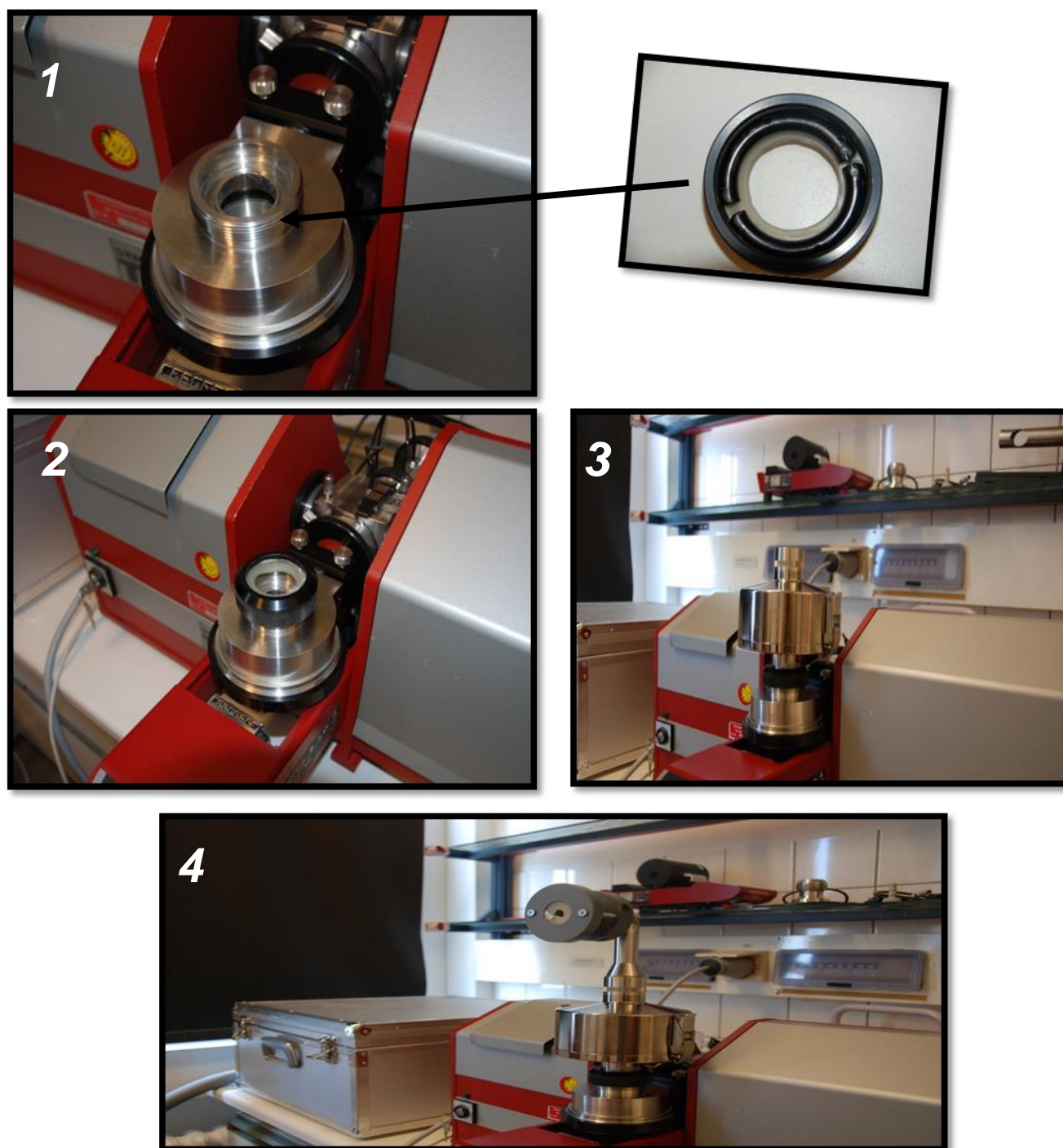


Figure 2-4: Steps 1 to 4 showing the assembly of the preseparator and the throat to the inhalation module of the Sympatec laser diffraction system. (1 & 2) A plastic ring and a rubber ring are placed to have an air tight connection with the preseparator. (3) Connecting the preseparator. (4) Overall view before placing the inhaler.

2.4.2 Next Generation Impactor

In accordance with (United States Pharmacopeial Convention, 2014) (USP) chapter 601 specification on aerosols, the aerosolization performance of each prepared formulation was assessed by a Next Generation Impactor (Figure 2-5) (NGI, Copley Scientific, Nottingham, UK) evaluating the aerodynamic particle size distribution. For using capsule based inhalers, each formulation sample was accurately weighed into size 3 hydroxypropylmethylcellulose capsules (HPMC, Quali-V[®] caps, SA, Spain). OP blends' samples were in (15 ± 0.1 mg) filled capsules, while BU, SS, and DSCG blends' samples were in (5 ± 0.1 mg) filled capsules. Prior to testing, NGI preseparator and tray cups were coated with a solution of Brij35:Ethanol:Glycerol at weight ratio of 15:51:34, respectively, to prevent powder particles from bouncing. For each experimental run, one capsule of the tested formulation was aerosolized and discharged into the NGI. Afterwards, the NGI apparatus is dismantled and the inhaler, the throat, the preseparator and tray cups were washed down with known volumes of the suitable solvent. The amount of drug deposited in each part is calculated by either HPLC or spectrophotometric assay. The method was repeated three times for each formulation in an environmental controlled chamber at relative humidity (RH) around 40% and temperature below 25°C. Copley software was used to calculate the emitted dose, the fine particle dose (FPD), the fine particle fraction (FPF) and the mass median aerodynamic diameter (MMAD).

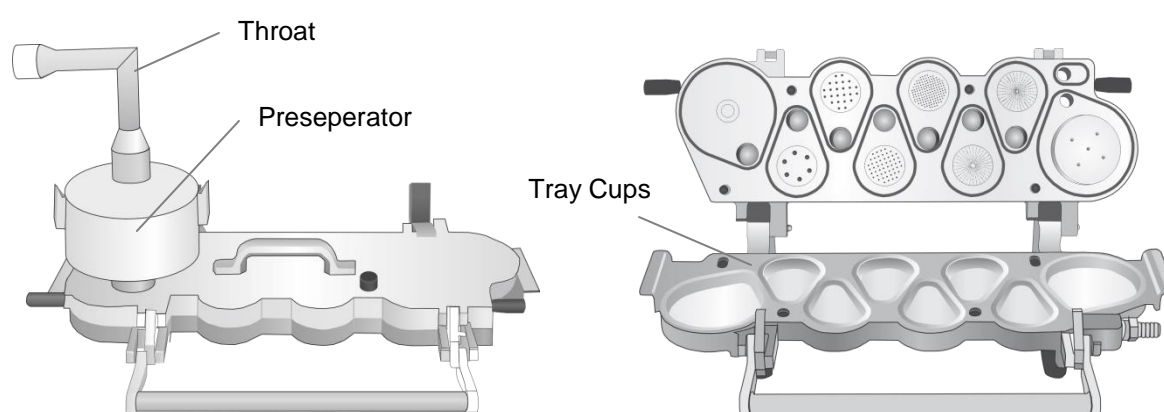


Figure 2-5: NGI closed (Left) and opened (right) schematic diagram

2.5 Drug assay

2.5.1 UV-spectrophotometric quantification

UV-spectrophotometric analysis was used to quantify OP at a wavelength of 240nm. Before all quantifications, control and calibration were evaluated in terms of linearity, assay precision, and accuracy by different concentrations of pure OP and OP in combination with trehalose. Trehalose had no significant absorbance at 240nm, and OP solutions were prepared by bi-distilled water; accordingly the quantification of OP was simple and sensitive for the tested concentrations.

2.5.2 Liquid Chromatography quantification

HPLC system (Agilent Technologies - Hewlett-Packard, Waldbronn, Germany) was used to quantify samples of BU, SS, and DSCG. The data was obtained and evaluated by LC/MS Chemstation software (Agilent Technologies, Germany).

2.5.2.1 Budesonide (BU)

Stationary Phase	LioChroCart® 125-4 LiChrospher® 100 RP-18 (5µm) With pre-column
Mobile Phase	75% Methanol 25% Water
Flow Rate	1 ml/min
Detection Wavelength	248nm
Injection Volume	100 µl
Calibrated Range	1 – 100 µg/ml

2.5.2.2 Salbutamol Sulphate (SS)

Stationary Phase	LioChroCart® 125-4 LiChrospher® 100 RP-18 (5µm) With pre-column
------------------	---

Mobile Phase	85% Buffer (3.45g Sodium dihydrogen phosphate in 1L of 0.05% triethylamine aqueous solution); pH adjusted to 3.0 with H ₃ PO ₄ (10% solution) 15% Methanol
Flow Rate	1 ml/min
Detection Wavelength	224nm
Injection Volume	50 µl
Calibrated Range	1 – 100 µg/ml

2.5.2.3 Di-sodium cromoglycate (DSCG)

Stationary Phase	LioChroCart [®] 125-4 LiChrospher [®] 100 RP-18 (5µm) With pre-column
Mobile Phase	60% Buffer (8.95g disodium hydrogen phosphate + 3.4g potassium dihydrogen phosphate in 1L Bidistilled water); pH adjusted to 3.3 by H ₃ PO ₄ (10% solution) 40% Methanol
Flow Rate	0.8 ml/min
Detection Wavelength	326nm
Injection Volume	100 µl
Calibrated Range	1 – 100 µg/ml

3. Chapter One

**Jet milled trehalose study and
oseltamivir phosphate aerosolization
optimization**

3.1 Introduction

Oseltamivir phosphate is the leading drug in the class of oral neuraminidase inhibitors (NAIs) which are the primary treatment option for influenza, and can also be used to limit the spread of infection in close proximity environments. OP is available only to be administered orally (Tamiflu™; Roche Laboratories, Nutley, NJ). Oseltamivir is a sialic acid analogue that competitively and reversibly inhibits the neuraminidase enzymatic active site specific for influenza virus A and B (Dreitlein et al., 2001, Englund, 2002, 2002; Oxford and Lambkin, 1998). It breaks the replication cycle when given during the start of infection at the virus highest activity (Gillissen and Höffken, 2002). Oseltamivir is effective against all avian and human influenza strains, including the highly pathogenic H5N1 strain.

Orally administered Oseltamivir Phosphate is a prodrug that is absorbed from the gastrointestinal tract with an absolute bioavailability of 75% - 80%. Then it is metabolized by the hepatic Carboxylesterase-1 family (CES1) into its active metabolite “Oseltamivir Carboxylate” as shown in figure 3-1 and not metabolized by the intestinal tissue or the plasma esterase’s (Hosokawa, 2008; Oo et al., 2003; Shi et al., 2006; Zhu and Markowitz, 2009). In adults, the standard oseltamivir treatment regimen is 75 mg twice daily for 5 days (Lindemann et al., 2010).

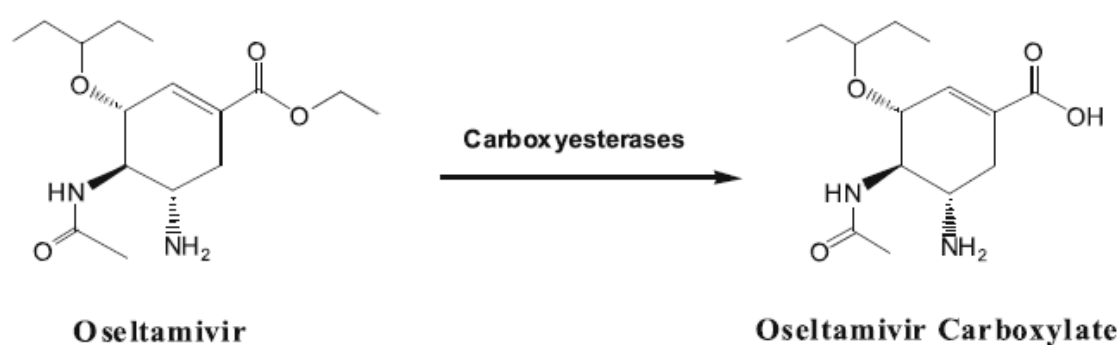


Figure 3-1: Bioconversion of Oseltamivir into Oseltamivir Carboxylate (Eisenberg, 2007).

Case reports indicate that standard doses of Oseltamivir can improve therapeutic outcomes and survival when initiated early in the infection cycle (Clercq, 2006). The use of higher doses of Oseltamivir drew attention for the treatment of avian influenza stains as the highly pathogenic H5N1. Furthermore, it was recommended by the World Health Organization (WHO) to treat patients with 150mg

twice daily. A treatment duration of 10 days was shown to be beneficial for infected patients (Dutkowski et al., 2010). Oseltamivir inhalative administration is therefore be considered as targeting the virus at the site of the infection instead of systemic administration of the drug, similar to aerosolized zanamivir that is another NAI and topically administered as a DPI with a daily dose up to 20mg (Beigel and Bray, 2008). One blister dose from Relenza[®] contains 5mg of zanamivir formulated with 20mg lactose monohydrate carrier (Claus et al., 2014). The lung which is the site of direct administration is rich with CES 1 enzyme (Hosokawa, 2008); accordingly the drug can be activated at the site of action. Subsequently, delivering oseltamivir directly into the lung by inhalation would lower the dose, lower the oral side effects (e.g.: nausea and vomiting) and give direct faster activity.

Previously, the feasibility of oseltamivir phosphate aerosolization was achieved using trehalose based DPI formulations with excellent indication of its safety on the lung cells. Besides, the study validated the high efficiency of the newly developed capsule-based inhaler (UNI-Haler) in dispersing highly agglomerated blends and its usefulness in aerosolizing oseltamivir phosphate was demonstrated (Aziz, 2011).

In this study chapter, three main targets were set;

1. To achieve an oseltamivir DPI formula with higher efficiency and better aerosolization performance using UNI-Haler for sustained comparison.
2. To take a further step showing the physicochemical characterization in relation to the aerosolization behavior of micronized grade trehalose dihydrate as a carrier in oseltamivir phosphate DPI formulations.
3. To evaluate the feasibility of bringing high drug doses into the lungs using trehalose as a fine carrier.

The main study design was set to use fine trehalose carrier instead of the commonly used particle size range of (40 μ m to 200 μ m). Also the design added into consideration the effect of small particle variation (\geq 5 μ m) of the API itself.

Based on a Design of Experiment (DOE), different micronized (D50 = 1.7 μ m, 2.4 μ m and 4.8 μ m) grade trehalose were investigated to optimize the fine particle fraction of inhaled oseltamivir in high dose blends (75% w/w). Furthermore, two OP particle size grades (D50 = 1.65 μ m and 1.88 μ m) were tested during the study to

measure the significance of small particle size changes on aerosol performance. Laser diffraction was used to evaluate the particle size distribution of jet milled trehalose and OP grades. Thermal behavior and crystalline structure were examined by differential scanning calorimetry, thermogravimetric analysis and X-ray powder diffraction. Likewise, micronized OP was tested for physical stability after mechanical milling by XRPD and DSC. Water sorption characteristics of trehalose were analyzed based on milled particles at different size grades. Moreover, specific surface area and the fluidization energy for the trehalose particles were correlated to the different size grade production by jet milling.

Subsequently, blends were prepared using a turbula mixer and de-agglomeration behavior was screened for all primary blends using laser diffraction. In view of that, aerosolization performance was evaluated for potential formulations utilizing inertial impaction. At the end of this chapter methodology, scanning electron microscopy visualized and evaluated the morphology of the particles in the blends to correlate its aerosolization performance.

3.2 Results

3.2.1 Prepared jet milled particles

From the factorial design (D-optimal charts refer to appendix), three trehalose batches (TR5, TR10, TR1010) were chosen based on relatively large, medium and small particle size diameter. The 4th (TR66) batch was chosen to compare similar particle size reached by different grinding conditions in terms of physicochemical properties. Four different batches of jet milled trehalose were successfully produced at different grinding conditions, evaluated and recorded (as shown in Table 3-1) for particle size distribution by laser diffraction, fluidization energy by FT4, and specific surface area by gas sorption analyzer.

Table 3-1: Particle size distribution, fluidization energy and specific surface area for jet milled trehalose batches (n=3)

Trehalose batch	Grinding condition		Particle size distribution (μm)				Fluidization energy (mJ)	Specific surface area (m^2/gram)
	Run 1	Run 2	D10	D50	D90	Span Value		
TR5	5 bar	_____	0.9	4.8	21	4.2	51	1.25
TR10	10 bar	_____	0.7	2.4	7	2.65	103	2.36
TR66	6 bar	6 bar	0.6	2.4	7.3	2.67	94	2.49
TR1010	10 bar	10 bar	0.6	1.7	4	2	134	2.73

On the other hand OP was only jet milled into two grades as shown in Table 3-2; both are fine particles ($D_{50} \leq 5\mu\text{m}$) to target possible deepest lung dispersion.

Table 3-2: Particle size distribution of jet milled OP grades

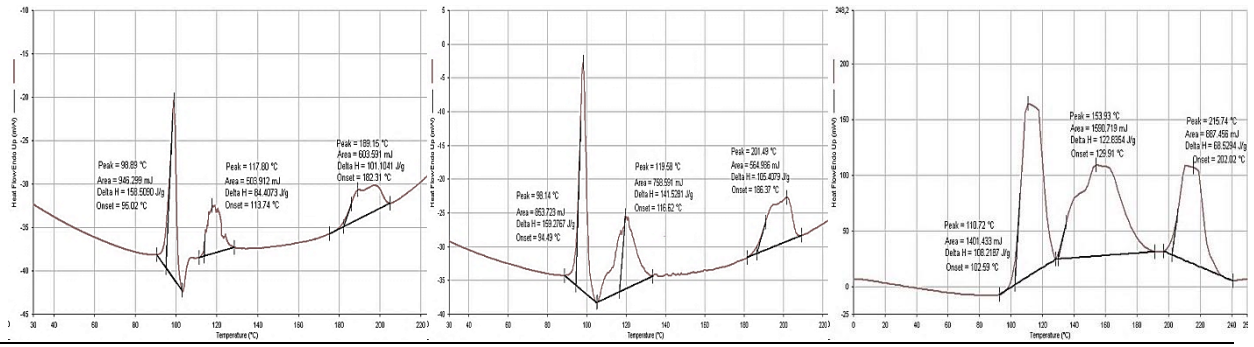
Oseltamivir phosphate batch	Grinding condition		Particle size distribution (μm)			
	Run 1	Run 2	D10	D50	D90	Span Value
OP10	10	_____	0.69	1.88	7.7	3.7
OP1010	10	10	0.67	1.65	5.1	2.7

3.2.2 Physicochemical characteristics

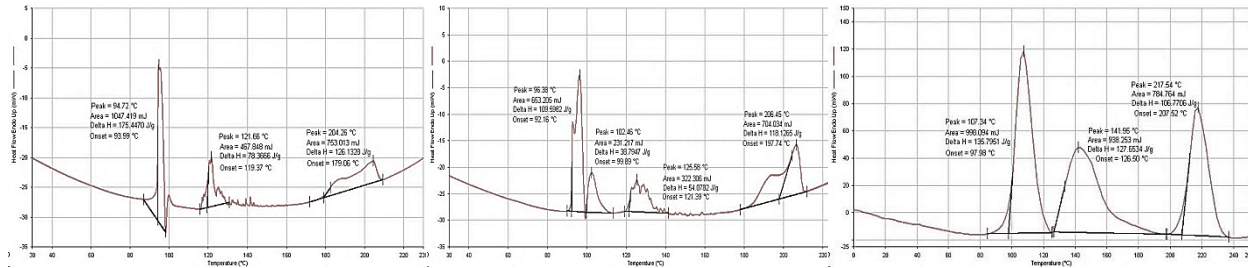
3.2.2.1 Thermal Behavior

DSC scans obtained, showed typical endothermic and exothermic events for trehalose dihydrate at both low ($5^{\circ}\text{C min}^{-1}$, $10^{\circ}\text{C min}^{-1}$) and high ($100^{\circ}\text{C min}^{-1}$) scanning rates (Figure 3-2). The first endothermic peak appeared around 100°C is related to the dehydration of the α -trehalose crystals (T_{α}). The second endothermic peak proceeded with an exothermic event was recorded around 120°C and according to literature it is correlated to the melting of (T_{α}) and the formation of polymorph β -trehalose crystals (T_{β}). The last endothermic peak at about 200°C indicates the melting of the more stable polymorph β -trehalose crystals (Jones et al., 2006; Sussich and Cesàro, 2008; Verhoeven et al., 2012). This study was made to evaluate the effect of micronization on such thermal behavior. At high scan rate, the finer the trehalose particles, the sharper the peaks. Furthermore, it was clear that decreasing trehalose particle size lead to a moderately faster dehydration process at lower temperatures as presented in Figure 3-3. As for the other thermal events melting/transition of T_{α} to T_{β} , and melting of T_{β} ; they were less affected by the particle size reduction as illustrated in Table 3-3.

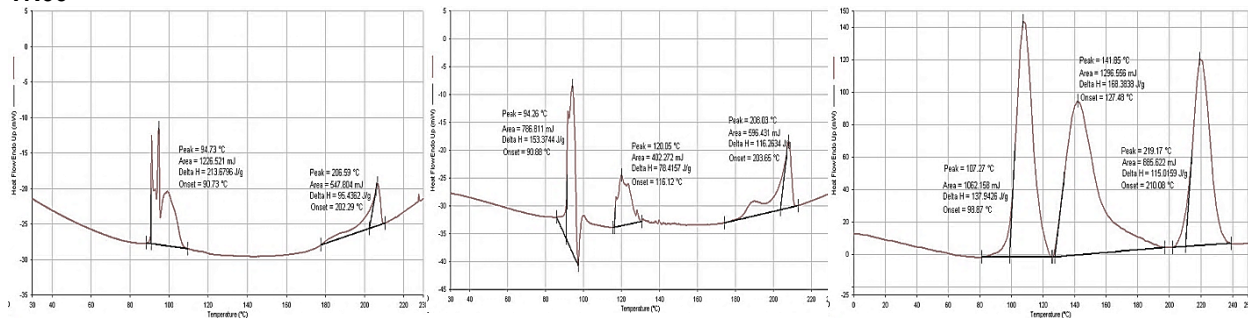
TR 16400



TR5



TR66



TR1010

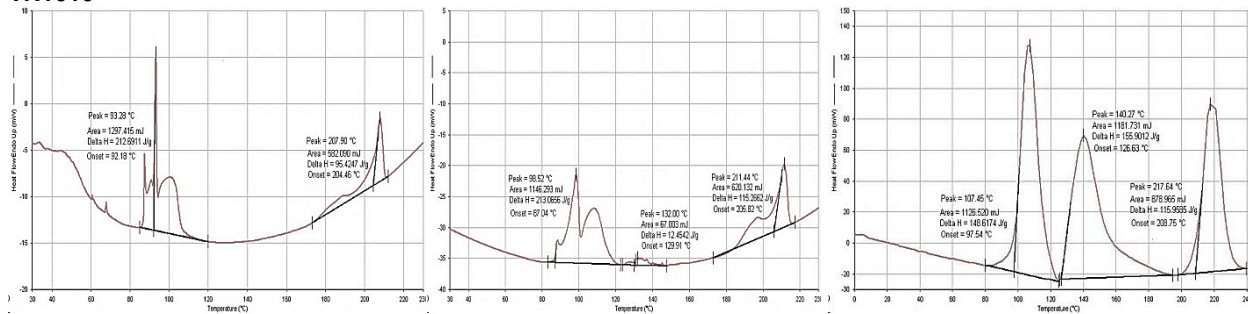


Figure 3-2: DSC thermograms at 5°C min⁻¹ (Left side) at 10°C min⁻¹ (Middle) and 100°C min⁻¹ (Right side) for different Trehalose batches

Table 3-3: Summary of transition temperatures at different scanning rate for milled trehalose grades compared to unprocessed trehalose (TR16400).

TR Grade	Dehydration of T α			Melting & Transition T α \rightarrow T β			Melting of T β		
	(5°C min-1)	(10°C min-1)	(100°C min-1)	(5°C min-1)	(10°C min-1)	(100°C min-1)	(5°C min-1)	(10°C min-1)	(100°C min-1)
TR 16400	95	95	102	113	117	129	182	186	202
TR5	95	92	98	119	126	126	179	206	207
TR66	94	91	98	—	120	127	201	202	210
TR1010	92	87	98	—	130	127	204	206	209

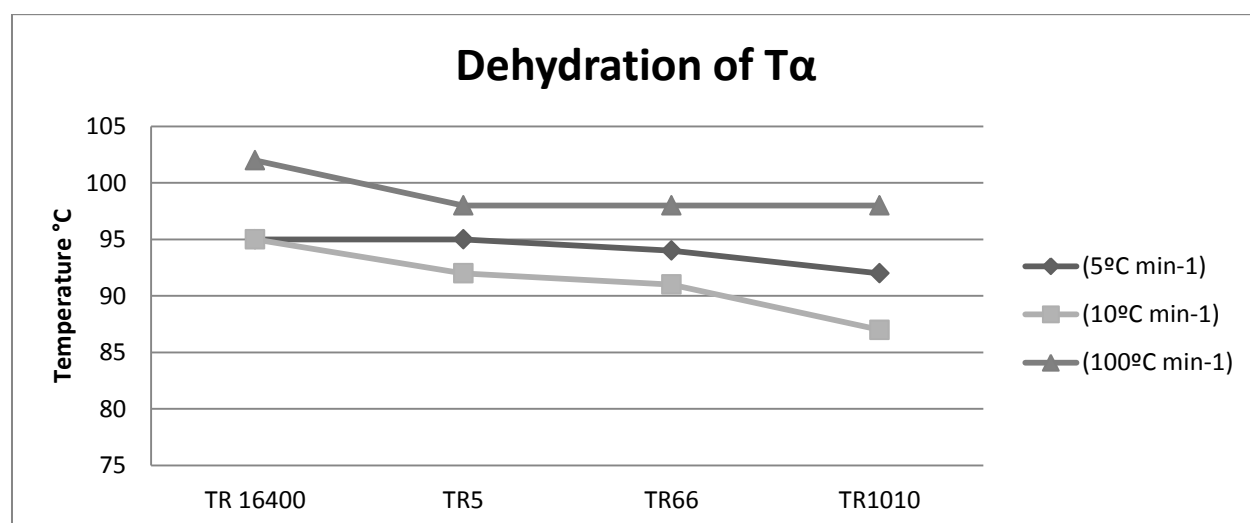


Figure 3-3: Onset of dehydration temperatures for T α crystals relative to the trehalose grade (particle size)

Thermo-gravimetric analysis presented in Figure 3-4 confirms previous observation, where both samples (largest and finest trehalose particles) lost about 9% water by weight. The dehydration started at 80 °C, but a faster loss of weight of finer TR1010 (ending at \approx 120°C) when compared to unprocessed TR16400 (ending at \approx 160°C). Mechanical processing as micronization into finer particle size did not remove the water content but facilitated the ease of water removal when exposed to thermal energy.

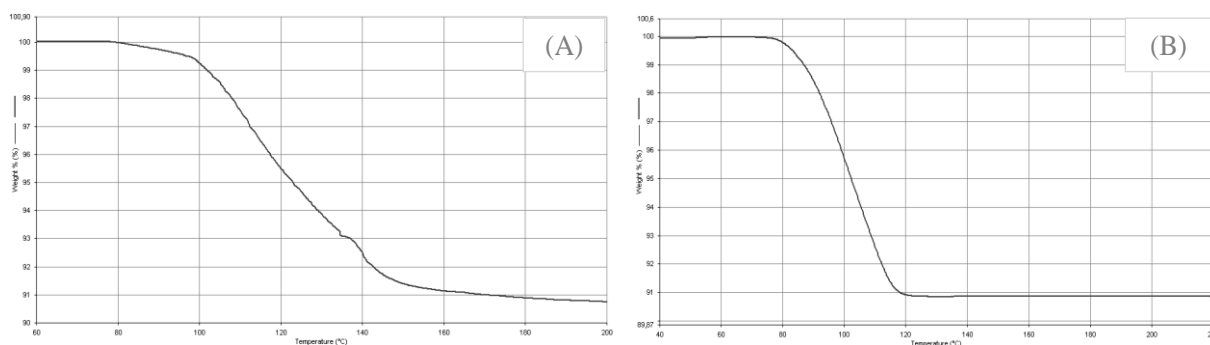


Figure 3-4: TGA of (A) TR16400 and (B) TR1010 showing the percent weight loss (Y-axis) with increasing temperature °C (X-axis).

3.2.2.2 Dynamic Vapor Sorption

Analysis of the vapor sorption characteristics of three micronized particle grades trehalose dihydrate compared to the unprocessed form (TR16400) are shown in Figure 3-5. In general, trehalose dihydrate accepts water moisture to be adsorbed at $\geq 15\%$ until it is steady at about 45% RH till 85% RH. As expected, the finer the trehalose particles the extra moisture it adsorbs to its surface. Observing at 50% RH, water sorption to TR5 ($D_{90} = 21\mu\text{m}$) was four times more than its sorption to the unprocessed sample (TR16400) with change of mass of about 2%. Furthermore, at 50% RH the change in mass of the finer trehalose TR1010 & TR66 was 2.6% & 3% respectively. Unexpectedly, TR1010 the finest micronized trehalose particles ($D_{90} = 4\mu\text{m}$) showed a lower moisture sorption than TR66 ($D_{90} = 7.3\mu\text{m}$). This can be explained by the high cohesive forces between the trehalose particles that might have limited any further water sorption.

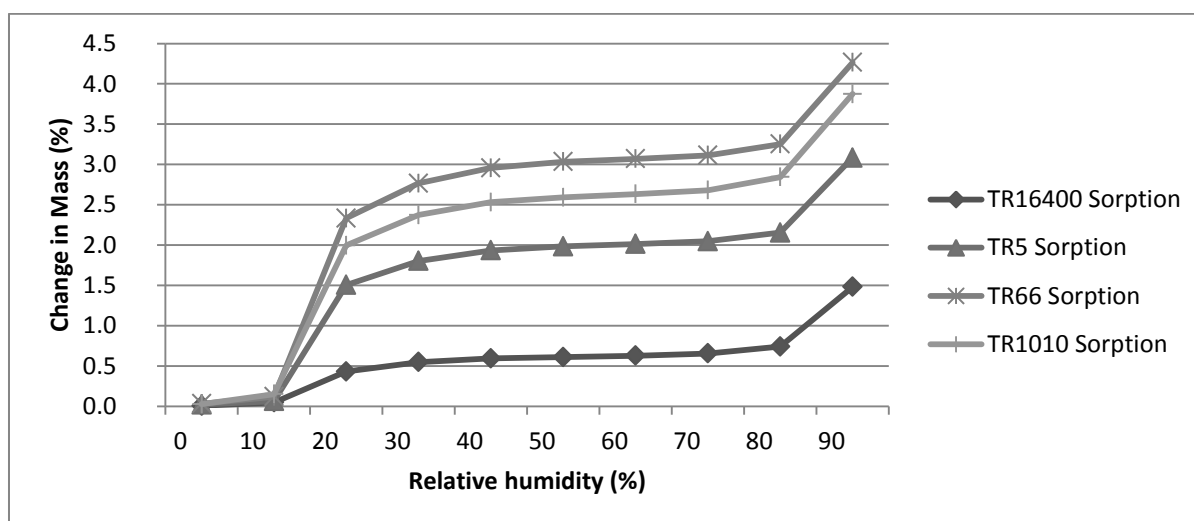


Figure 3-5: DVS profile of different micronized particle grade trehalose dihydrate.

3.2.2.3 Crystalline structure

XRPD spectra obtained for trehalose dihydrate before and after micronization shown in Figure 3-6 are clearly similar to those in literature (Jones et al., 2006; Sussich et al., 1998). This confirms the preserved structure of the trehalose dihydrate crystal even after micronization. Micronizing the trehalose particles into fines did not change the peaks detected, but only reduced their detected intensity where the finest particles (TR1010) gave the lowest detected intensity.

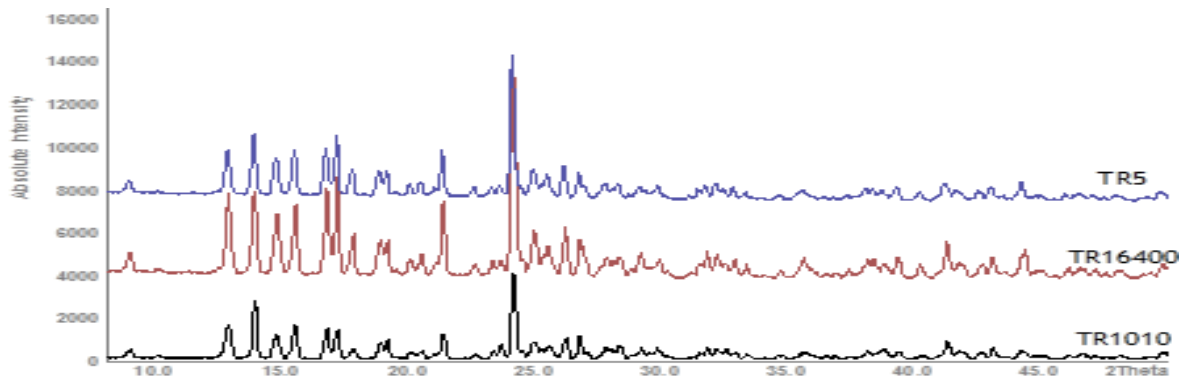


Figure 3-6: XRPD spectra of trehalose dihydrate before micronization (TR16400) and after micronization (TR5 and TR1010).

3.2.2.4 De-agglomeration behavior

From the de-agglomeration behavior of micronized trehalose dihydrate presented in Figure 3-7; (TR5) the least fine particles showed the highest de-agglomeration when aerosolized at different airflow rates. Furthermore, TR10 and TR66 having similar PSD, had similar de-agglomeration behavior as shown. Accordingly, in jet milling conditions, using either one or two micronization runs to reach similar PSD, did not affect the de-agglomeration behavior.

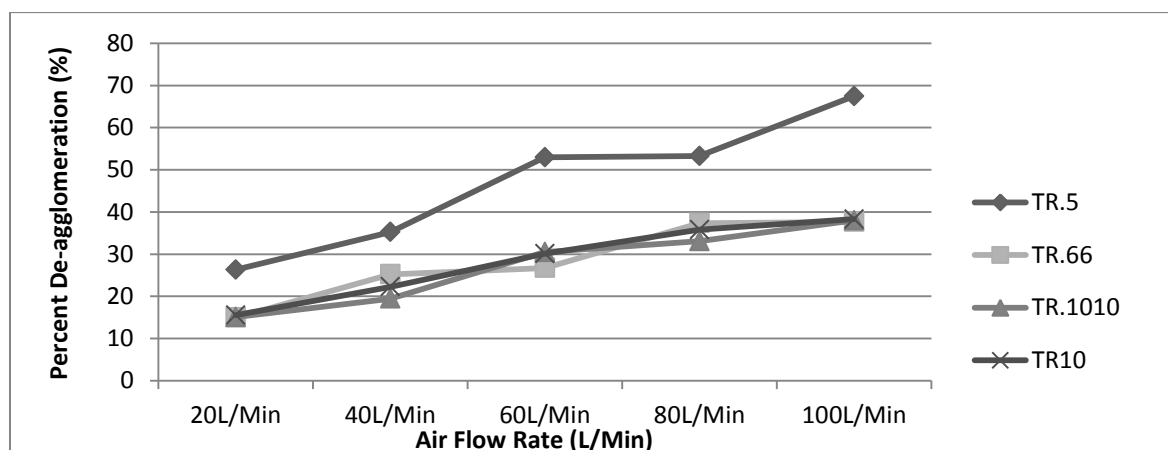


Figure 3-7: Percent De-agglomeration of tested trehalose grades under different airflow rates.

3.2.2.5 Oseltamivir physical stability

By jet milling under highest pressure for 2 runs, the OP particles kept its thermal behavior constant. From the unprocessed (OP) to the finest particles (OP1010), a small increase by less than 1°C of the only endothermic peak was observed as in Figure 3-8. This indicates a minor change in the amorphous part or the limited occurrence of impurities.

Furthermore, by observing XRPD spectra in Figure 3-9, there is no change in the crystalline pattern for both fine jet milled OP1010 compared to unprocessed OP.

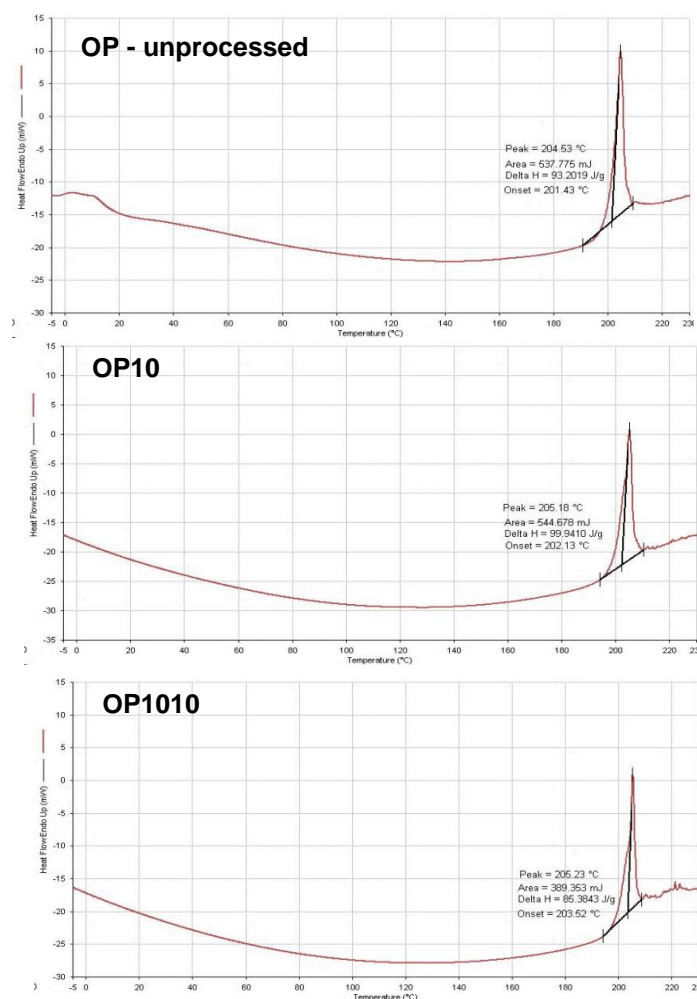


Figure 3-8: DSC thermograms of OP grades

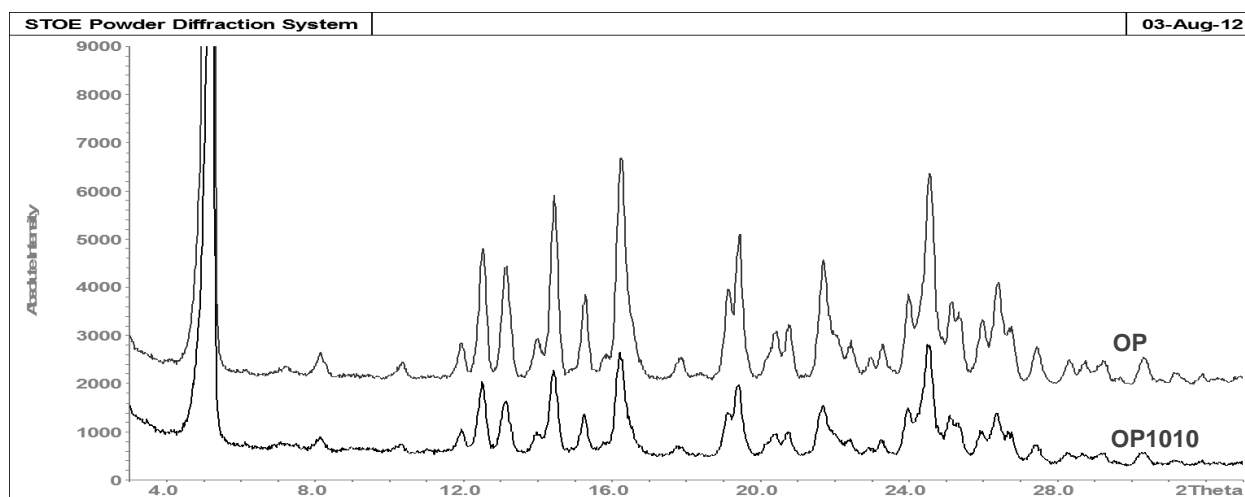


Figure 3-9: XRPD spectra for OP and OP1010

3.2.3 Blends and homogeneity

From jet milling, three particle size grades of trehalose and two grades of oseltamivir were produced; accordingly six homogenous blends were prepared as shown in Table 3-4. All DPI blends prepared were considered homogenous as their relative standard deviation (RSD) was below 6% (Jones et al., 2010).

Table 3-4: Prepared OP/TR formulations showing RSD% for UV-absorbance and OP concentration.

#	Blend		Top	Mid	Bottom	Mean	RSD%
1	OP10/TR5	Conc. (mg/ml)	0.21	0.21	0.22	0.21	2.71
2	OP10/TR66	Conc. (mg/ml)	0.22	0.22	0.22	0.22	0.00
3	OP10/TR1010	Conc. (mg/ml)	0.20	0.21	0.21	0.21	2.79
4	OP1010/TR5	Conc. (mg/ml)	0.20	0.20	0.21	0.20	2.84
5	OP1010/TR66	Conc. (mg/ml)	0.20	0.20	0.21	0.20	2.84
6	OP1010/TR1010	Conc. (mg/ml)	0.20	0.22	0.21	0.21	4.76

3.2.4 Aerosolization performance

3.2.4.1 Laser diffraction

In the second part of the de-agglomeration analysis by laser diffraction, OP/TR-formulations were tested at the same airflow as it would be aerosolized by UNI-haler in the cascade impaction at 4 kPa pressure drop across the device. Figure 3-10 shows how close it would be to the Rodos module full de-agglomeration when using the UNI-haler depending on different PSD. Trehalose particles (TR5) that are about 4-5 times larger than the OP1010 PSD, gave the highest de-agglomeration percentage of about 98%. This indicates the highest potential of using TR5 to give the best aerosolization of finest OP.

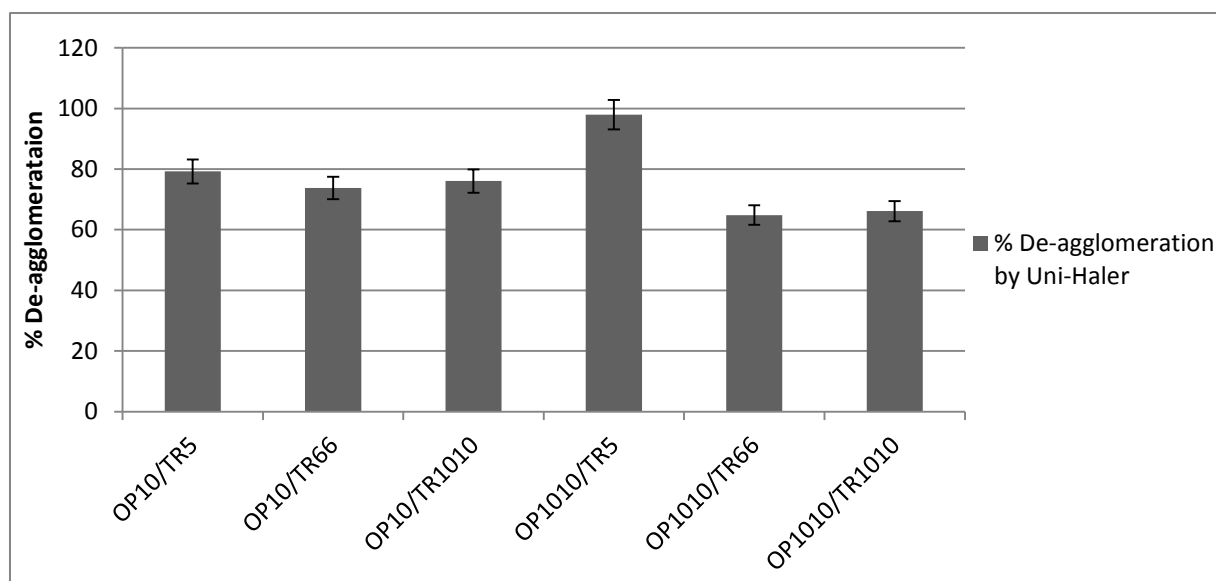


Figure 3-10: Average percent de-agglomeration of all OP blends prepared at airflow 57L/min using the UNI-Haler (n=3).

3.2.4.2 Cascade impaction

For all six DPI formulations with high drug load (75%) of $15\text{mg} \pm 0.1\text{ mg}$ filled capsules, the aerosolization performance at 4 kPa pressure drop was observed with excellent results ($\geq 60\%$ FPF) as shown in Figure 3-11. It was observed that formulations with OP1010 showed slightly higher FPF% than their counter using the less fine OP10. (OP1010/TR5) and (OP1010/TR1010) gave similar highest FPF values of 66% and 67% respectively.

On the other hand, only the fine drug binding larger carrier in (OP1010/TR5) gave most reproducible results with FPD of 8.2mg as shown in Figure 3-12. While the interaction of the fine drug with a similar sized carrier gave slightly higher FPF% and similar FPD of 8.2mg, it also showed higher capsule retention and larger MMAD as shown in Figure 3-13. The formulation (OP1010/TR5) using trehalose as an inert carrier with a particle size range 4-5 times larger than the fine OP; gave the most reproducible FPF% and FPD values with lowest MMAD of $1.4\mu\text{m}$.

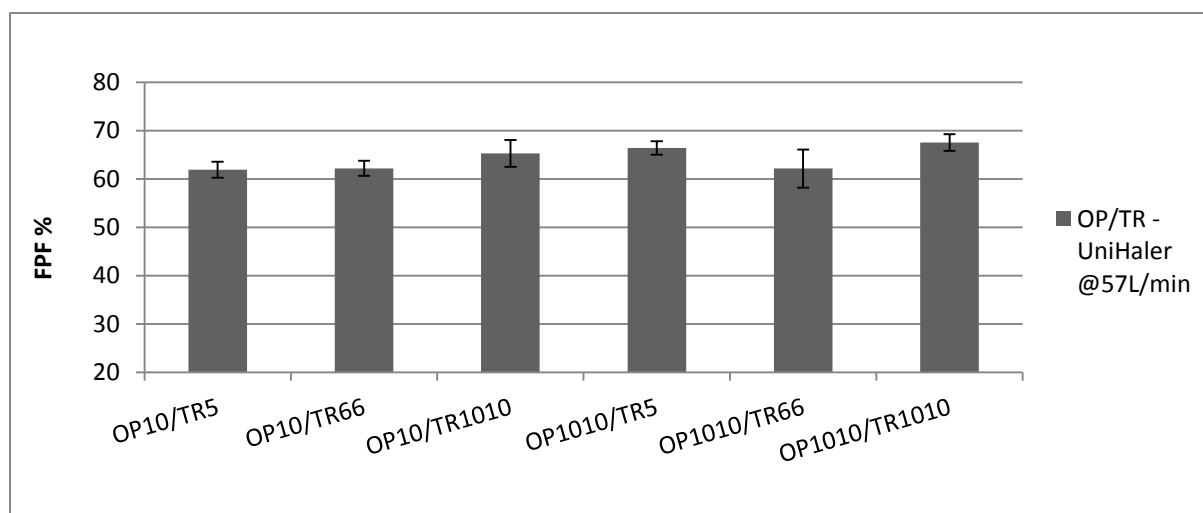


Figure 3-11: Average FPF% \pm SD of aerosolized OP/TR formulations using UNI-Haler @ 57L/min (n=3).

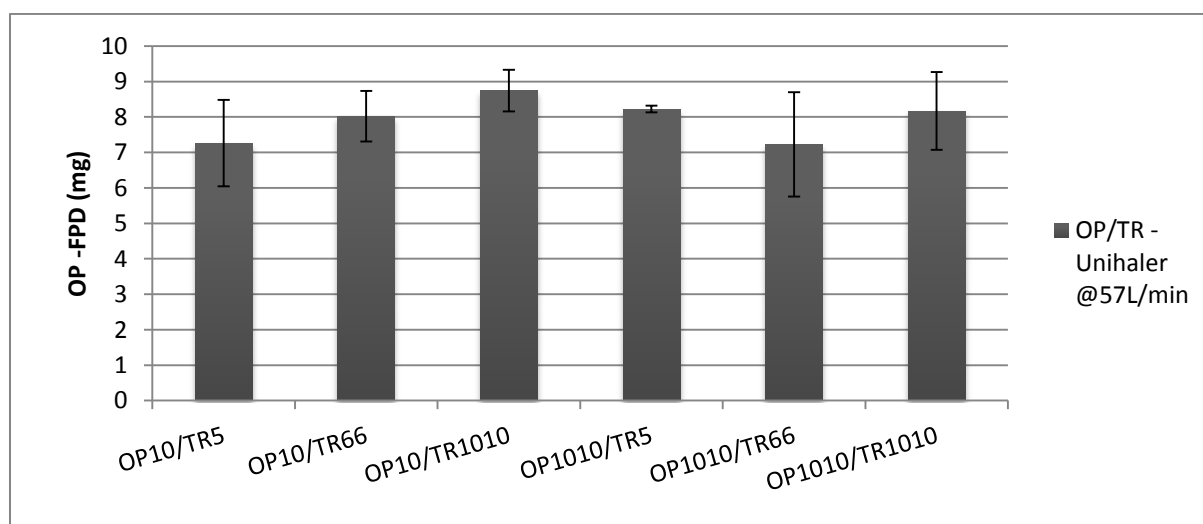


Figure 3-12: Average FPD \pm SD (mg) of aerosolized OP/TR formulations using UNI-Haler @ 57L/min (n=3).

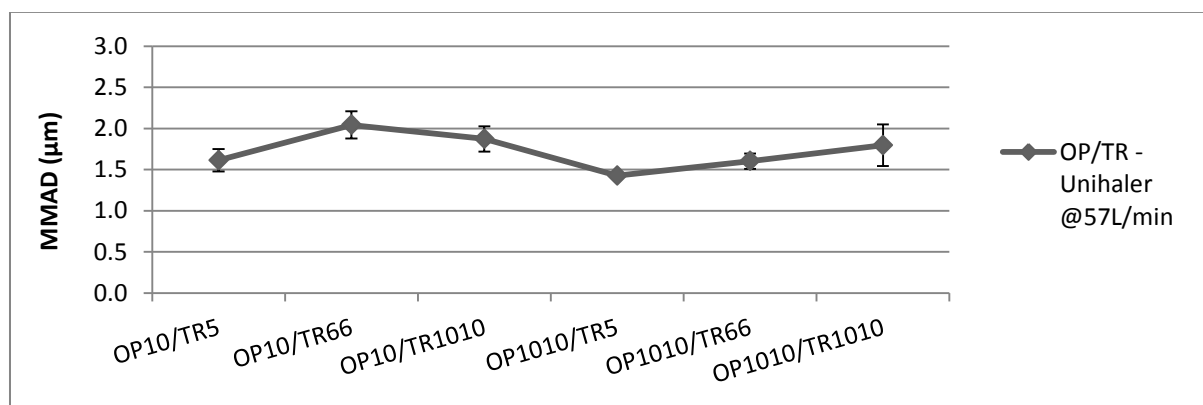


Figure 3-13: Average MMAD \pm SD (μm) of aerosolized OP/TR formulations using UNI-Haler @ 57L/min (n=3).

Analysis of the aerosolization performance of the OP/TR formulations at higher flow rate was done with the low resistance inhaler Aerolizer[®]. Four blends were chosen to be tested that included either finest trehalose carrier or finest OP. As shown in Figure 3-14, again all blends showed excellent dispersion with FPF $\geq 60\%$. Aerosolization at 100L/min showed a different trend from that at 57L/min, where we can say that; the finest the total particles, the higher the FPF%. OP1010/TR1010 showed highest and reproducible FPF of 75%. Compared to the lower flow rate of 57L/min, the FPF has increased for all tested blends by 2-10% with better reproducibility and higher FPD values as shown in Figure 3-15. On the other hand, the MMAD values shown in Figure 3-16 were similar to previously aerosolized at 57L/min, with lowest value for (OP1010/TR5) of 1.4 μm . In general, the smaller the MMAD the more effective de-agglomeration has occurred, releasing OP closer to its average particle size distribution. Nevertheless, all the tested formulations showed similar effective de-agglomeration process as read MMAD $\leq 2 \mu\text{m}$ under both high and medium flow rate. This further proves the consistent efficiency of the prepared formulations in aerosol generation under different airflows.

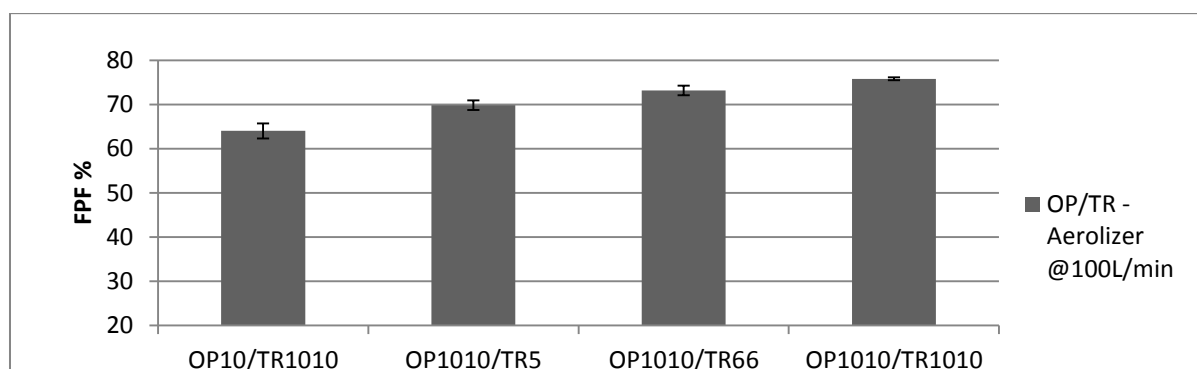


Figure 3-14: Average FPF% \pm SD of aerosolized OP/TR formulations using Aerolizer @ 100L/min (n=3).

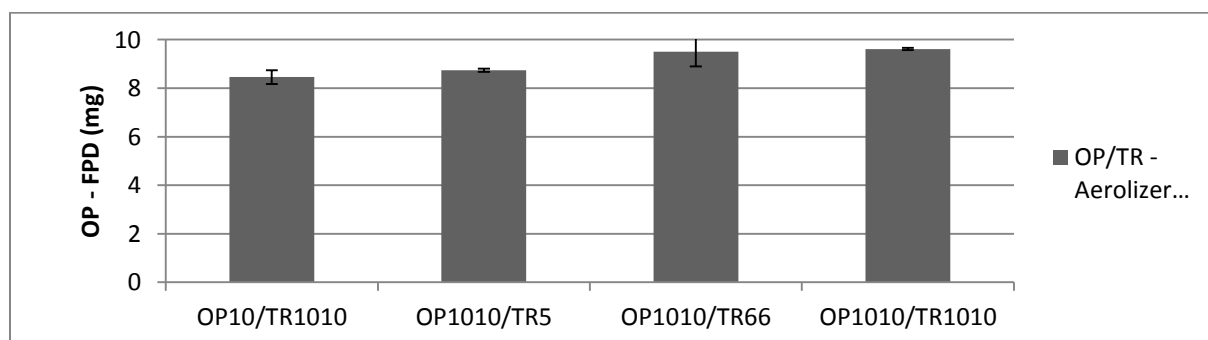


Figure 3-15: Average FPD \pm SD (mg) of aerosolized OP/TR formulations using Aerolizer @ 100L/min (n=3).

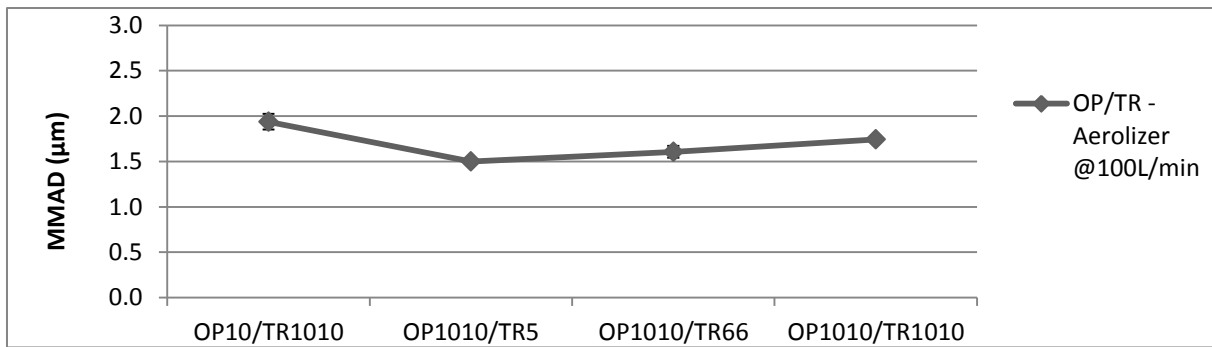


Figure 3-16: Average MMAD \pm SD (μm) of aerosolized OP/TR formulations using Aerolizer @ 100L/min (n=3).

Figure 3-17 and Figure 3-18 show OP1010 particle deposition profiles from TR5 carrier on each NGI stage at air flow = 57 L/min and 100 L/min respectively. As indicated in the 57 L/min profile using the Unihaler, the finest jet milled OP1010 exhibited low particle deposition on stage 1 (cutoff diameter point of 8.06 μm) and high particle deposition on stages number 4–6 reaching its maximum of about 2.7mg on stage number 5 (cutoff point of 0.94 μm). However, compared with the 100 L/min profile using the Aerolizer, the particles exhibited slightly higher particle deposition on stage 1 and high particle deposition on stages number 3–5 reaching its maximum of about 2.4mg on stage number 4 (cutoff point of 1.66 μm). Although, the particles were deposited deeper at 57 L/min relative to the deposition profile at 100L/min, yet the inhaler entrapment for particles was higher about 7.5% from the total dose.

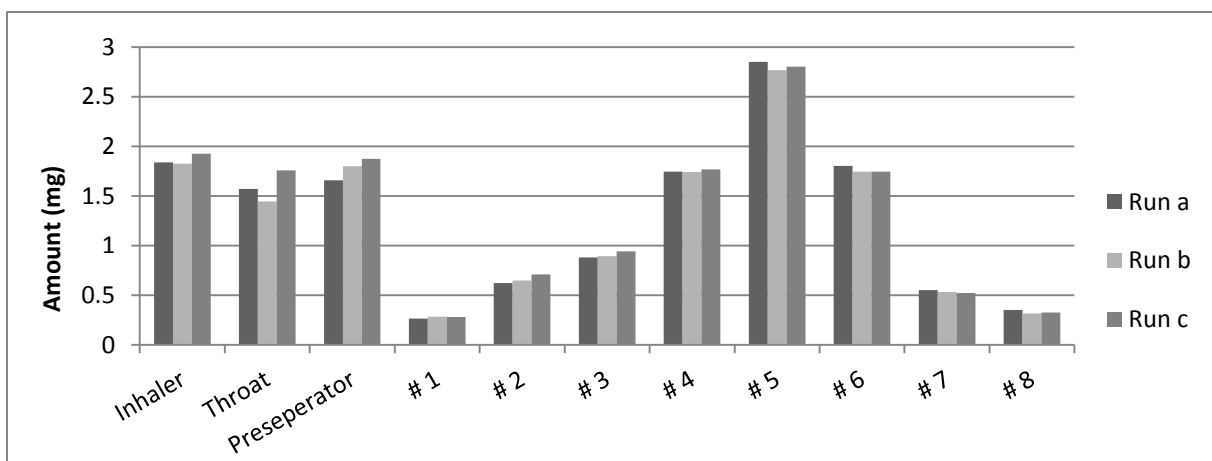


Figure 3-17: OP1010/TR5 - Stage distribution by Unihaler @ 57L/min (n=3)

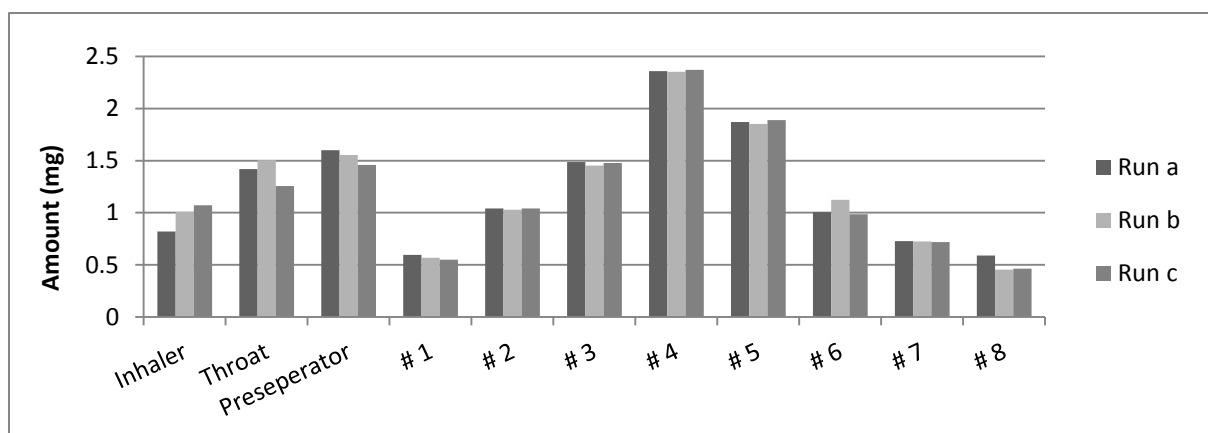
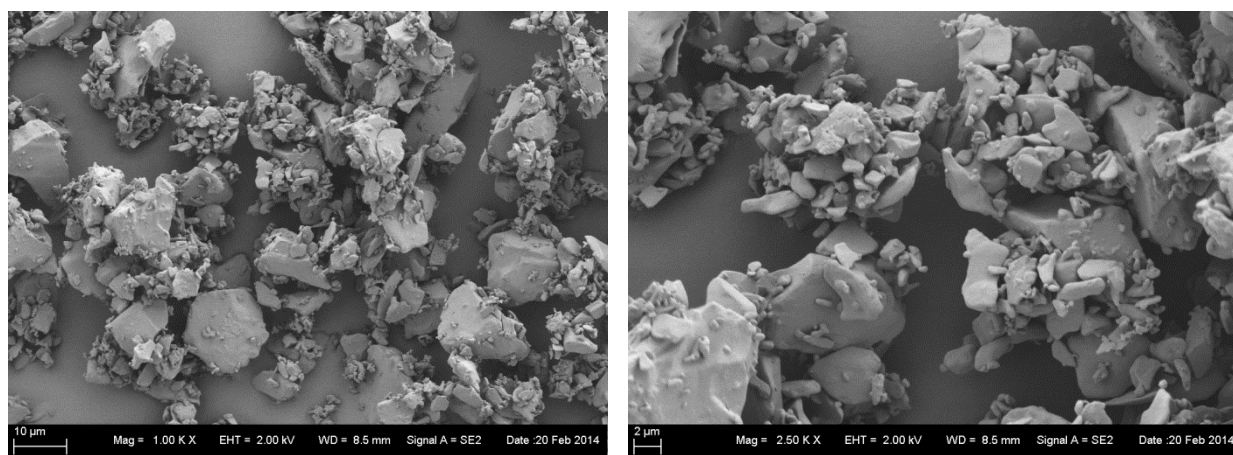


Figure 3-18: OP1010/TR5 - Stage distribution by Aerolizer @ 100L/min (n=3)

3.2.5 Scanning electron microscopy

Trehalose particle morphology of largest (TR-5) and smallest (TR-1010) PSD were presented by SEM images under different magnification powers as listed in Figure 3-19. Both qualities were captured in pure and blend formulations with OP1010. As observed jet milled trehalose qualities were of irregular shape while the OP1010 gave rod shaped morphology. When the relatively cohesive OP1010 particles are blended with TR-5, the rod shaped particles are totally covering and rounding larger particles of trehalose in a separate agglomerated pattern. However, when the OP1010 rod particles are in formulation with the fine TR1010, a more one phase agglomerated rods with the irregular trehalose particles imbedded within are observed.

Jet milled Trehalose: TR5



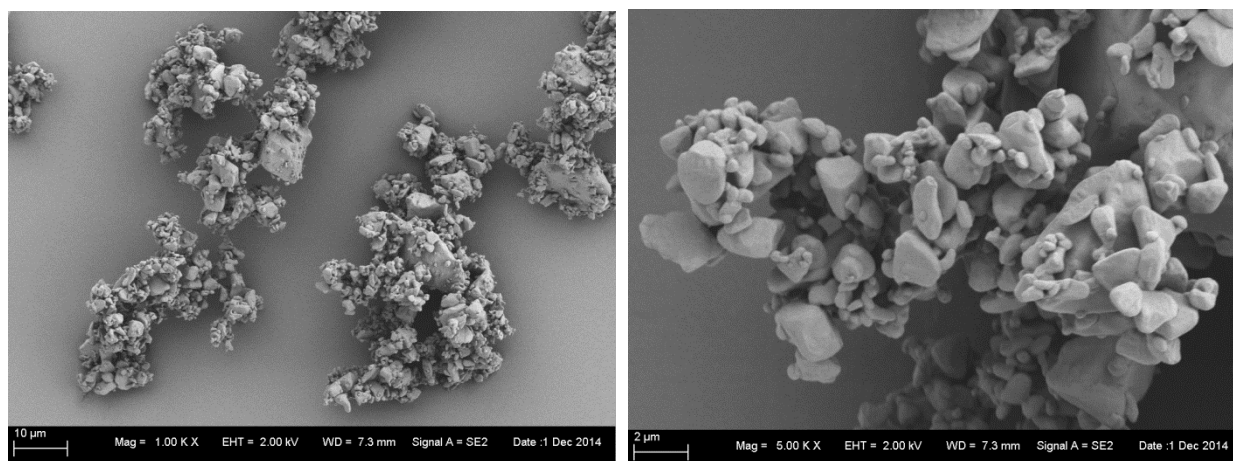
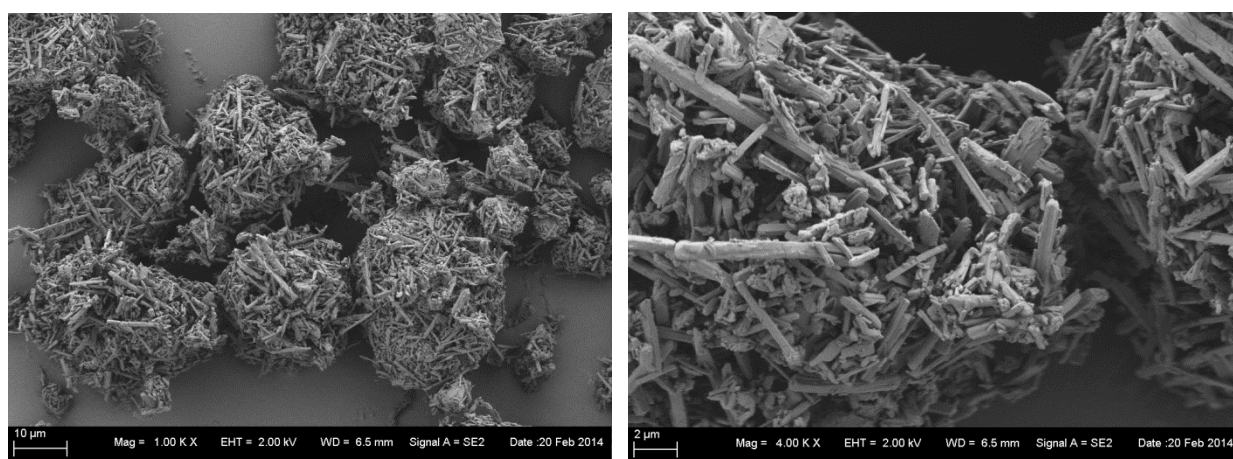
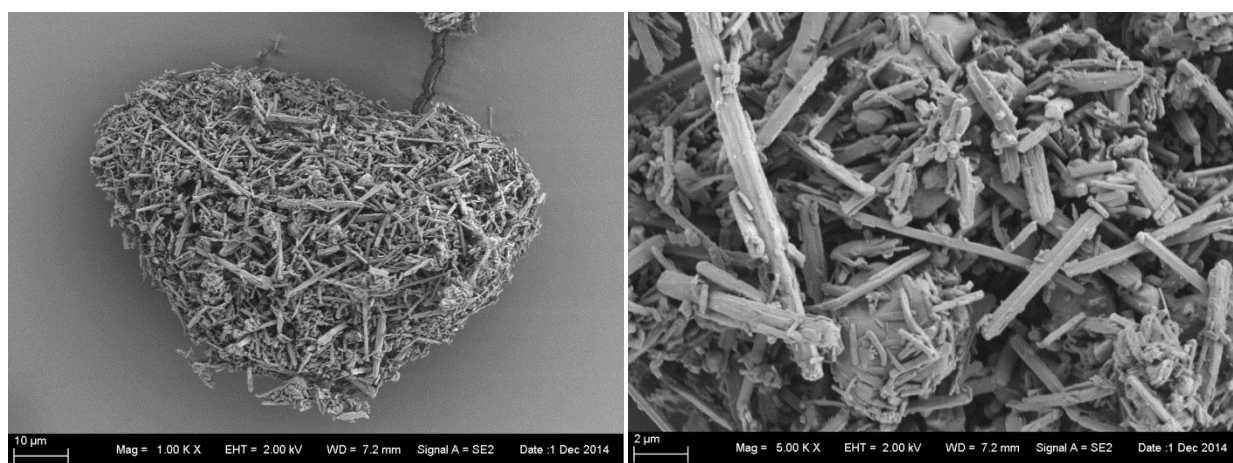
Jet milled Trehalose: TR1010**Blend: OP1010 / TR5****Blend :OP1010 / TR1010**

Figure 3-19: SEM images of jet milled trehalose qualities (TR5 and TR1010) and in OP1010 blends under magnification power 1KX (left) and 5KX (right).

3.3 Discussion

This study chapter clearly demonstrated that trehalose micro-particulates produced by jet milling were successfully able to aerosolize oseltamivir phosphate with excellent results. Different batches were produced by jet milling based on the particle size distribution of both trehalose carrier and OP particles. Focusing on the physicochemical analysis, there was no significant change observed in crystalline structure, water sorption or thermo-gravimetric behaviors that would dramatically alter the aerosolization behavior. On the other hand, the larger the particle size the less the specific surface area lowering the fluidization energy required for easier flowability. Furthermore, where TR10 behaved similarly to TR66, no significant differences observed in terms of the physical characteristics of particles with similar size distribution produced by jet milling but at different number of runs under different grinding pressure.

The crystalline irregular particles of trehalose with a fine size range were able to give optimum physicochemical interaction in the binary formulations with OP finest particles under the studied conditions for the drug to be aerosolized efficiently. The studied trehalose particles (TR-5) and (TR-1010), was able to disperse and aerosolize OP1010 with the highest recorded FPF% under both high and medium flow rates. On the other hand, trehalose grade with widest particles size span (TR-5) showed more consistent and highest performance at the medium flow rate. While at the high flow rate, TR-1010 with the smallest PSD and span value showed the most reproducible highest performance. This can mean that, fine trehalose carrier micro-particulates in binary formulations of high drug load may perform best with low resistant inhalers yet they de-agglomerate formulations' drug particles with similar effectiveness under medium resistance.

Particle surface properties have an influential role in the performance variation between different produced batches. In general, jet milling lead to surface heterogeneity of particles implying a non-homogenous energy distribution and morphology. Two strategies regarding the de-agglomeration behavior of the particles can be concluded from the results of this study. First, active sites with high energy have higher preference to bind strongly with the API small particles than the surface sites with lower energy. Accordingly for the high OP dose formulation evaluated, the few high energy active sites of the fine trehalose particles would be saturated easily

and the majority of the OP particles are binding relatively loose to the less energetic surface sites leading to lower adhesion and easier de-agglomeration. Secondly, irregular shaped particles or rough particles with asperities may lead to strong binding between particles by mechanical interlocking or it may limit the closeness of two particles and reduce the Van der Waals forces. It can be assumed that the irregular shaped fine particles of the trehalose reduced both the mechanical interlocking and the Van der Waals forces by being placed into the higher ratio of the fine rod shaped OP particles. This would be achieved by introducing air space in between the particles that facilitate the de-agglomeration process upon aerosolization.

4. Chapter Two

Trehalose particle engineering by spray drying

4.1 Introduction

As discussed earlier in DPI formulations, reduced inter-particulate interactions can lead to better aerosolization and dispersion. For that reason, spray dried particles with spherical morphology, narrow micron size range distribution and relatively smooth surface might reduce mechanical interlocking, van der Waals, and electrostatic forces. Spray drying is an established technique that is well described and studied in optimizing particle physical properties by plentiful literature. In pharmaceutical industry, the versatile input factors of the method enabled the production of engineered dry particles suitable for parenteral, nasal, and pulmonary delivery (Vehring et al., 2007; Vicente et al., 2013). In general spray drying techniques are composed of three sequential steps; atomization, droplet drying and particle collection. As represented in schematic diagram Figure 4-1, initially, the target particles are in solution or suspension pumped through feeding nozzle to be dispersed via flow of carrier gas as droplets in the drying chamber. The droplet size formed is the limiting factor for the particles size to be produced. Then the dispersed droplets undergo evaporation and solute condensation depending on the drying temperature and time. Afterwards, the dry particles are collected by a cyclone (Nandiyanto and Okuyama, 2011; Yang et al., 2014). Spray drying parameters such as solids concentration, solvent type, feeding rate, inlet/outlet temperatures, and flow rate can be optimized to target a specific physical property of the produced particles (Li et al., 2014; Vicente et al., 2013).

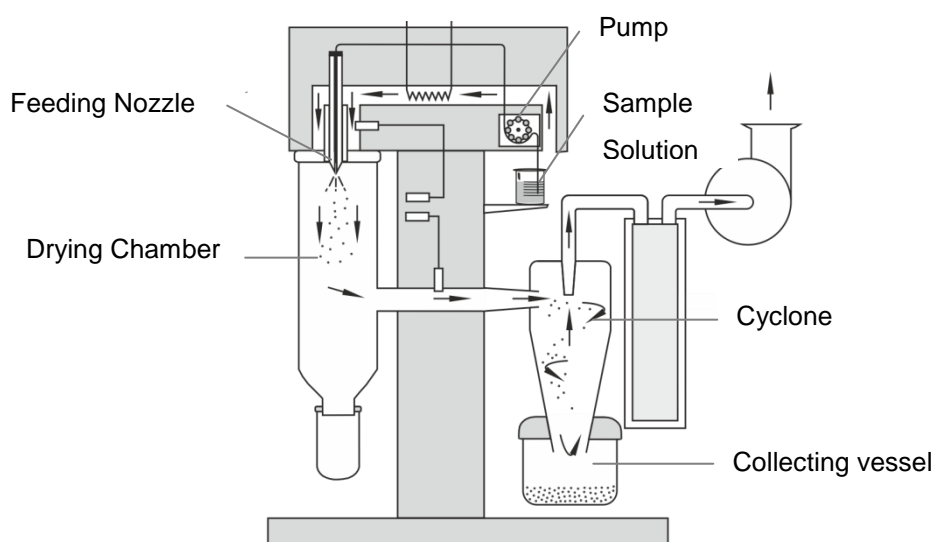


Figure 4-1: Spray drying process schematic diagram

Inhalable trehalose microparticles have been previously produced and examined under different parameters, but mainly to reach a potential stabilizing excipient with bio therapeutic drugs as proteins and peptides. These studies mainly targeted spray dried amorphous microparticulate trehalose via dilute organic solutions (Li and Mansour, 2011; Ogáin et al., 2011).

The purpose of this chapter is the production of smooth spherical trehalose particles by spray drying via aqueous solution with relatively large particle sizes and the study of their thermal and crystalline characteristics. The study design considered trehalose particles that would be suitable as a DPI formulation carrier, where the produced size would be in a similar range as the jet milled quality that showed successful aerosolization behavior in the previous study chapter for later comparison.

Based on a design of experiment, four spray drying parameters were tested in controlling particle size and yield; feed concentration, inlet temperature (T_{in}), pump rate, and gas flow. The produced particles were then dispersed under 3bar with Rodos module for PSD analysis by laser diffraction. Afterwards, X-ray powder diffraction revealed the absence of crystallinity of trehalose particles after spray drying and vapor sorption behavior of the particles was tested under different cycles of RH% by DVS. Consequently, recrystallization trial of a spray dried amorphous trehalose sample was done at 55% RH to target spherical crystalline particles. Moreover, thermal behavior and detection of glass transition of the amorphous particles were examined by modulated-DSC. Lastly in this chapter, particle morphology and surface were imaged and examined by scanning electron microscopy.

4.2 Results

4.2.1 Spray dried Produced trehalose

First experimental design, took into consideration four factors each with 3 levels; Feed concentration (10, 25 and 40%w/v), T-inlet (75, 85 and 95°C), Pump rate (10, 15, and 20%) and Gas flow (30, 40 and 50mm). However due to environmental conditions of high relative humidity (80-90%), some runs with low T_{in} , high pump rate and their interaction, lead to insufficient drying process (sticky product) and yield of less than 10%. Accordingly, such products were not possible to analyze their PSD and the design calculation was incomplete. In a second experimental design trial, T_{in} was set at 95°C and the pump rate was set at 10%. It was observed that feed concentration and gas flow were the most significant parameters affecting the particle size and both tested over 3 levels as previous without affecting the drying efficiency. From the graphical presentation in (Figure 4-2) and statistical calculation, the particle size of the spray dried trehalose was significantly affected by gas flow, feed concentration, and their interaction. The summary statistics presented, shows two parameters; the model fit (R^2) and the future prediction precision (Q^2). Both parameters were near perfect model value of 1 with difference between them of less than 20%. In general, increasing the feed concentration, results in more solid in the dispersed droplets leading to larger particles. While, increasing the gas flow, results in more dispersed smaller droplets leading to smaller particle upon drying.

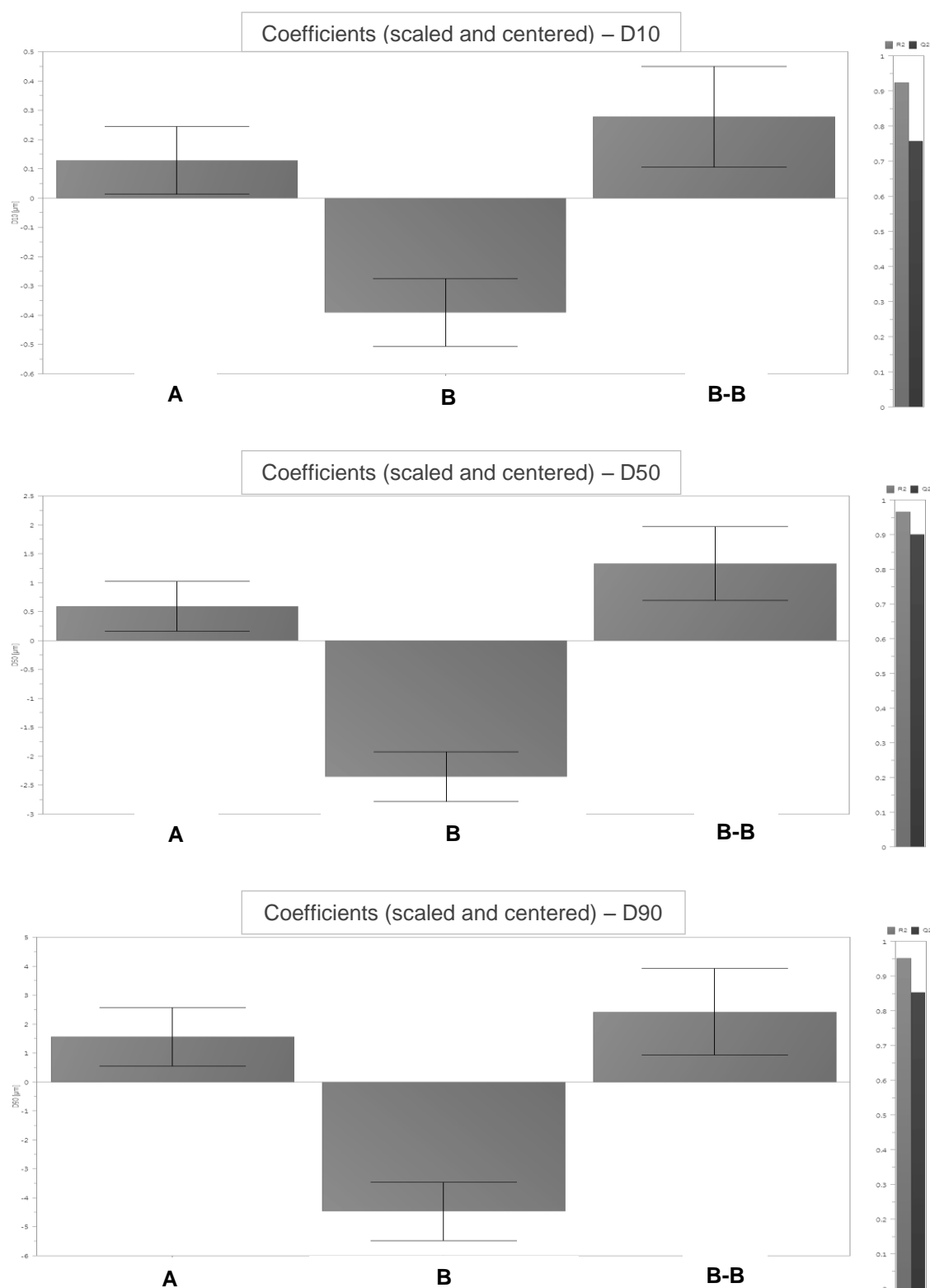


Figure 4-2: DOE graphs presenting coefficients significantly affecting SD trehalose PSD outcome of D10, D50 and D90 with excellent model fit and precision ($R^2 > 0.9$ & $Q^2 \geq 0.75$); on the X-axis (A) Concentration, (B) Gas flow and (B-B) Gas flow – Gas flow interaction, while the Y-axis shows the change in μm .

For further physicochemical analysis, three batches were chosen based on particle size distribution as shown in Table 4-1.

Table 4-1: Spray dried three trehalose batches of relatively small, medium and large PSD

Sample Name	Feed Conc. %(w/v)	T-inlet (°C)	Pump rate (%)	Gas flow (mm)	PSD (µm)			
					d10	d50	d90	Span value
L-4913	40	95	10	30	1.78	9.05	19.64	1.97
M-2914	25	95	10	40	0.80	4.11	9.47	2.1
S-1915	10	95	10	50	0.62	2.25	5.57	2.2

4.2.2 X-ray powder diffraction

Under spray drying conditions for the three chosen batches, it was confirmed as seen by the XRPD pattern (Figure 4-3), that trehalose lost its crystalline structure. Initially, trehalose dihydrate gave its default intense sharp peaks as seen previously in chapter one. The drying process was sufficient to remove water molecules in solution droplets before the formation of any crystal lattice leaving solid dry amorphous trehalose particles in all three batches.

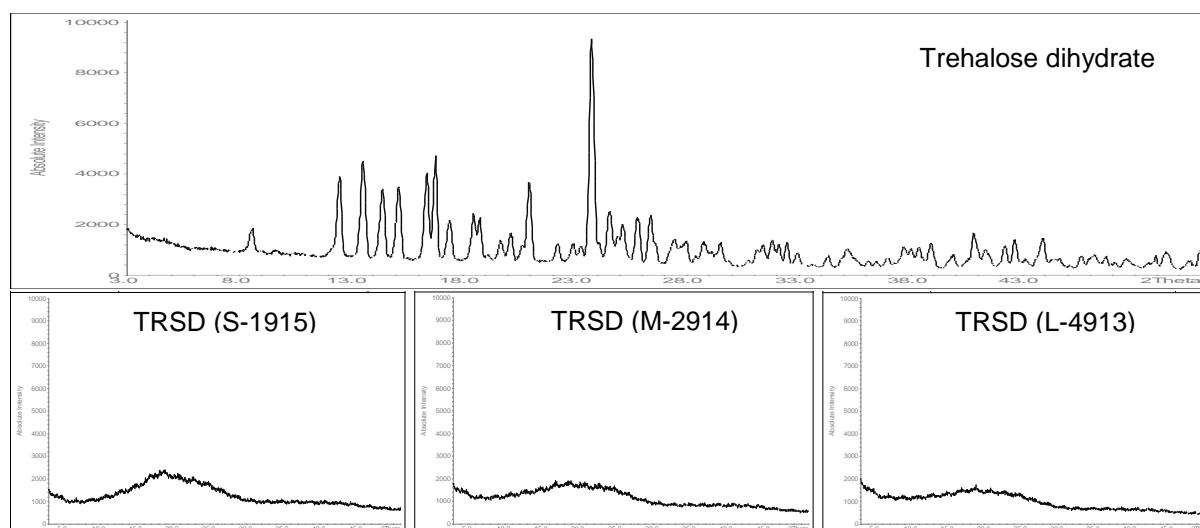


Figure 4-3: XRPD spectra of SD trehalose and raw trehalose dihydrate.

4.2.3 Dynamic Vapor Sorption

The vapor sorption profile in Figure 4-4 illustrates the capacity of the amorphous trehalose particles to water molecules in a cycle up to 70% RH. Raw trehalose dihydrate particles can only adsorb water molecules of less than 1% from its mass. On the other hand spray drying producing amorphous trehalose particles, lead to increased water adsorption capacity of about 10 times at RH \geq 50%. The TR-SD particles showed constant increase in water sorption as soon as the RH is above 0% till reaching plateau at 50% RH. Comparing the water sorption profile of the three TRSD batches (small, medium and large); a slight variation is observed where the larger the particle size distribution the less water capacity.

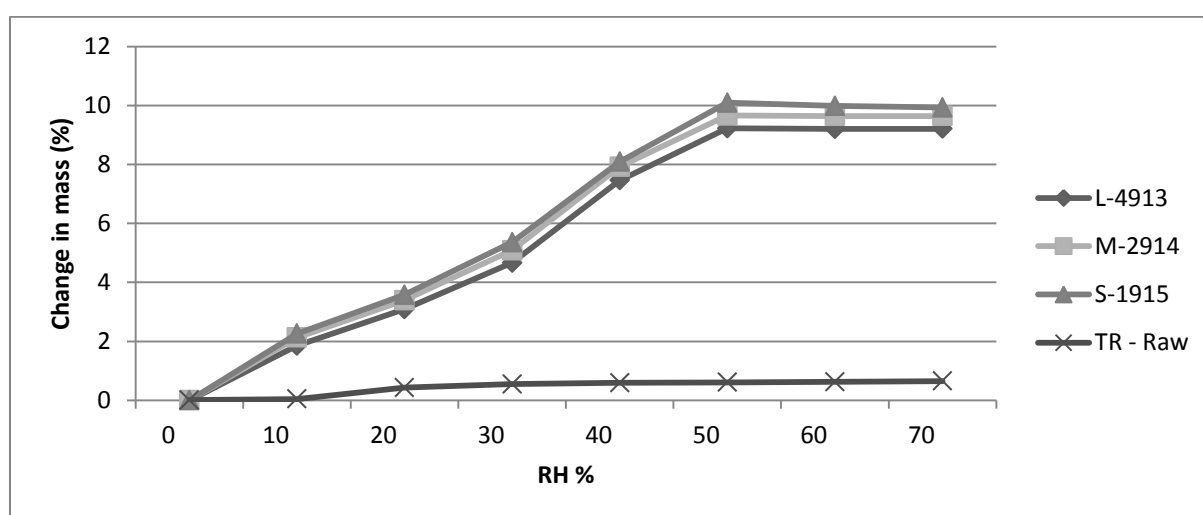
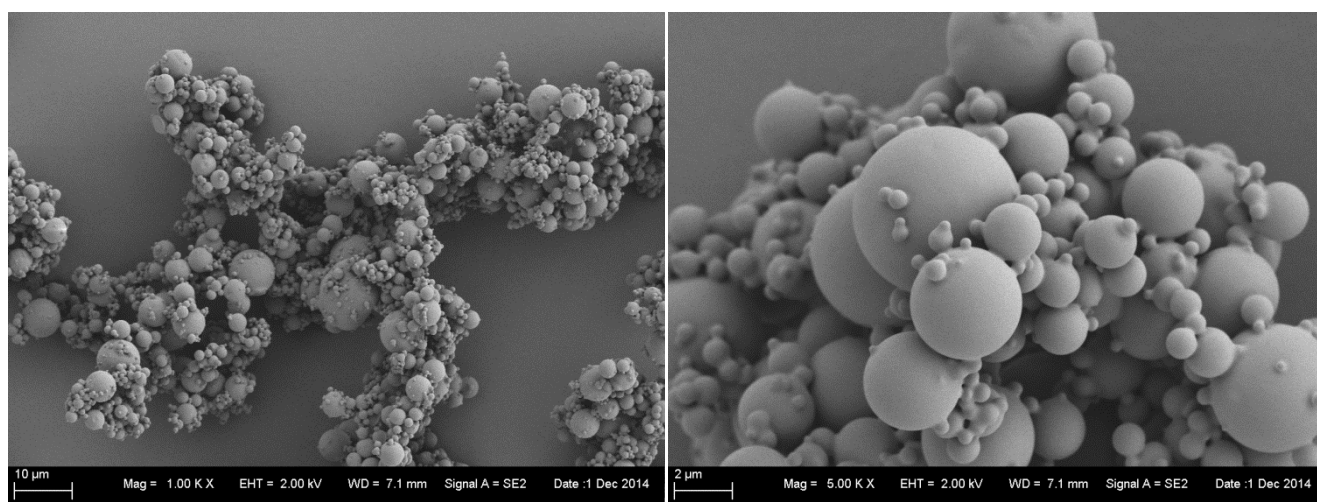


Figure 4-4: DVS profile of spray dried trehalose batches and trehalose dihydrate (TR - Raw)

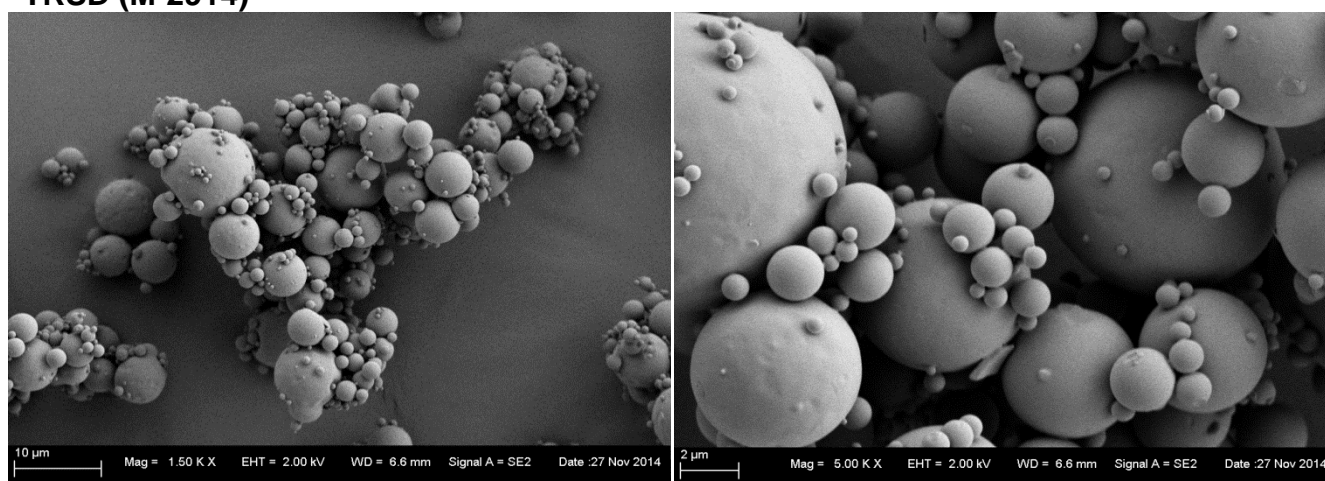
4.2.4 Scanning electron microscopy

The SEM images of all three spray dried trehalose batches are displayed in Figure 4-5. The magnification power showing the smallest particle sized batch (S-1915) was 1K X and 5K X, the medium particle sized batch (M-2914) was shown under 1.5K X and 5K X, while the large particle sized batch was shown under 1KX and 2.5K X. It was clearly obvious the successful production of smooth spherical particles for all batches. However, larger particles tend to have a less smooth surface as seen specifically in L-4913 sample.

TRSD (S-1915)



TRSD (M-2914)



TRSD (L-4913)

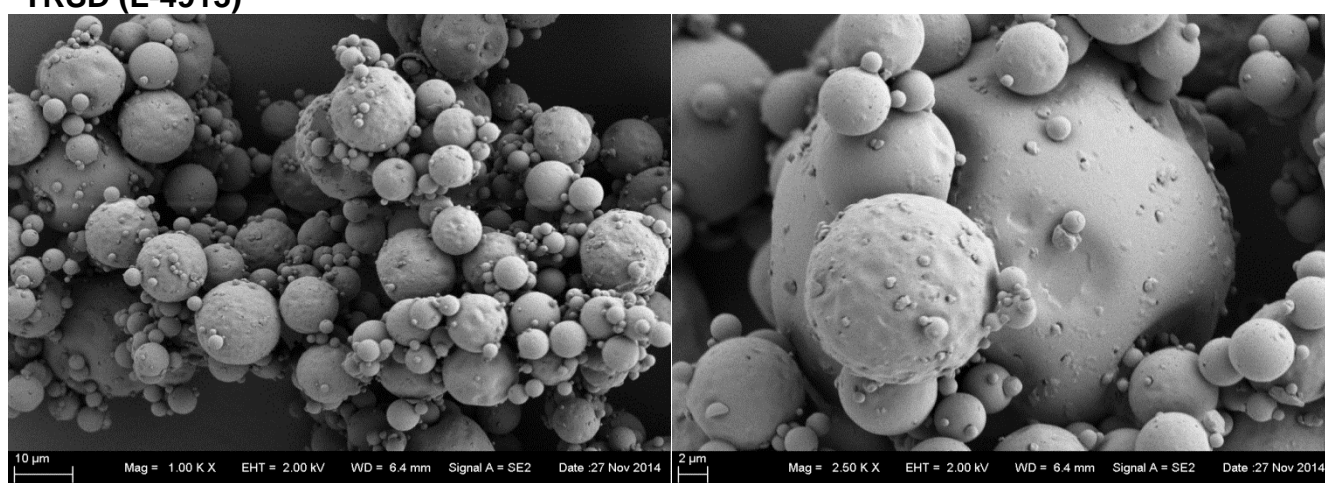


Figure 4-5: SEM images of spray dried trehalose (TRSD) batches.

4.2.5 Recrystallization of spray dried trehalose

In target of crystalline spherical trehalose particles, recrystallization of amorphous spherical spray dried trehalose trial was conducted. TRSD (M-2914) was conditioned in room temperature at 50% RH for 24hrs. Particle size distribution and modulated differential scanning calorimetric measurements were recorded every 2hr interval as illustrated in Table 4-2. The initial produced powder of trehalose particles by spray drying, as seen in Figure 4-6, showed amorphous glassy to rubbery phase transition (T_g) at around 59.7°C with no observation for the endothermic transition events (dehydration & melting) normal to trehalose dihydrate.

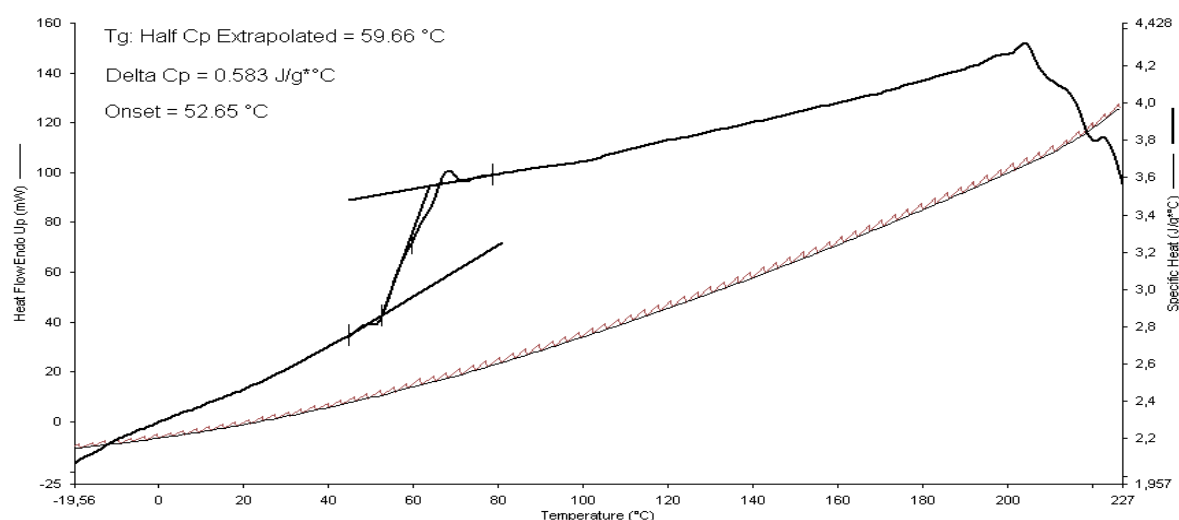


Figure 4-6: mDSC thermogram of TRSD (M-2914)

Conditioning the TRSD sample in 50% RH for 6hrs, was enough for the particles to adsorb water molecules restoring some crystallinity and preserving its powder form. Observing Table 4-2, with time during the 6hrs, the particles tend to increase in size and have a reduced T_g that reached 18°C. Furthermore, after 6hrs the appearances of endothermic peaks (dehydration and melting) are observed with weak intensity along with lowest T_g recorded as seen in Figure 4-7. Conditioning at 50% RH for more than 6hrs, lead to the formation of sticky stone like product. Accordingly, particle size distribution was not possible to be measured for samples more the 6hrs, while the DSC results showed similar endothermic peaks (dehydration and melting) as the raw trehalose dihydrate and no T_g was detected.

Table 4-2: Particle size distribution, glass transition onset and dehydration peak recorded at different time intervals for TRSD (M-2914) conditioned at 50%RH

Time (hr.)	Particle Size Distribution (μm)				Glass transition onset (T_g) $^{\circ}\text{C}$	Dehydration Peak (T_E) $^{\circ}\text{C}$
	D10	D50	D90	Span Value		
0	0.81	4.11	9.85	2.2	52.7	_____
2	0.84	4.26	10.14	2.18	38.8	_____
4	1.05	4.96	10.99	2.0	25.7	_____
6	1.52	5.91	11.97	1.77	18.2	101
8	_____				_____	92
24	_____				_____	90

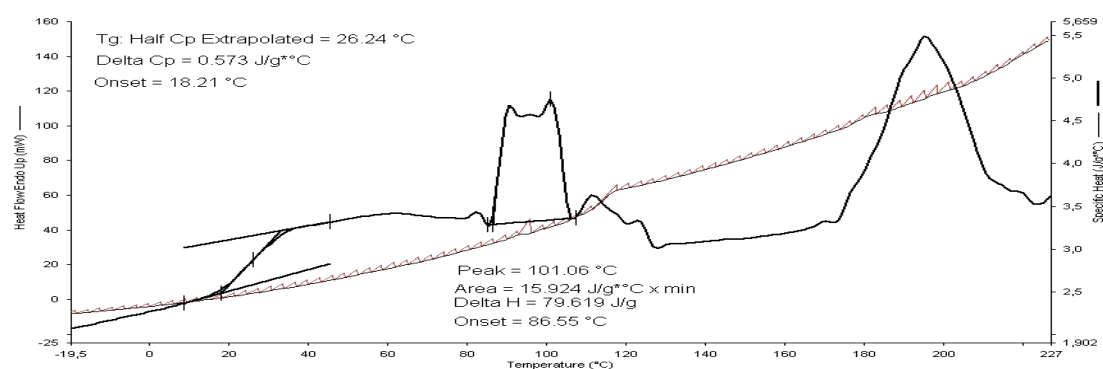


Figure 4-7: mDSC thermogram of TRSD (M-2914) conditioned at 50%RH for 6hrs.

Partially crystalline spray dried trehalose particles imaged by SEM, showed intact smooth spheres similar to the previously examined amorphous TRSD (2914). As observed in Figure 4-8, the particles are smooth and spherical but formed bridge like formation in between may be due to capillary bridges by water interface. The fused spherical particles still preserved suitable size distribution that is slightly larger compared to the spray dried batch.

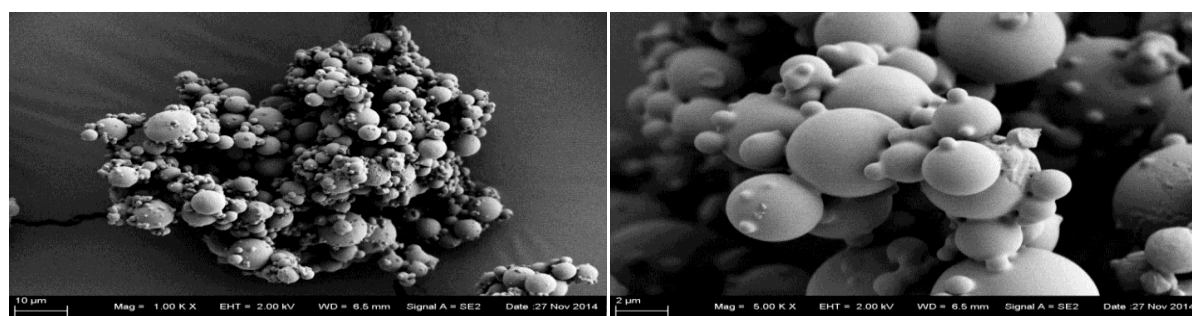


Figure 4-8: SEM images of recrystallized-TRSD conditioned at 50%RH for 6hrs (REC.M-2914).

4.3 Discussion

As presented in this study chapter, trehalose micro-particulates can be successfully produced by spray drying. Operating simple spray-drying technique with varying concentrations of aqueous solvent solution at different gas flows; the micro-particulates were successfully produced with smooth spherical morphology, amorphous and relatively large particle size up to $20\mu\text{m}$ with narrow size distribution (span value range of 1-2). Furthermore, amorphous particles with lowest possible water content would decrease the capillary forces between particles leading to better de-agglomeration performance. Nevertheless, crystalline particles would possess more stability especially towards water moisture adsorption and degradation in high relative humidity. In remark to that, Relative Humidity is an indispensable factor that significantly affects the production process of particles by spray drying as well as the physical stability that can affect the results of the thermal and crystallinity measurements. As it was mentioned earlier, high relative humidity has limited the possibilities for the production of the target particles in a dry powder form. Certainly, the water content in the dispersed solution particles in the drying chamber evaporates more efficiently in a relatively dry air flow rather than saturated with moist. On the other hand, trehalose has different physical phases that have been studied in many literatures to elucidate the biological protective function against dehydration stress. They have also shown the transformation from one phase to another under thermal, dehydration and rehydration processes were humidity played an essential role between these transitions.

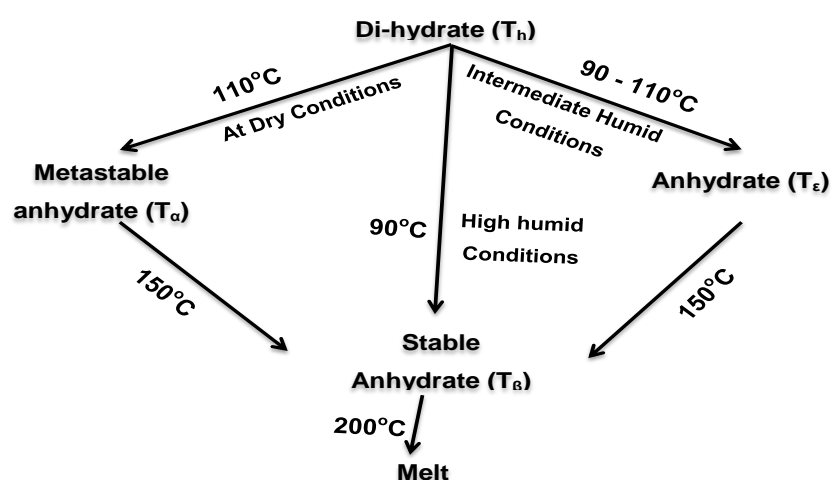


Figure 4-9: Trehalose phase and state transition under thermal and humidity conditions (adapted from Furuki et al., 2005)

As illustrated in Figure 4-9, four different crystalline forms have been recognized and demonstrated showing the transition states under different conditions. In accordance to (Furuki et al., 2005), the findings from chapter one and two demonstrate that the transition observed by DSC occurred through the intermediate humidity route that gave the anhydrate (T_g) at about 90°C. Indeed the amorphous spray dried trehalose particles, showed quick rehydration behavior over 8hrs reaching the dihydrate crystal at 50% RH in room temperature. This fast rehydration process can also be explained by the small particle size that has high surface to volume ratio accepting water molecules easier. Yet again at intermediate humidity of the room conditions, thermal behavior of the partially recrystallized trehalose particles showed similar behavior with (T_g) observed at about 90°C. The partially crystallized rehydrated particles behaved as a mixture of crystalline dihydrate and amorphous particles where glass transition was spotted at a very low temperature of 18 °C by mDSC, hydration and phase transitions peaks were observed by DSC and the XRPD patterns showed XRPD pattern with lower intensity than the fully crystalline particles.

In conclusion of this chapter, the production of smooth spherical SD trehalose particles was successful in the desired particle size range. The particles produced were amorphous particles which can be considered as an inferior option in terms of physical DPI carrier stability compared to the crystalline particles of trehalose. In trial to produce more stable crystalline particles, only partial recrystallization of the smooth spherical SD trehalose particles was achieved, maintaining the produced morphology and size range. Full crystallization of spherical smooth particles could not be achieved due to the formation of sticky stones like structures instead of the required flowing powder particles under further exposure to the crystallization conditions. However, the produced trehalose particles either amorphous or partially crystalline might have the potential as an inert carrier to effectively aerosolize DPI formulations. Indeed, spray dried trehalose was previously observed for its protective activity as a carrier for potent bio-macromolecules (Rahimpour et al., 2014), accordingly the produced SD trehalose particles could be of further use in such DPI formulations. Consequently in the coming chapter, the produced SD trehalose particles are to be initially tested for their performance as DPI carrier despite their physical stability drawback.

5. Chapter Three

**Aerosolization performance of SD vs.
JM Trehalose formulations**

5.1 Introduction

Each specific drug/carrier combination in formulations requires a different design of physiochemical properties to reach optimum aerosolization behavior. The idea of reaching and setting one rule that fits all is totally unrealistic. As it has been studied in numerous literatures, contradicting observations can be perceived each with argue and reason, yet they prove the idea of tailored formulations for each API.

In some studies, elongated lactose and mannitol carrier particles with higher surface area relative to more spherical particles were capable to flow deeper in the air stream due to better aerodynamics thus improving the overall aerosolization performance of salbutamol sulphate. It was also reported that increasing the surface smoothness of the carrier particles increases the aerosolization performance of the API (Kaialy et al., 2010; Larhrib et al., 2003; Young et al., 2002, Zeng et al., 2000a, 2000b). Indeed, DPI formulations with irregular carrier shapes such as elongated, needle-like, or even pollen shaped particles (Hassan and Lau, 2011) have all resulted in increased aerosolization performance of various drugs under different concentrations and flow rates. However, other studies demonstrated that spherical spray dried lactose and mannitol particles with rough surfaces (increased surface area) achieved better aerosolization performance than using irregular shaped or smooth particles with various drugs (Kawashima et al., 1998; Littringer et al., 2012). Another key factor that considerably affects the aerosolization performance is the carrier particle size which is also still to date not fully understood. In contrast to the usual carrier size (40-200 μm) used in DPI formulations, several studies have found an increase in aerosolization performance with decreasing carrier size. Lactose grade with particle size $\leq 32\mu\text{m}$ showed the best aerosolization performance of budesonide using different concentrations at 4KPa pressure drop compared to larger particles (Kaialy et al., 2012; Steckel and Müller, 1997). Furthermore, salbutamol sulphate with lactose carrier (Zeng et al., 2000a), disodium cromoglycate with lactose and dextrose monohydrate carriers (Braun et al., 1996), also proved that smaller carrier particle size lead to improved aerosolization performance. It was concluded from these results, that smaller carrier particles had less mechanical interaction with the API particles that lead to the improved de-agglomeration behavior, hence better aerosolization performance.

In summary, optimized aerosol generation can be achieved; by surface smoothing or roughing, by formatting into irregular or spherical morphology and even by reduction of the carrier particle size. It all depends on the interaction either physically or chemically between the specific ingredients particles used in the formulation and the ease of flow of those particles. From here comes the necessity of new DPI carriers with particle engineering -specifically trehalose- with the potential to diversify the use of new API in DPI formulations and enhance the aerosolization performance for the model inhaled drugs.

On the other hand, by studying the API particle properties and their effect on the aerosolization performance, it was pointed out that aerodynamic particle diameter for all APIs should be in the range of 1 – 5 μm for optimum performance. Nevertheless different API particles hold diverse surface adhesive and cohesive characteristics. Thus for each API, morphological engineering is required to control the surface interactions that would generate optimized aerosolization performance. API engineered particles by spray drying is not always spherical; they may have surface convolutions, voids, holes and asperities (Johnson, 1997) that determine the surface roughness.

Some studies on salbutamol sulphate showed better achievable aerosolization performance with coated smoother elongated surfaces (Raula et al., 2009). While in another study by (Steckel and Brandes, 2004) on salbutamol sulphate, they produced spray dried low density porous irregular shaped particles with lower surface area that showed more homogenous PSD and resulted in better aerosolization performance than the jet milled irregularly shaped drug particles. Another study formulated budesonide as porous particles with a sponge-like morphology that was tested at both high and low flow rates with excellent performance (Duddu et al., 2002). The model of having a less smooth API particle surface was further proved by (Chew, Nora Y K et al., 2005) when achieved a significant improvement in the aerosol performance of the powder as the degree of surface corrugation of spray dried particles increased.

Targeting optimum performance, API in DPI also requires particle modification regarding morphology and surface characteristics, but the particle size distribution must be limited to the range of 1 – 5 μm .

This study chapter aimed two main objectives; 1) Aerosolization performance comparison between different qualities of spray dried and jet milled trehalose particles as an inert carrier in DPI formulations. 2) The correlation of surface morphology and dispersive energy to the aerosolization performance. The study design was based on the previously produced trehalose particles by jet milling and spray drying in combination with model inhaled COPD drugs that were also produced each as two qualities by jet milling and spray drying. Budesonide and salbutamol sulphate were used as model hydrophobic and hydrophilic APIs respectively. Additionally, the aerosolization behavior of spray dried trehalose in case of hygroscopic drug was evaluated using Disodium cromoglycate as the model drug in formulations.

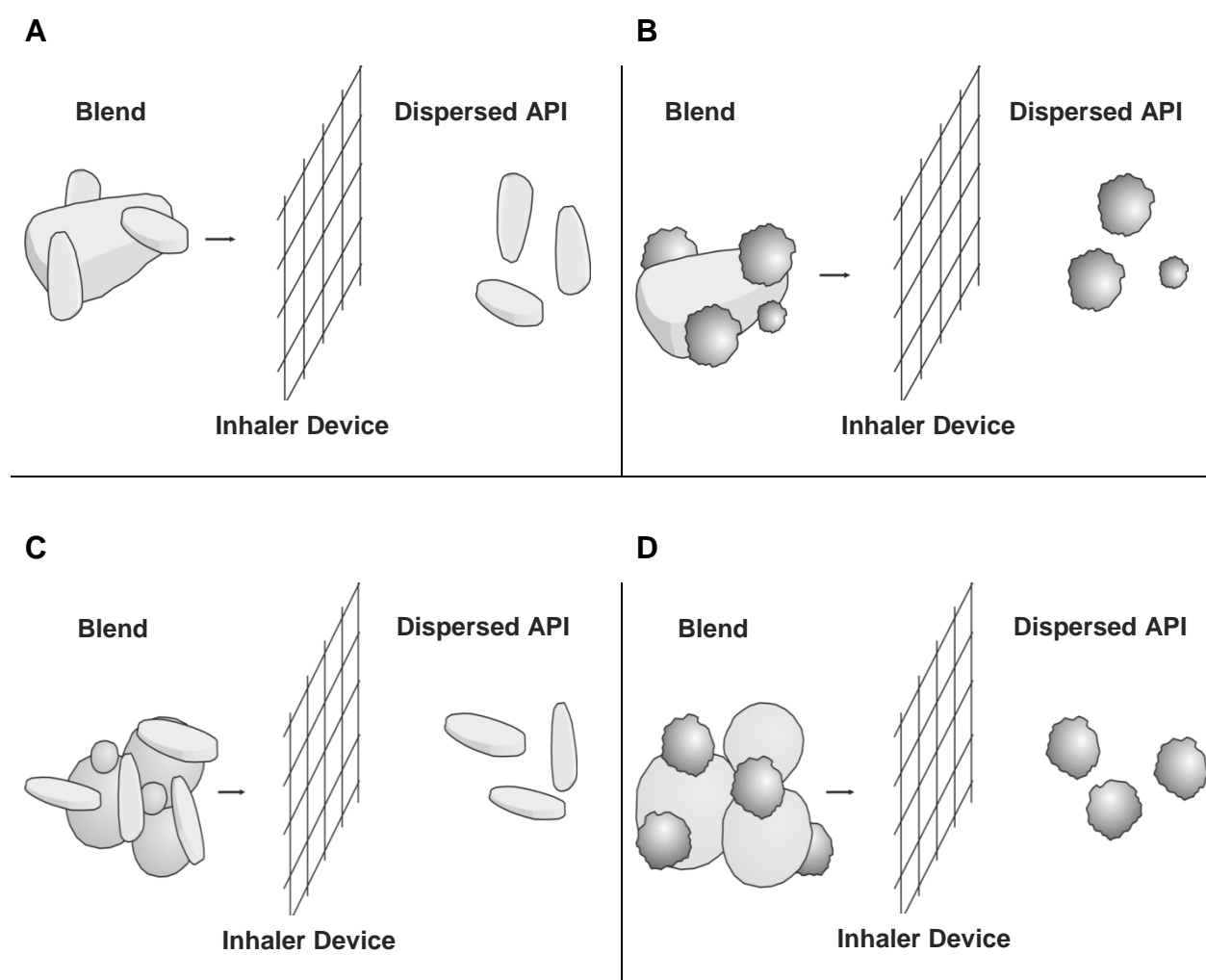


Figure 5-1: Schematic diagram of the four main binary blend categories prepared and tested for aerosolization performance; A) jet milled API / jet milled trehalose, B) spray dried API / jet milled trehalose, C) jet milled API / spray dried trehalose, D) spray dried API / spray dried trehalose

In general, the binary blends prepared were of four categories as illustrated in Figure 5-1 based on the morphology of the drug and carrier particles; either irregular by jet milling or spherical by spray drying. In addition, each category had different factors tested within, based on different produced qualities/batches from the trehalose and the different types of API used. Thus a total of 27 blends were prepared, tested for homogeneity and analyzed for aerosolization performance. All blends were analyzed by cascade impaction using capsule based Aerolizer at 100L/min and some were further tested by multi-dose Easyhaler at 50L/min to associate with the air flow effect on the aerosolization performance. The Aerolizer (Figure 5-2-A) represents the model inhaler for low resistance single dose devices. Prior to cascade impaction, the capsules were filled with 5mg powder loaded with 20% drug. Additionally, Easyhaler (Figure 5-2-B) was the model inhaler for medium resistance reservoir multi-dose devices. Its storage container was also filled with blends containing 20% API for comparable results. In attempt to correlate the aerosolization performance with particle surface energy and morphology, inverse gas chromatography was used to measure and calculate the dispersive surface energy, while SEM images showed the particle surface morphology in blends.

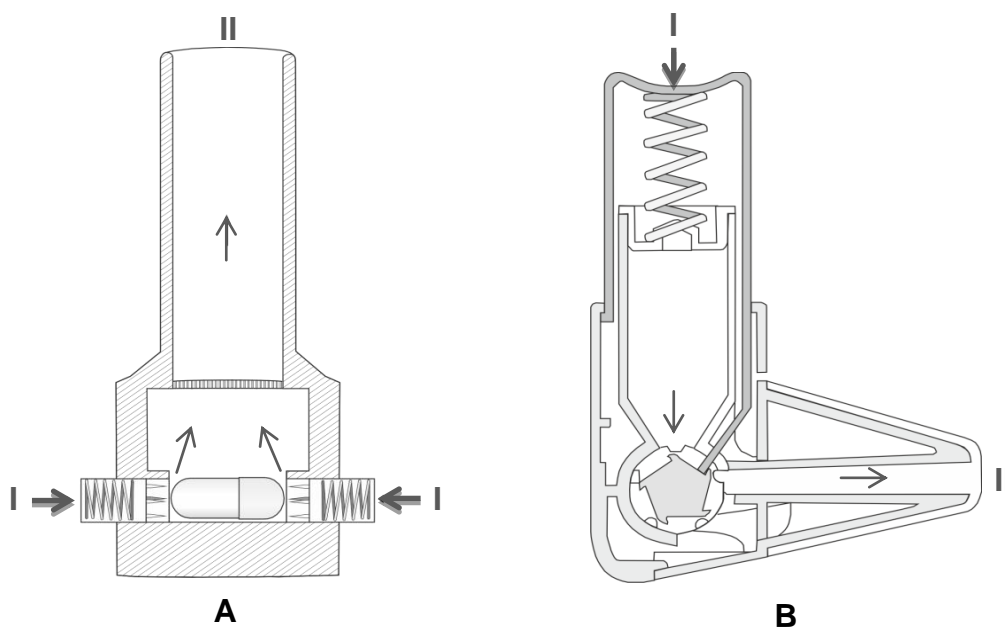


Figure 5-2: Schematic diagram of A) Aerolizer® and B) Easyhaler®, showing I) Pressing direction and II) powder flow and exit.

5.2 Results

5.2.1 Choice of trehalose and API qualities

As previously studied, micron sized trehalose particles were successfully produced to be tested as inert carrier for DPI formulations by two methods; spray drying (SD) and jet milling (JM). Accordingly from each produced quality, batches for aerosolization performance analysis (listed in Table 5-1) were mainly chosen based on the particle size distribution. The choice took into consideration relatively large (L-4913), medium (M-2914) and small (S-1915) amorphous spray dried trehalose particles. Also included the medium sized in a recrystallized form (REC.M-2914) as a side trial for the effect of water content in trehalose particles. Furthermore, jet milled trehalose batches of relatively large (TR-5) and small (TR1010) crystalline particles were of similar particle size as the spray dried batches to compare the effect of particle morphology on the aerosolization performance.

For testing the aerosolization performance of trehalose as an inert carrier, trehalose was to be blended with a model inhalable drug. Besides, the trehalose efficiency to disperse the drug should be related to the interaction with the API's physicochemical nature. Thus, budesonide, salbutamol sulphate and disodium cromoglycate were chosen to represent model hydrophobic, hydrophilic, and hygroscopic drugs respectively for analysis. In addition that all the API batches were in the inhalation size grade, each was of two qualities; spray dried and jet milled as shown in Table 5-2. Although, all produced API qualities had a similar aerodynamic particle size range, yet the morphology was divergent as investigated by SEM and presented in Figure 5-3. Spray dried budesonide (BU-SD) showed incomplete spheres with concave sides; while the jet milled quality (BU-JM) was of irregular shape with rough surface. Spray dried salbutamol sulphate (SS-SD) showed spherical particles with corrugated surface while the jet milled (SS-JM) particles showed rod shaped with smaller irregular particles. Spray dried disodium cromoglycate (DSCG-SD) showed convoluted brain like structure in a spherical format, but the jet milled (DSCG-JM) showed irregular shaped particles with scaly rough surface.

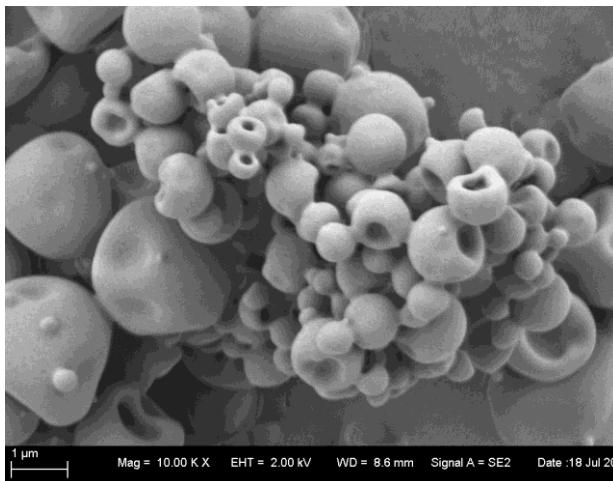
Table 5-1: Particle size distribution of spray dried and jet milled trehalose batches prepared for blending formulations.

PSD	Spray dried				Jet milled	
	L-4913	M-2914	S-1915	Rec.M-2914	TR-5	TR-1010
D10	1.78	0.8	0.62	1.52	0.96	0.75
D50	9.05	4.11	2.25	5.91	5.05	2.23
D90	19.64	9.47	5.57	11.97	18.33	6.13
Span value	1.97	2.11	2.20	1.77	3.44	2.41

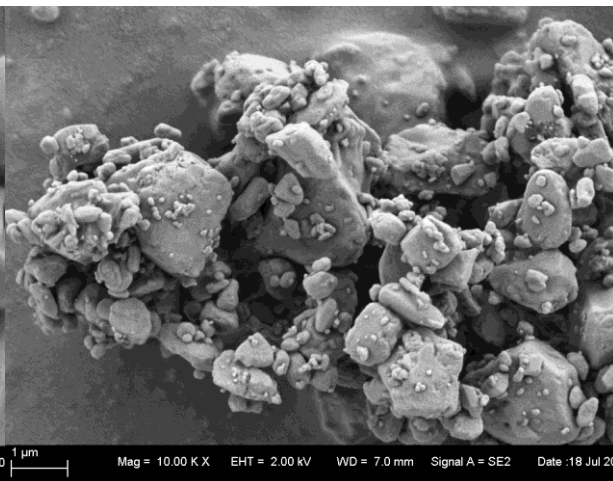
Table 5-2: Particle size distribution of spray dried and jet milled model API for formulations analysis.

PSD	Salbutamol sulphate		Budesonide		Di-sodium cromoglycate	
	SD - SS	JM - SS	SD - BU	JM - BU	SD - DSCG	JM -DSCG
D10	0.64	0.8	0.75	0.55	0.66	0.66
D50	2.23	2.33	1.77	1.43	2.29	2.34
D90	5.65	5.76	3.58	4.16	5.34	5.82
Span Value	2.25	2.13	1.60	2.52	2.04	2.21

BU-SD



BU-JM



SS-SD



SS-JM



DSCG-SD



DSCG-JM

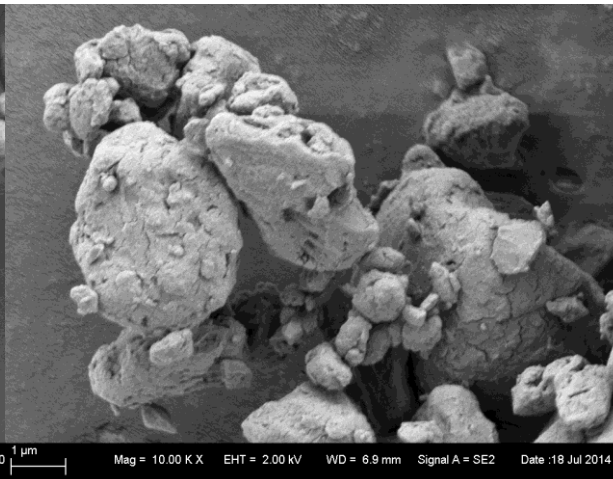


Figure 5-3: SEM Images of spray dried (Left) and jet milled (Right) API particles under 10000X magnification power.

5.2.2 Blends preparation

As described in the methodology section, blending was done mainly with a turbula mixer to produce 20% drug loaded formulations. As shown in Table 5-3, 27 DPI blends were successfully prepared and considered homogenous as their RSD% was significantly below 6%. The blends prepared can be classified into three main groups as follows;

- A. Hydrophobic budesonide (BU-SD or BU-JM) / trehalose SD (L-4913, M-2914, S-1915) or trehalose JM (TR-5, TR1010).
- B. Hydrophilic salbutamol sulphate (SS-SD or SS-JM) / trehalose SD (L-4913, M-2914, S-1915, REC.M-2914) or trehalose JM (TR-5, TR1010).
- C. Hygroscopic disodium cromoglycate (DSCG-SD or DSCG-JM) / trehalose SD (L-4913, M-2914, S-1915).

Table 5-3: Homogeneity of all binary prepared blends by turbula mixing, showing RSD% calculated based on average values for each top, middle, and bottom samples.

Blend #	Blend Code	Prepared Concentration		Homogeneity	
		Blend Conc. (mg/ml)	API Conc. 20% (mg/ml)	SD	RSD %
1	BU-SD / L-4913	0.3 mg/ml	0.06 mg/ml	0.002	3.246
2	BU-SD / M-2914			0.002	2.564
3	BU-SD / S-1915			0.001	1.742
4	BU-JM / L-4913			0.001	1.648
5	BU-JM / M-2914			0.001	1.842
6	BU-JM / S-1915			0.002	3.857
7	BU-SD / TR-JM 5	0.25 mg/ml	0.05 mg/ml	0.002	4.416
8	BU-SD / TR-JM 1010			0.002	3.114
9	BU-JM / TR-JM 5			0.001	1.738
10	BU-JM / TR-JM 1010			0.001	2.949

Table 5-3 continued

11	SS-SD / L-4913	0.3 mg/ml	0.06 mg/ml	0.002	3.122
12	SS-SD / M-2914			0.002	3.862
13	SS-SD / S-1915			0.001	1.945
14	SS-JM / L-4913			0.000	0.803
15	SS-JM / M-2914			0.003	4.404
16	SS-JM / S-1915			0.001	1.508
17	SS-SD / TR-JM 5	0.5 mg/ml	0.1 mg/ml	0.001	1.323
18	SS-SD / TR-JM 1010			0.001	1.265
19	SS-JM / TR-JM 5			0.001	1.168
20	SS-JM / TR-JM 1010			0.004	3.974
21	SS-JM / REC.M-2914	0.4 mg/ml	0.08 mg/ml	0.003	3.869
22	DSCG-SD / L-4913	0.3 mg/ml	0.06 mg/ml	0.001	2.113
23	DSCG-SD / M-2914			0.001	1.593
24	DSCG-SD / S-1915			0.002	2.477
25	DSCG-JM / L-4913			0.000	0.706
26	DSCG-JM / M-2914			0.001	1.263
27	DSCG-JM / S-1915			0.001	1.337

5.2.3 Aerosolization performance by NGI

5.2.3.1 Hydrophobic Budesonide (BU) blends

In addition to the prepared binary blends, carrier free formulations of spray dried (BU-SD) and jet milled (BU-JM) budesonide were also tested as a 100% control in 1 mg filled capsule for comparison with the 20% of 5mg blends filled capsules. As illustrated in the FPF% chart for the budesonide formulations (Figure 5-4), aerosolization performance was generally very good as they were all above 50%. It was obvious that 1 mg carrier free formulations showed highest FPF% range where the BU-SD released about 85 % fines and BU-JM released 76% fines. This might indicate that the aerosolization behavior of the spray dried quality was relatively better than the jet milled quality for the hydrophobic drug. After comparing the binary blends, the indication of better aerosolization of BU-SD than the BU-JM is further

proved with all qualities of trehalose. From these results, we can interpret that the physical properties of BU particles with concave sided spheres may give less mechanical interlocking, better flowability or better aerodynamic properties than the irregularly shaped rough particles.

In the next observation, the difference in the PSD of spray dried trehalose, slightly affected the performance of the BU-SD dispersion (72% – 78% FPF), while it had a greater effect on the BU-JM dispersion. The Largest SD trehalose PSD (L-4913) gave best performance with BU-JM by 68% FPF, while the smallest SD trehalose PSD (S-1915) showed the lowest dispersion efficiency of BU-JM with FPF of 52%. On the other hand, the smallest jet milled quality of trehalose (TR-1010) showed slightly better aerosolization performance than the larger (TR-5) when tested with both BU-SD and BU-JM. Through the whole chart, the highest achieved FPF% was about 81% with the binary blend (BU-SD / TR-1010) and 85 % by the carrier free (BU-SD).

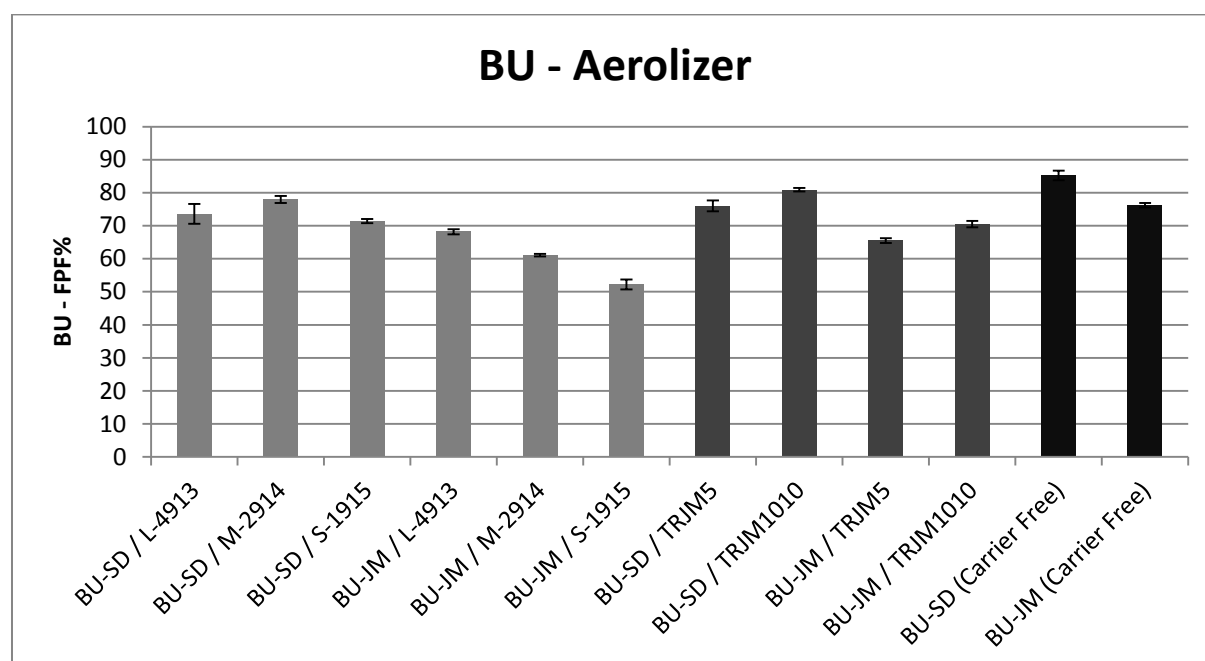


Figure 5-4: FPF% chart for Budesonide with different Trehalose batches and carrier free formulations, aerosolized at 100L/min by Aerolizer (n=3 ±SD).

Changing focus to the FPD chart (Figure 5-5), (BU-SD / TR-1010) was able to deliver the highest amount (750µg) of fine BU-SD, even more than the carrier free form that delivered 660µg. This indicates that, finest trehalose carrier (TR-1010) was able to release BU-SD and disperse it from the most efficient formulation with least capsule retention. From this point, it was concluded that using fine jet milled

trehalose particles as an inert carrier for BU, would be beneficial for lowering the adhesion to the capsule walls and gives more efficient formulations than the carrier free.

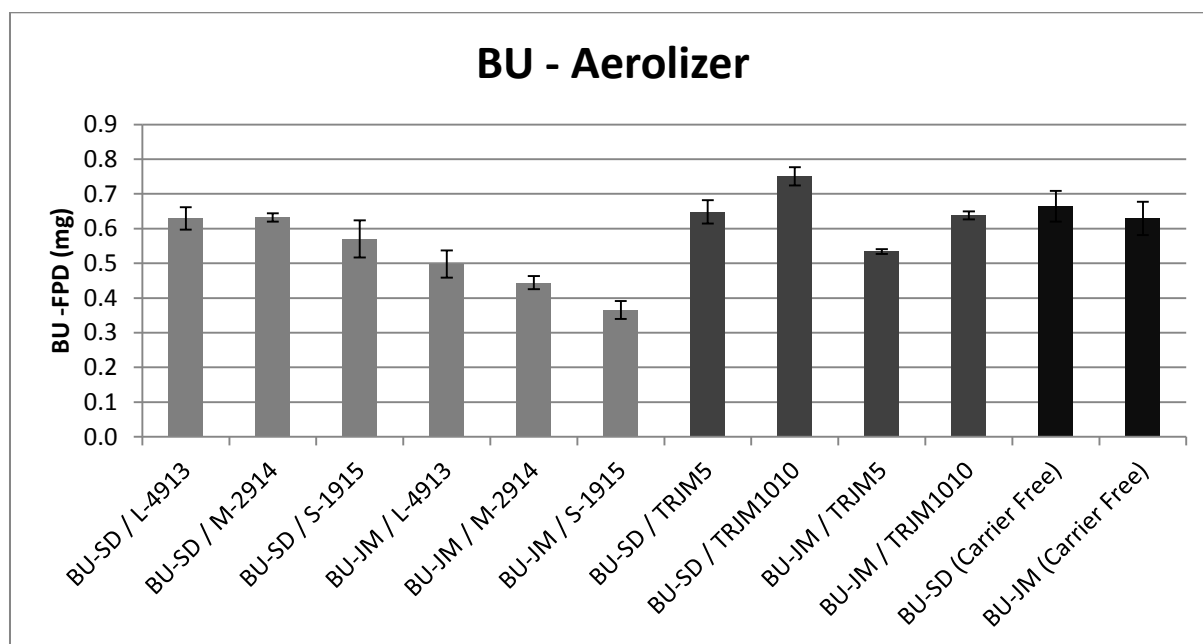


Figure 5-5: FPD chart for Budesonide with different Trehalose batches and carrier free formulations, aerosolized at 100L/min by Aerolizer (n=3 \pm SD).

To observe the aerosolization behavior of the budesonide formulations containing spray dried trehalose batches only at medium flow rate, cascade impaction analysis took place using the Easyhaler device at 45L/min. In contrast to the results from the high flow rate previously observed, the formulations with BU-JM showed better aerosolization performance in terms of FPF% than their counter formulation with BU-SD as presented in Figure 5-6. The highest achieved FPF of BU-JM was about 31% by both the larger trehalose particles (L-4913 & M-2914). Further insight on the performance of trehalose particles to disperse budesonide particles at the lower flow rate can be observed by the FPD chart in Figure 5-7.

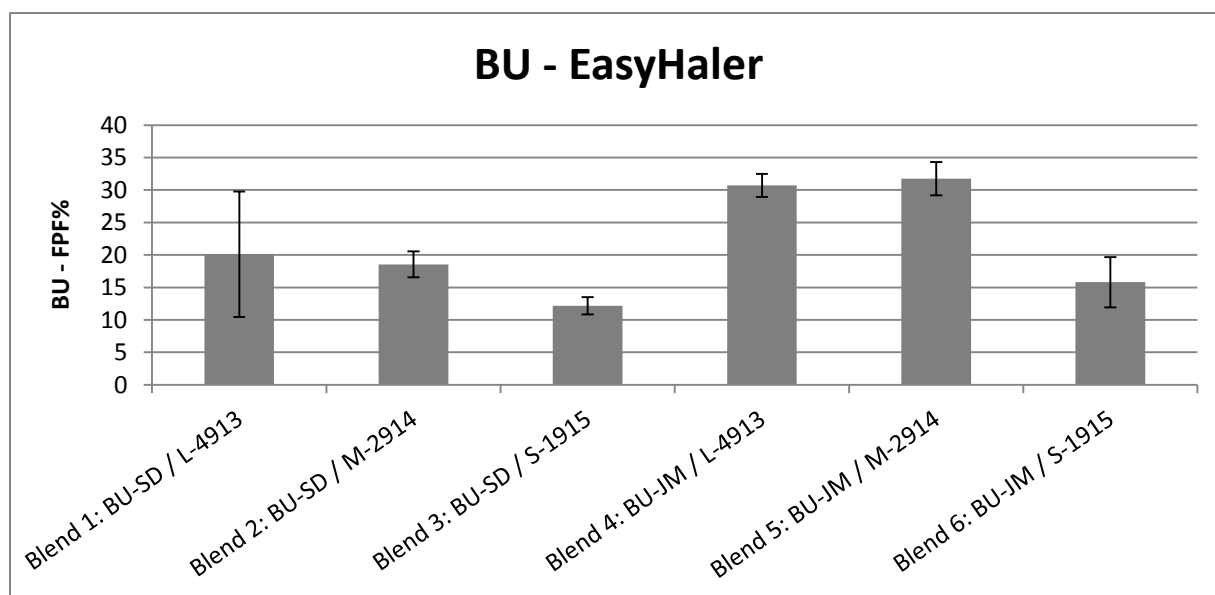


Figure 5-6: FPF% chart for Budesonide formulations with spray dried trehalose batches, aerosolized at 45L/min by Easyhaler (n=3 \pm SD).

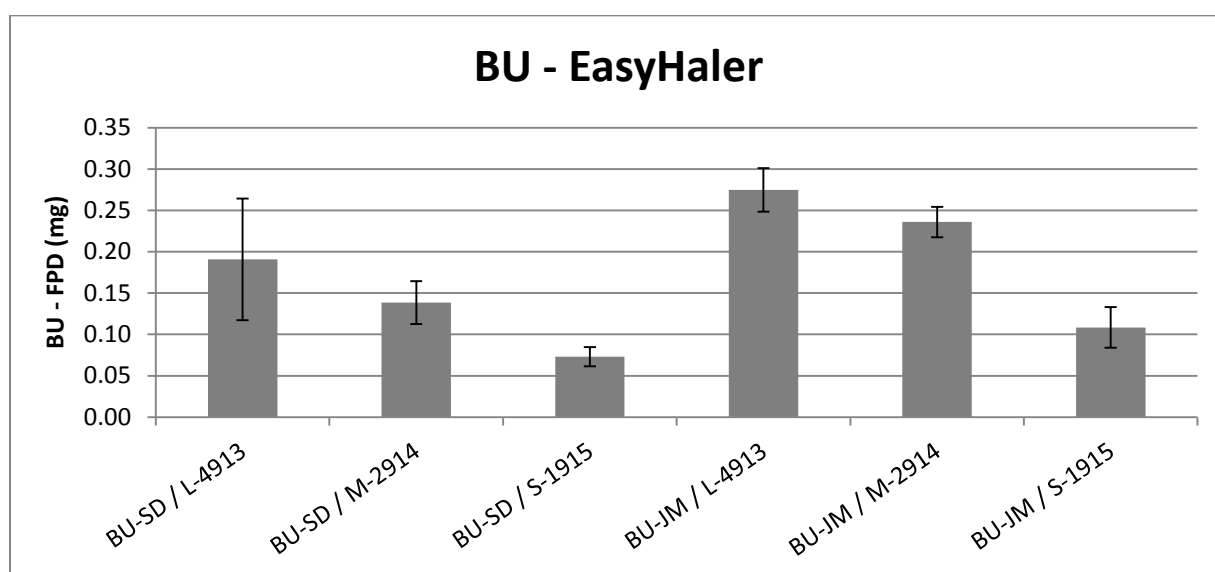


Figure 5-7: FPD chart for Budesonide formulations with spray dried trehalose batches, aerosolized at 45L/min by Easyhaler (n=3 \pm SD).

Despite of the overall lower dispersion efficiency, spray dried trehalose behaved in a similar trend compared to its aerosolization performance at high flow rate of 100L/min. Indeed relatively larger trehalose particles were able to disperse and deliver higher fine particle dose from both qualities of the budesonide, achieving maximum delivery of 270 μ g from (BU-JM / L-4913). A major problem encountered by using the Easyhaler at flow rate of 45L/min, was the dose uniformity reflected by the fluctuating standard deviation for each formulation's runs. It was observed that the dose uniformity was highly affected by the handling of the inhaler while pressing to

load the dose. Slight shaking or tapping might have increased the amount loaded thus the total amount released. This observation can be correlated to the generally reduced flowability of the formulations fine particles. Further looking at the data from the NGI runs, High BU fraction on throat and preseparator suggest that the powder was not effectively de-agglomerated upon aerosolization under 45L/min and was released in the form of bulk agglomerates. These agglomerates were entrapped by the throat and preseparator which could not pass deeper onto the NGI stages.

In comparison with using the Aerolizer, the capsule retention at 100L/min was $\leq 3\%$ from the total filled powder for all the formulations tested. Certainly the particles were effectively de-agglomerated by the Aerolizer even before leaving the capsule due to the high flow and further dispersed by the inhaler grid to reach deeper onto the NGI stages as observed earlier.

5.2.3.2 Hydrophilic Salbutamol sulphate (SS) blends

In addition to the prepared binary blends, carrier free formulations of spray dried (SS-SD) and jet milled (SS-JM) salbutamol sulphate were also tested as a 100% control in 1 mg filled capsule for comparison with the 20% of 5mg blends filled capsules. As illustrated in the FPF% chart for the salbutamol sulphate (Figure 5-8), aerosolization performance showed more significant differences compared to the results of the hydrophobic budesonide formulations. Once more, it was obvious that 1 mg carrier free formulations showed highest FPF% range where the SS-SD released about 42 % fines and SS-JM released 74% fines. Nevertheless, this indicates that the aerosolization behavior of the jet milled quality was significantly better than the spray dried quality for the hydrophilic drug unlike the hydrophobic budesonide aerosolization behavior. When coming to compare the binary blends, the fact of better aerosolization of SS-JM than the SS-SD is further proved with all qualities of trehalose.

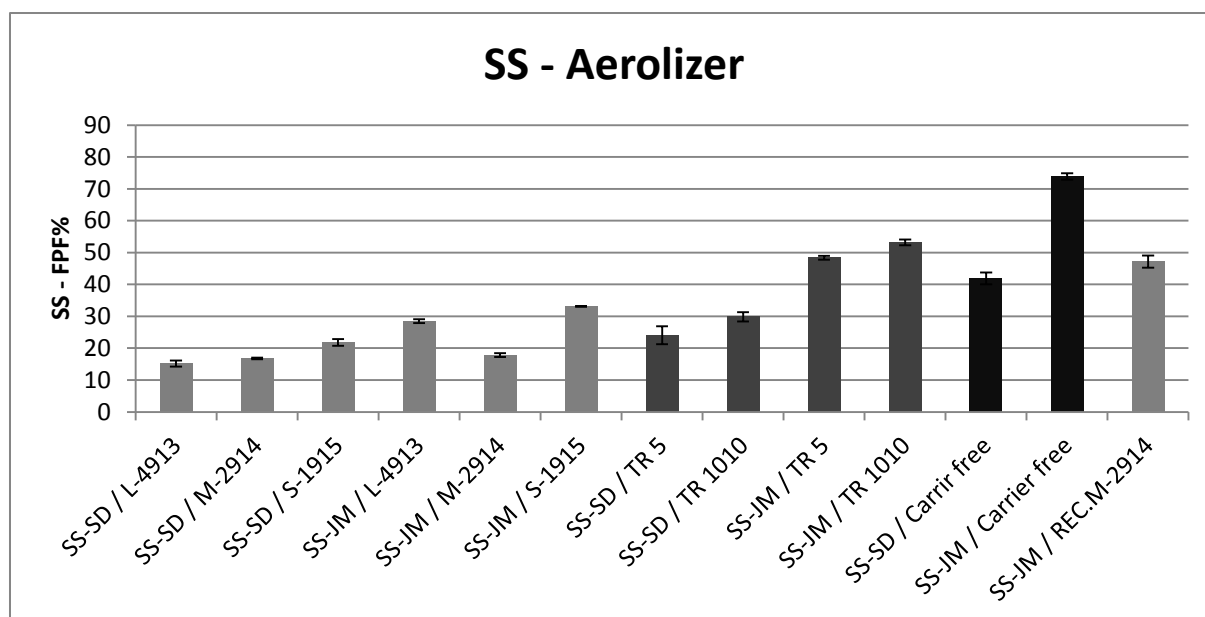


Figure 5-8: FPF% chart for Salbutamol sulphate with different Trehalose batches and carrier free formulations, aerosolized at 100L/min by Aerolizer (n=3 ±SD).

In the following observation, the difference in the PSD of spray dried amorphous trehalose particles, slightly affected the performance of the SS-SD dispersion (15% – 22% FPF), while it had a greater effect on the SS-JM dispersion (17% – 33% FPF). Furthermore, the smallest SD trehalose PSD (S-1915) gave best performance with SS-JM and SS-SD. while the largest SD trehalose PSD (L-4913) showed the lowest dispersion efficiency of SS-SD with 15% FPF and comparable performance to (S-1915) with SS-JM releasing 28% FPF. Unexpectedly, the medium sized trehalose particles M-2914 showed the lowest performance with SS-JM releasing only 17% FPF. However, the partially recrystallized (REC.M2914) which has similar PSD as (M-2914) showed the best performance compared to the spray dried trehalose qualities with 47% FPF.

On the other hand, jet milled crystalline trehalose qualities in formulations, showed better aerosolization performance than their counterpart of amorphous spray dried trehalose particles. The smallest jet milled quality of trehalose (TR-1010) showed slightly better aerosolization performance than the larger (TR-5) when tested with both SS-SD and SS-JM. Through the whole chart, the highest achieved FPF% was about 53% with the binary blend (SS-JM / TR-1010) and 74 % by the carrier free (SS-JM).

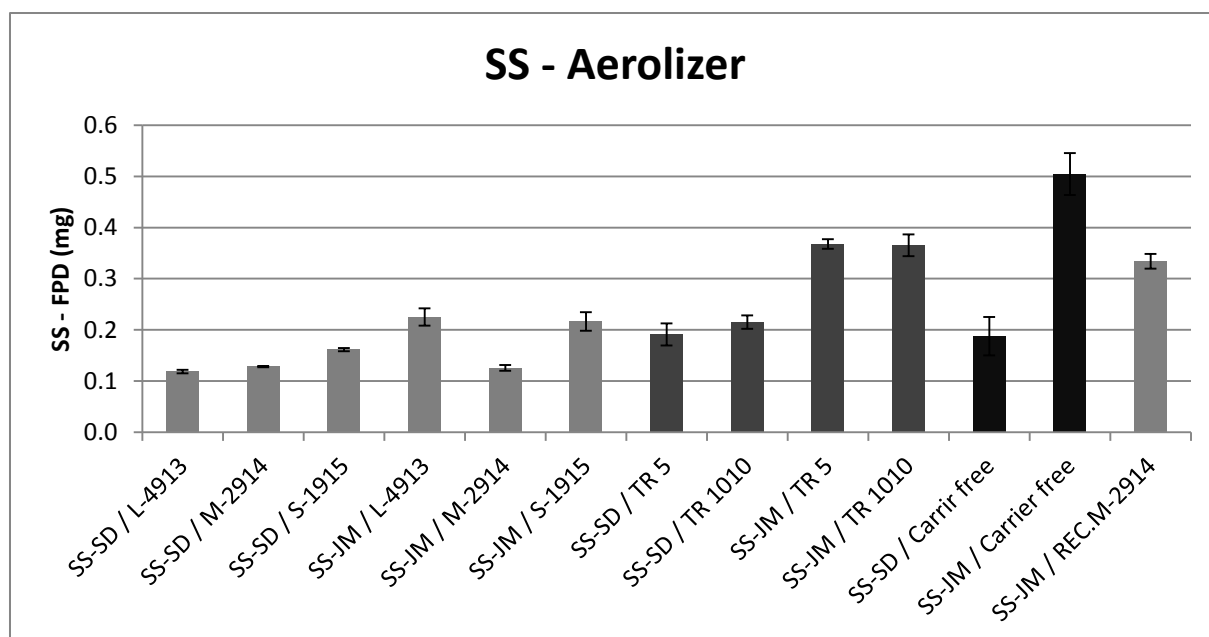


Figure 5-9: FPD chart for Salbutamol sulphate with different Trehalose batches and carrier free formulations, aerosolized at 100L/min by Aerolizer (n=3 \pm SD).

For further insight on the aerosolization performance, Figure 5-9 shows the fine particle dose of salbutamol sulphate that was actually released and dispersed deep in the impactor. It is observed that particle size distribution differences within trehalose qualities did not have substantial effect on the performance. The jet milled trehalose qualities both TR-5 and TR-1010 performed similarly by releasing 370 μ g SS-JM. The spray dried trehalose (L-4913 & S-1915) also gave similar results of about 220 μ g SS-JM. Instead, performance differences were observed depending on the quality of the trehalose particles to release the hydrophilic SS-JM. The performance order of the formulations based on the physical form of the trehalose carrier particles can be set as; (amorphous SD-trehalose < partially crystalline SD-trehalose < fully crystalline JM-trehalose). This behavior can be correlated to the moisture content of trehalose particles, where the more the trehalose particles are crystalline the less the binding with the hydrophilic SS, the easier the de-agglomeration and dispersion.

5.2.3.3 Hygroscopic Disodium cromoglycate (DSCG) blends

The binary blends prepared, focused to present the performance of the amorphous spray dried trehalose as a carrier in aerosolizing the highly hygroscopic DSCG. In addition to the prepared binary blends, carrier free formulations of spray dried (SS-DSCG) and jet milled (DSCG-JM) disodium cromoglycate were also tested as a

100% control in 1 mg filled capsule for comparison with the 20% of 5mg blends filled capsules. However, DSCG-JM and DSCG-SD carrier free formulations failed to be discharged efficiently showing capsule retention of $\geq 60\%$ and accordingly FPF% was not calculated. It was observed that, the performance of the tested formulations did not depend solely on the variation of the SD-trehalose particle sizes with each DSCG quality. Indeed, two more factors governs the performance outcome; firstly the hygroscopic nature of DSCG particles and their interaction with the amorphous trehalose particles. Secondly, the different surface morphology which was shown as convoluted brain like spheres for DSCG-SD and irregular particles for DSCG-JM with scaly rough surface.

At start, SD-trehalose carrier was successful in efficiently discharging both qualities of DSCG. The relatively medium (M-2914) and large (L-4913) trehalose particles did release both DSCG qualities with average capsule retention of $\leq 3\%$. Nevertheless, the smallest PSD trehalose batch (S-1915) performed the least in releasing DSCG upon aerosolization. (DSCG-SD / S-1915) formulation showed average capsule retention of about 20%, while (DSCG-JM /S-1915) formulation showed average capsule retention of about 7.5% of the total capsule filled powder. For further analysis of the aerosolization behavior Figure 5-10 represents the performance of amorphous spray dried trehalose particles in dispersing hygroscopic DSCG in terms of FPF%. The largest PSD trehalose batch (L-4913) had similar performance aerosolizing DSCG-SD by 18% FPF and DSCG-JM by 16% FPF. On the other hand, the smallest PSD trehalose batch (S-1915) showed performance variation, where DSCG-SD was dispersed by 8% FPF and DSCG-JM by lowest achieved performance of 1% FPF. In general, both trehalose qualities (L-4913) and (S-1915) showed relatively better aerosolization behavior in terms of releasing higher fraction of DSCG-SD compared to DSCG-JM. Unexpectedly, the medium PSD trehalose batch (M-2914) showed an opposing behavior, where it gave the best aerosolization performance with DSCG-JM reaching 28% FPF releasing 230 μg and lowest performance with DSCG-SD getting 7% FPF releasing 60 μg .

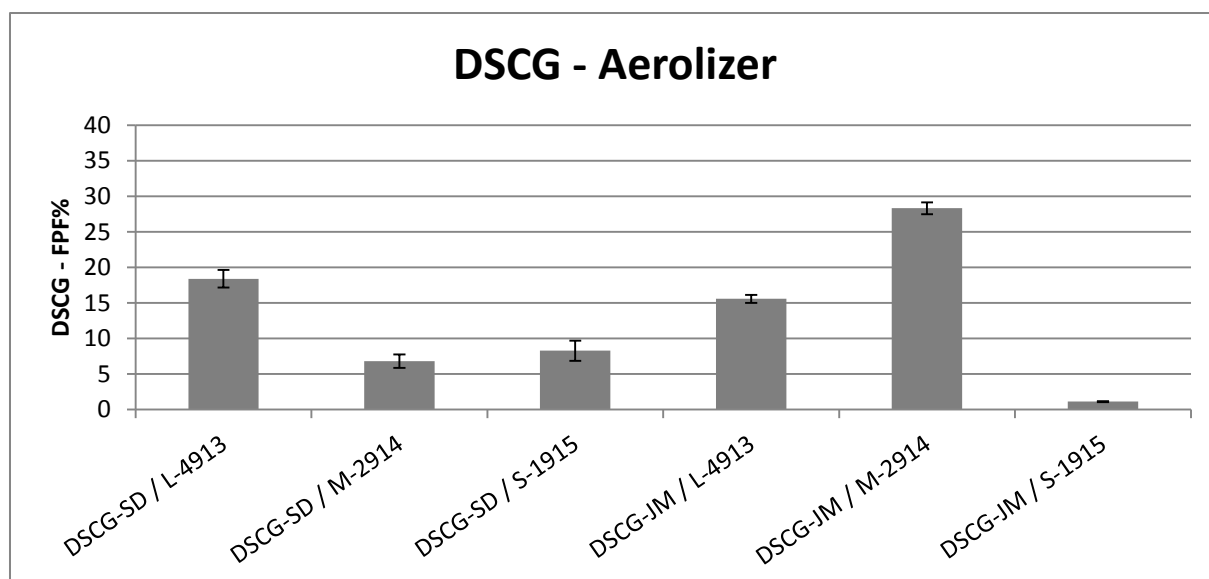


Figure 5-10: FPF% chart for Disodium cromoglycate with spray dried Trehalose batches, aerosolized at 100L/min by Aerolizer (n=3 \pm SD).

By observing the results of the NGI stage distribution presented in Figure 5-11, trehalose PSD different batches had a noticeable effect on the aerodynamic particle size distribution among the NGI stages. Based on the high affinity of the hydrophilic DSCG to bind with the hydrophilic trehalose particles, and the mechanical interaction of the different morphologies, strong agglomerates were formed with a relative variation in size. The larger trehalose particles (L-4913) formed larger agglomerates that were caught early in the throat, yet they can release some loose fines giving relatively higher DSCG fraction deeper on the NGI stages. This shows the least morphological influence of DSCG qualities when using the largest SD-trehalose quality. Indeed, smaller PSD of the used trehalose particles in the formulations showed more profound DSCG morphological influence on the aerosolization behavior. The medium sized trehalose particles (M-2914) also formed some large agglomerates that were caught early in the throat, but not as large as the agglomerates formed by (L-4913). Accordingly, for the (DSCG-SD / M-2914) a higher fraction of the agglomerates were formed in size to be captured by the preseparator and not releasing much loose fines to reach deeper. Focusing on (DSCG-JM / M2914), also medium sized agglomerates were formed that were similarly captured by the throat. Nevertheless, the irregular DSCG-JM particles was most effectively released as fines to reach deeper and not to be captured as much by the preseparator, thus this formulation showed highest achieved FPF%. The smallest sized trehalose particles (S-1915) have showed the least particle deposition in the

throat for both DSCG qualities, but highest particles deposition in the preseparator. This can be related again to the size of the agglomerates that were able to pass the throat but not the preseparator. Besides, the formed agglomerates of (DSCG-SD / S-1915) may have been more compact than (DSCG-JM / S-1915) to be able to give 7% more fines by reaching stage 2 on the NGI.

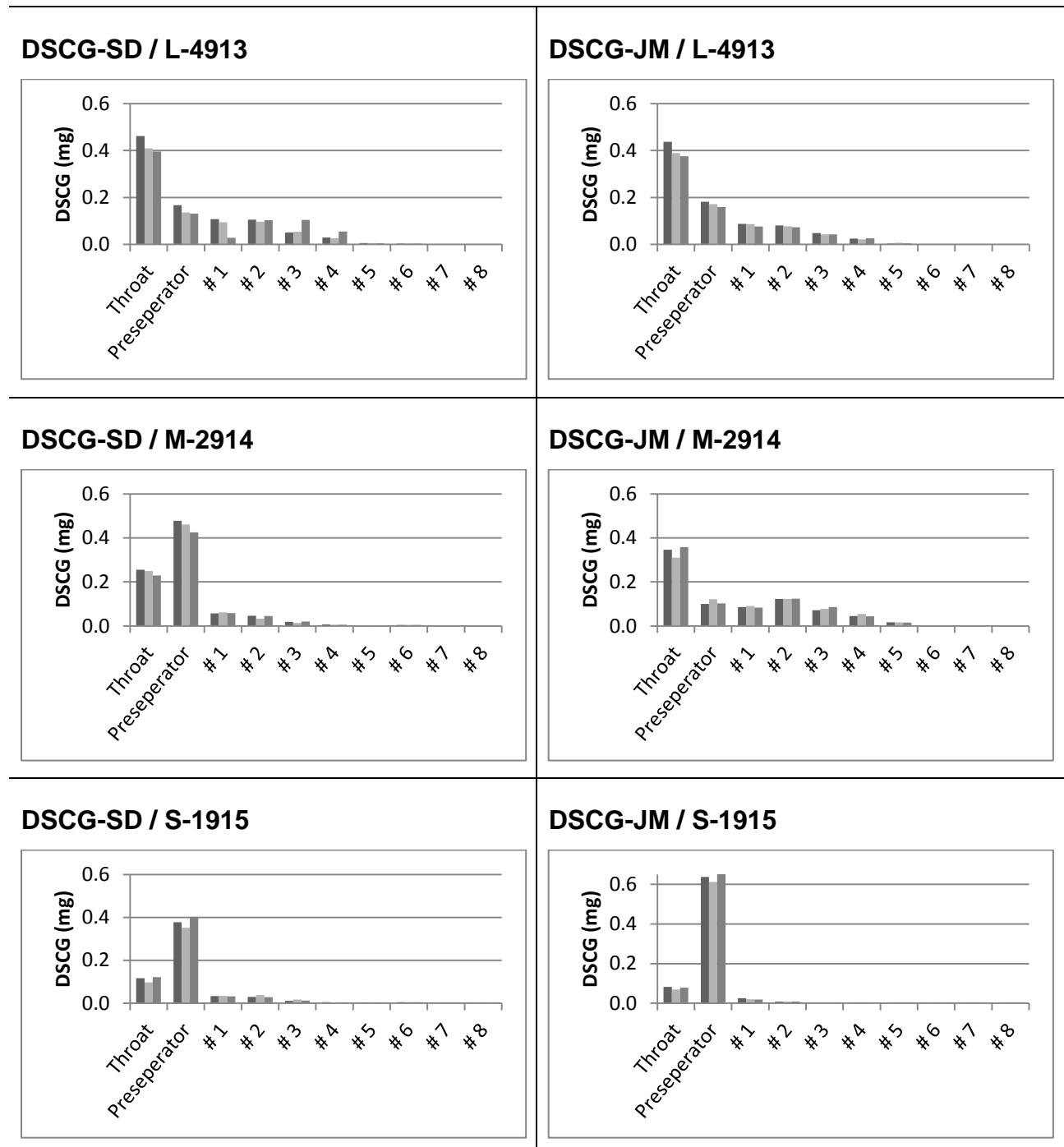


Figure 5-11: DSCG - NGI stage distribution at 100L/min by Aerolizer (n=3)

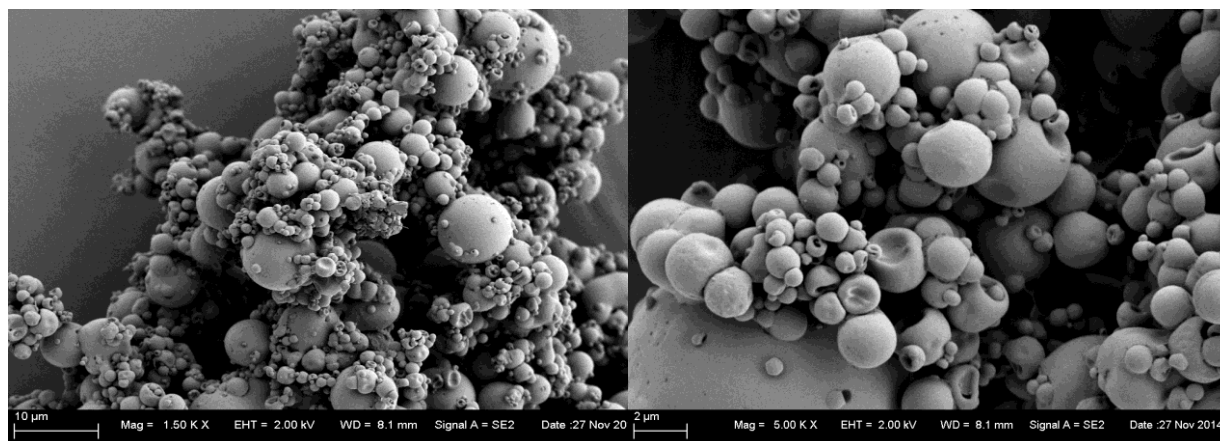
5.2.4 SEM

Morphology of particles in blends was detected under different magnification power of a scanning electron microscope to observe the interaction between API's and trehalose particles. Images shown in Figure 5-12 are for blends of different trehalose qualities that showed different morphological agglomerations with each tested API resulting in different aerosolization performances as previously illustrated. In (BU-SD / M-2914), large agglomerates of differently sized spherical particles were observed. Zooming in shows that the hydrophobic BU have smaller sized semi spheres with concave sides that gave a loose structure in combination with the relatively larger spherical trehalose carrier particles. In (BU-JM / M-2914), smaller agglomerates were observed compared to the previous. However zooming in shows that the irregularly shaped BU fine particles were scattered with high surface contact on the obviously larger spherical trehalose carrier particles. Relative to the aerosolization performance observed earlier, BU-SD was easier to de-agglomerate from the spherical trehalose particles and disperse than the BU-JM. In (BU-SD / TR5) and (BU-SD / TR1010), small agglomerates that were connected in an irregular loose structure were observed. Zooming in, showed that each TR5 irregular particle had higher surface contact with more BU-SD particles than the finer TR1010 particles in the other blend. This was previously demonstrated by the tested aerosolization performance of the fine TR1010 in releasing highest FPF of BU-SD.

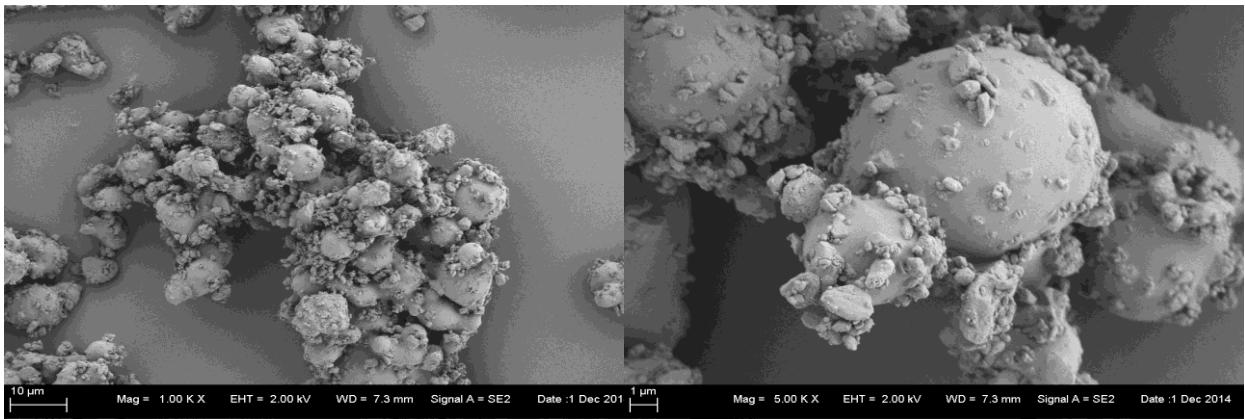
Generally for the hydrophilic drugs (SS and DSCG), they showed more compact or denser agglomerates in combination with the hydrophilic trehalose carrier particles due to the higher binding affinity. In (SS-SD / M-2914), agglomerates of differently sized spherical particles were observed. The agglomerates were not seen as large single units; rather they were smaller dense units. Zooming in, showed that SS-SD particles were spherical with some surface corrugation and size variation. Larger SS-SD particles were in minimum contact with the spherical trehalose particles, but the smaller SS-SD particles filled the small gaps in between leading to a tighter arrangement. Indeed, this formulation showed poor aerosolization performance as previously examined. In (SS-JM / M-2914), large dense agglomerates were observed of rod shaped SS-JM with spherical trehalose particles in between. Compared to (SS-SD / M-2914) it showed denser and larger agglomerates, nevertheless it gave similar aerosolization performance due to the

aerodynamically favored rod shaped SS-JM that may be released off the agglomerates' outer surface upon aerosolization. In (SS-JM / TR5) and (SS-JM / TR1010), agglomerates that were connected in an irregular structure were observed. Zooming in, shows that the agglomerates are formed by asymmetrical buildup of fines from rod shaped SS-JM particles and irregular trehalose particles. In these two formulations, the assembly of particles gave the least observed mechanical interlocking resulting in better aerosolization performance compared to other SS formulations with trehalose. In (SS-JM / REC.M-2914), small dense agglomerates were observed of rod shaped SS-JM with spherical trehalose particles in between. Zooming in, shows that the rod shaped SS-JM were buildup on surface of the partially crystalline trehalose particles that had shaped bridge like formation in between spheres. In contrast to the amorphous similarly sized (M-2914), (REC.M-2914) limited the trapped rods of SS-JM in between the spheres, forming smaller agglomerates and resulting in a comparable dispersion performance as the fully crystallized Jet milled trehalose. In (DSCG-JM / M-2914), large dense agglomerates were observed of irregular shaped DSCG-JM particles alongside with spherical trehalose particles. Zooming in, shows that the highly hygroscopic nature lead to fused particles inside the core of the agglomerates, holding loose fines of DSCG-JM on surface. This comes in accordance to the aerosolization performance observed, where the large agglomerates were held early by the throat, and fines were able to de-agglomerate and disperse.

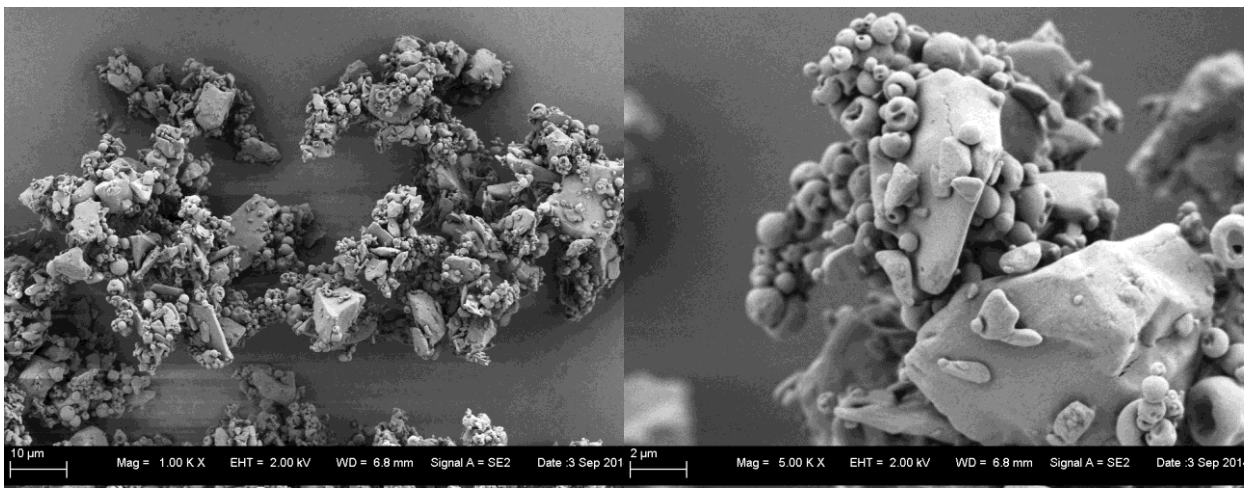
BU-SD / M-2914



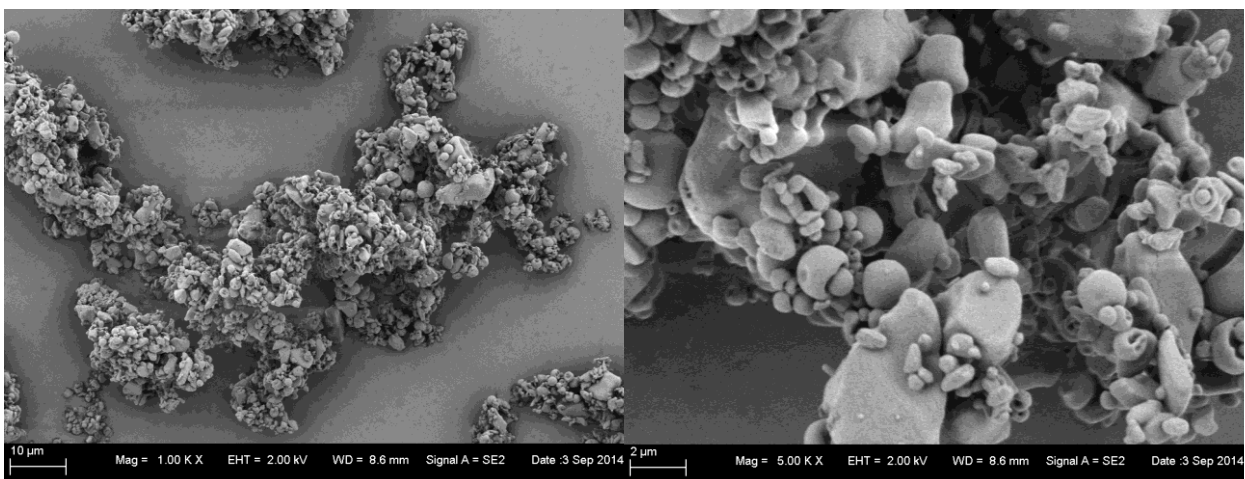
BU-JM / M-2914



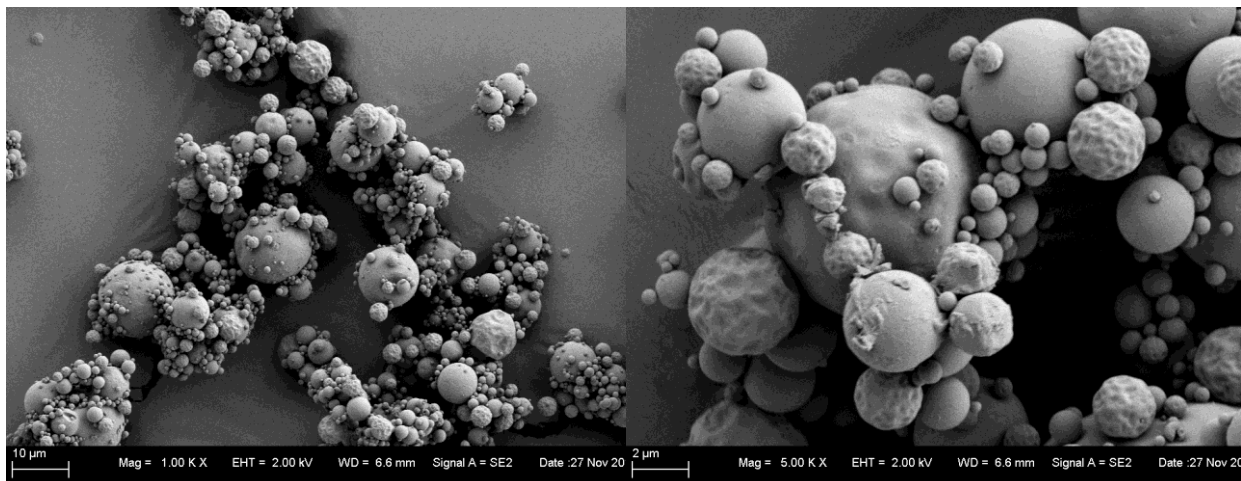
BU-SD / TR5



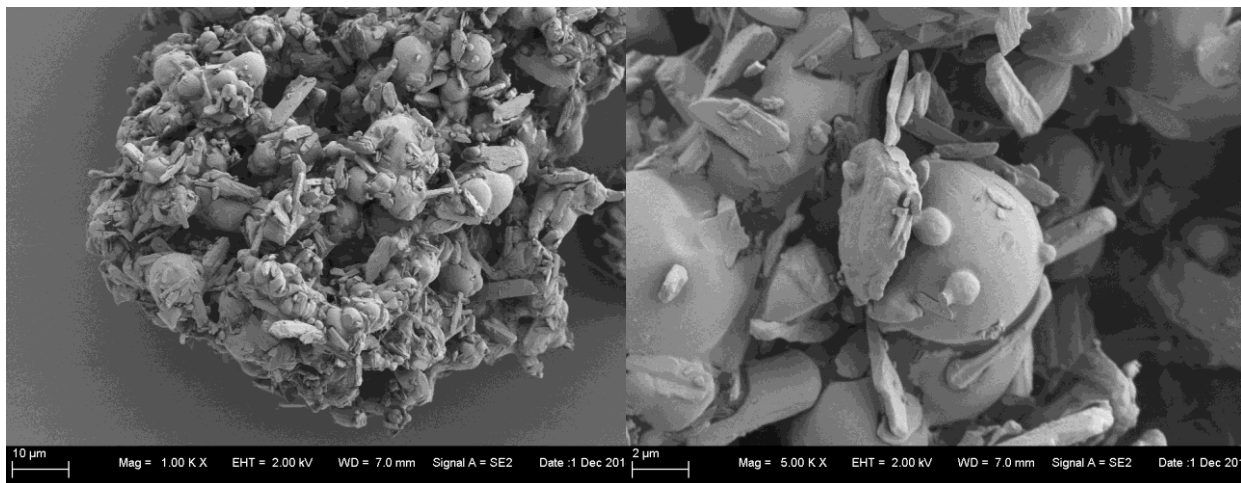
BU-SD / TR1010



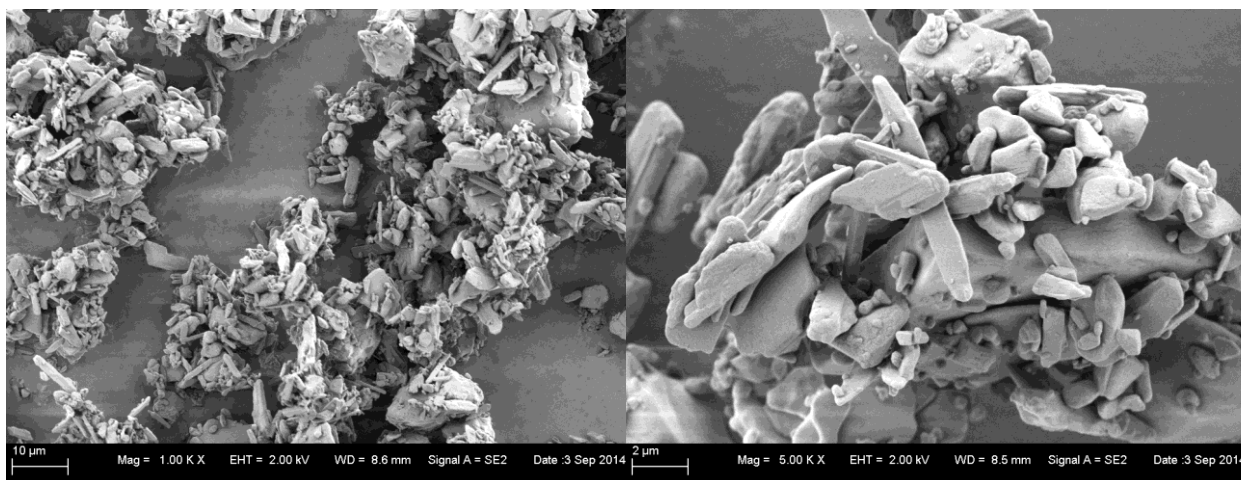
SS-SD / M-2914



SS-JM / M-2914



SS-JM / TR5



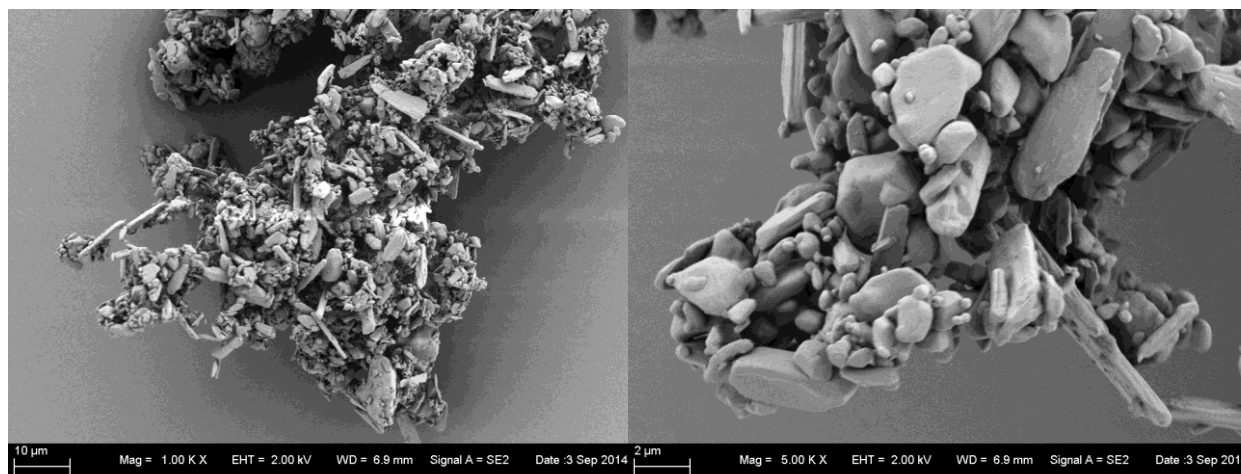
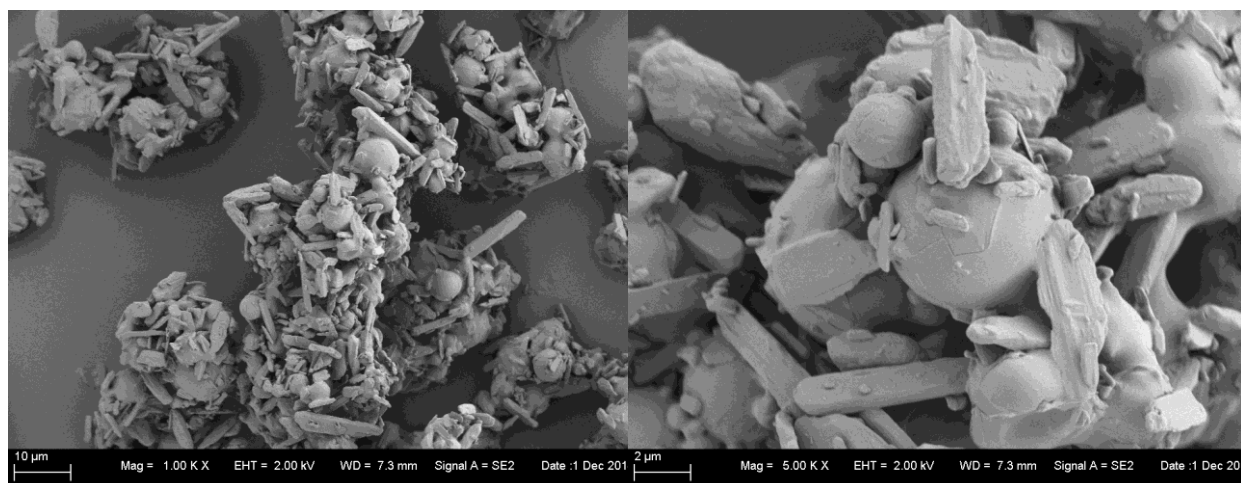
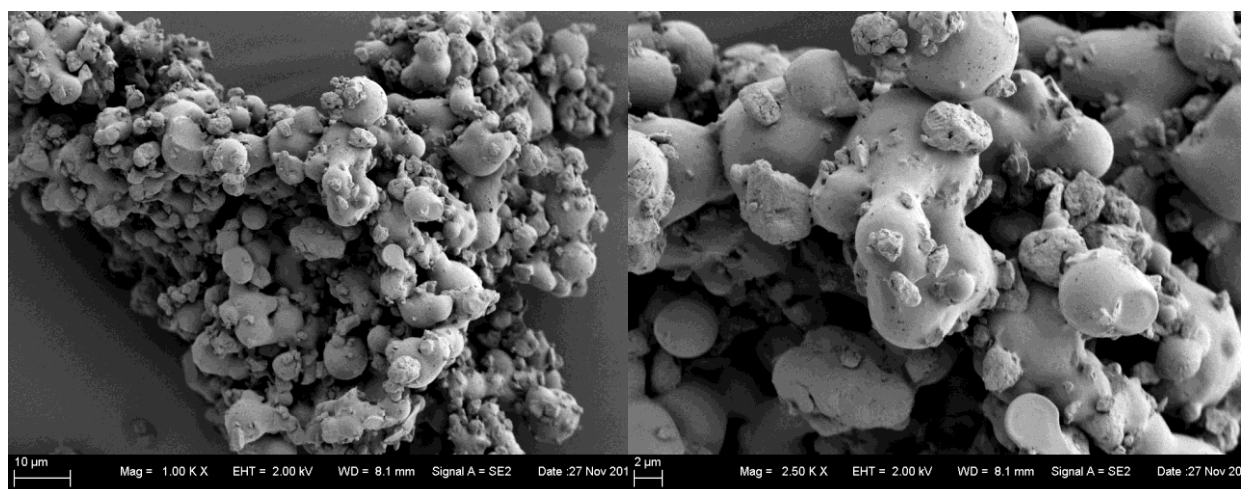
SS-JM / TR1010**SS-JM / REC. M-2914****DSCG-JM / M-2914**

Figure 5-12: SEM images under magnification power 1000X (left) and 5000X (right) of 10 blends as listed.

5.2.5 Surface energy measurements

The surface free energy of any material can be classified into non polar forces as Van der waals and polar forces such as acid/base interactions. Van der Waals forces constitute the major part of the dispersive component of the surface free energy (γ^D) which is a measure for the non-polar interaction sites of a surface. The theory developed by (Fowkes, 1964) is the base in calculating (γ^D), taking into account the interaction with the non-polar liquid probes. In this case, the work of adhesion is ($W = 2 \gamma^D$). The dispersive surface energy (work of adhesion), is expressed in units (J/m^2) and the total surface energy is the additive effect of both the dispersive (γ^D) and polar (γ^P) components (Grimsey et al., 2002). The particle molecular nature, size, morphology, surface area, water content, and the processing conditions by which it was produced, all governs the resulting surface energy. In a number of studies, the aerosolization performance was correlated with the surface energy of the particles for both the APIs and the carriers. In general there was an inverse relation detected, increasing the total surface energy either dispersive or polar forces for various APIs with lactose carrier, decreased the resulting aerosolization performance (Das et al., 2009). On the other hand, this surface energy can vary between the adsorption strength of particles of the same material (Cohesion) or the adsorption strength between particles of different material (Adhesion). If particles are highly cohesive or highly adhesive, this will lead to poor flowability and dispersibility. Accordingly, some studies used tensile strength method and the atomic force microscopy to measure and relate the Cohesion/Adhesion balance (CAB) of API particles in regards to the carrier particles. It was perceived that a slightly cohesive drug-carrier formulation than being adhesive may give better aerosolization performance (Jones et al., 2008). The surface energy measurements can be set as a good qualitative method to predict the performance of a new DPI formulation.

The dispersive surface energy (γ^D) was measured for all API and trehalose qualities by IGC. The values shown in Figure 5-13 demonstrate the consistency of trehalose low (γ^D) that valued in the range of (40 mJ/m^2) under all preparation conditions. This similarity can be related to the average particle size of each quality that had a close range of D50 from $2.2\mu\text{m}$ to $9\mu\text{m}$. While different trehalose qualities of significantly different moisture content, processing condition and morphology did

not affect the dispersive surface energy of fine trehalose particles, rather they might have affected the polar surface energies. It was considered that the dispersive surface energies of the pure material tested an indication for their cohesive attractions. On the other hand, the tested (γ^D) values for APIs showed that spray dried qualities were always lower than their jet milled qualities as presented in Figure 5-14. Furthermore, both qualities of the DSCG particles showed the highest measured (γ^D) of about (70 mJ/m²). This was in agreement to their highly hygroscopic nature and observed poor flowability resembling high cohesive attractions. The measured (γ^D) of SS-JM was about (58 mJ/m²) resembling intermediate cohesive attractions, while SS-SD particles showed the lowest measured (γ^D) of (42 mJ/m²) resembling relatively lowest cohesive attractions. As for the hydrophobic BU-JM and BU-SD, both showed relatively intermediate cohesive attractions as presented by the measured (γ^D) of (60 mJ/m² and 53 mJ/m²) respectively.

In regards of the hydrophilic API aerosolization behavior previously discussed, highly cohesive material as DSCG formed strong agglomerates and showed poor dispersibility upon aerosolization. Although DSCG can adhere to trehalose due to hydrophilic affinity (polar interaction), yet the adhesion force was not enough to overcome the cohesion forces and disperse the fines efficiently. In contrast, SS-SD having lowest dispersive surface energy showed lowest cohesion forces and higher adhesion forces when in formulation with trehalose particles. This also resulted in reduced observed flowability and dispersibility. SS-JM carrier free particles having an intermediate dispersive surface energy, showed the highest achieved dispersibility for a hydrophilic drug, signifying a balance between the particles' cohesive and adhesive forces. SS-JM in formulation with trehalose particles as carrier, have showed a reduced aerosolization performance from the carrier free formula. This indicates the increased adhesion forces of SS-JM to the trehalose particles due to hydrophilic affinity, overcoming the cohesion forces thus resulted in lower dispersibility. In regards of the hydrophobic BU qualities, BU-SD presented relatively intermediate cohesive forces, while BU-JM had higher dispersive surface energy and thus higher cohesive forces. BU-SD carrier free formulation recorded the highest achieved aerosolization performance in terms of FPF%. This indicates the most achieved balanced cohesion and adhesion forces for optimum dispersibility. Trehalose particles in blend with BU-SD might have increased the adhesion slightly over the

cohesion in balance, resulting in a general reduction in performance but still with excellent dispersibility values. BU-JM behavior was similar with an overall reduced dispersibility compared to BU-SD due to the higher cohesive attraction forces noted.

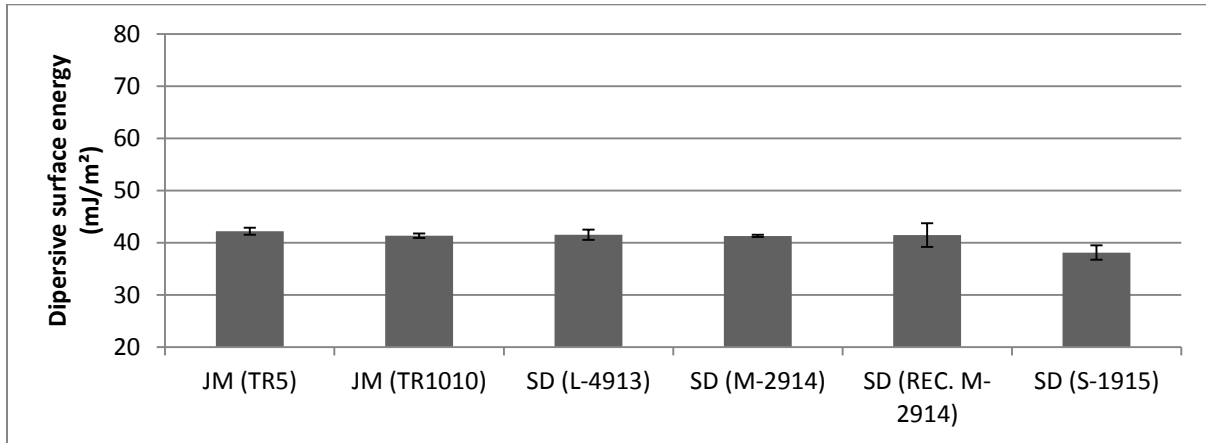


Figure 5-13: Dispersive surface energy of different JM and SD trehalose batches

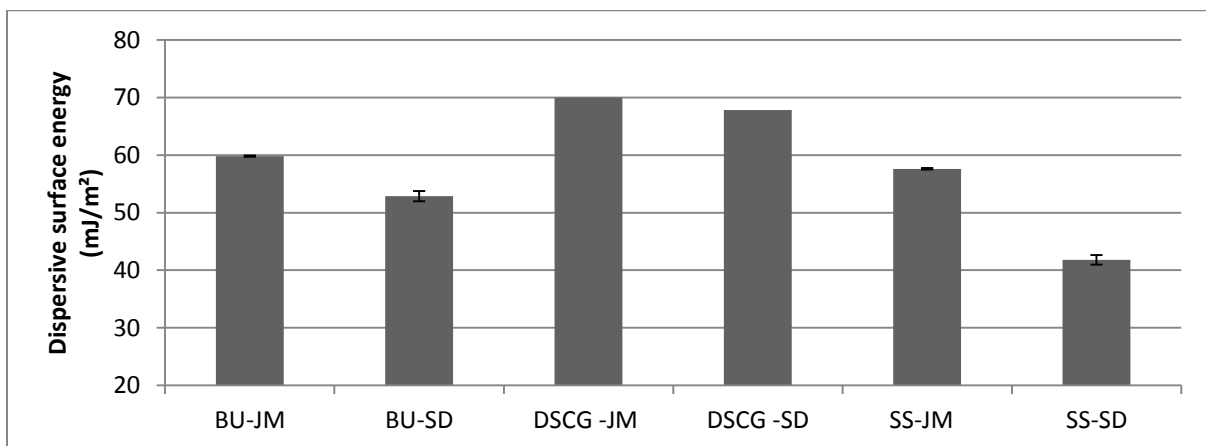


Figure 5-14: Dispersive surface energy of JM and SD qualities of BU, SS and DSCG

5.3 Discussion

A DPI carrier potentiality is mainly determined in-vitro by cascade impaction to observe the achieved aerodynamic aerosolization performance in terms of dispersed fine particle fraction. After the successful production of the inhalable trehalose particles in two qualities by spray drying and jet milling, cascade impaction proved that fine trehalose particles can achieve excellent aerosolization performance in different DPI formulations. The performance study distinguished between the different trehalose batches based on the prepared particle morphology, PSD, hygroscopicity and surface energy under constant factors as flow rate, inhaler device and drug ratio in formulations.

Despite the PSD differences, the jet milled trehalose quality that showed irregular morphology with rougher surface than the SD quality lead to better aerosolization performance dispersing both the hydrophobic BU model drug and the hydrophilic SS model drug from prepared formulations. The concurrent steps of the formulations aerosolization can be briefed in particle fluidization, then drug dispersion and final deposition. It was observed that particle morphology in terms of aerodynamics had a great impact on the fluidization threshold and dispersion. Indeed, at similar particle size distribution, rod shaped particles of the hydrophilic SS were easier to fluidize and disperse compared to the spherical particles. Besides, hydrophobic BU particles in the concaved spheres morphology were slightly easier to fluidize than the irregular shaped fine particles. Additionally the morphological influence on aerosolization performance was interconnected with the crystallinity and hygroscopicity of the particles. The jet milled trehalose qualities showed crystalline less hygroscopic nature that had lower binding affinity to APIs compared to the amorphous SD quality. This was further proved when the partially recrystallized trehalose spherical particles showed improved aerosolization performance with SS compared to the amorphous spherical particles.

In case of formulations with 20% hydrophobic BU, all of the trehalose fine particle batches either SD or JM showed very good performance over 50% FPF. From the presented results, the finest jet milled trehalose particles that had a similar size range as the BU particles performed best with 81% FPF delivering 750 μ g fine dose. When considering the formulation of 20% hydrophilic SS, again the jet milled trehalose particles performed best, but with least variation between the relatively

large and small PSD batches (TR-5) and (TR1010) respectively. Both jet milled grades dispersed SS particles in the range of 50% FPF delivering 370 μ g fine dose. In general, the overall performance of the finest trehalose particles showed best dispersion behavior with the hydrophobic BU and the hydrophilic SS. On top, the carrier PSD influence on the aerosolization performance was interconnected to the APIs' particles surface energies either dispersive surface energy or polar interactions. In general fine particles possess high contact surface area that gives high dispersive surface energy. However, high surface energy does not necessarily mean poor dispersibility, it can relate to a high cohesive force that can be balanced with an opposing adhesion force to optimize the aerosolization performance. Hydrophobic BU particles exhibited adhesion attractions to the fine trehalose particles that balanced the intermediate cohesive forces resulting in small agglomerates that are easily dispersed upon aerosolization. On the other hand, hydrophilic SS-JM particles exhibited stronger adhesion attractions to the fine trehalose particles that slightly exceeded the intermediate cohesive forces, resulting in larger agglomerates with lower dispersibility compared to BU formulations. Furthermore, SS-SD particles showed least cohesion forces that were highly exceeded by the adhesion attractions when in blend with fine trehalose leading to poor dispersibility. As for the DSCG particles, the exceedingly high cohesive forces lead to capsule release failure upon aerosolization. This behavior was counteracted by high adhesion attractions exhibited by the addition of SD-trehalose particles in binary blends. However the cohesion/adhesion interactions were not balanced enough to disperse DSCG efficiently from the prepared formulations.

From the results and observations of this chapter, hydrophobic API as BU with inhalable particle size of less than 5 μ m, carrying relatively intermediate dispersive surface energy, may have given best reached aerosolization performance in combination with hydrophilic irregularly shaped carrier particles of trehalose in a similar fine particle size distribution. These formulations have showed least mechanical interlocking and van der Waals interactions that lead to optimum aerosol generation. On the other hand, the SS hydrophilic API model has shown most excellent results when in crystalline rod shaped particles again with the fine hydrophilic irregularly shaped carrier particles of trehalose. Nevertheless, hydrophilic API had more affinity to agglomerate and bind to the trehalose particles. As also investigated, the amorphous spherical fine particles of trehalose have shown

excellent aerosolization performance of formulations with the hydrophobic BU and was effective to reduce entrainment of highly hygroscopic DSCG. It is still slightly less performing compared to its crystalline irregular shaped particles, but now it might have potential with highly cohesive API particles for its added adhesion counter attractions.

In summary, optimum dispersibility and aerosolization performance, is achievable by balancing the formulations' cohesion-adhesion attractions. Certainly the interactions between particles are not limited to the total surface energy measured by IGC, but also to the positioning and orientation of the particles in contact based on morphology and size. Thus deviations from predicted performances by energy measurements can be practical by aerosolization performance studies.

6. Conclusion and future perspectives

Dry powder inhalation therapy with all its enumerated advantages is one of the most attractive pharmaceutical fields for development in treatment of many pathological diseases. The developmental processes targeting optimal aerosol generation are mainly focusing on two directions; developing an efficient dry powder formulation and developing an inhaler device with efficient mechanism. The study aims to utilize trehalose particles as an inert fine carrier to improve DPI aerosolization performance, diversify the potential delivery of new drugs in DPI formulations and the feasibility of bringing high drug dose into the lungs. In view of that, fine jet milled trehalose of different size qualities were produced, characterized and evaluated for optimized aerosolization of high OP dose in binary dry powder inhalation formulations. Hereafter, surface engineered particles of trehalose were produced by simple spray drying methodology and physicochemically characterized. Subsequently, the aerosolization behavior of fine spray dried and fine jet milled trehalose carrier based DPI formulations were assessed with low dose model pulmonary drugs under constant factors as flow rate, inhaler device and drug ratio in formulations. The aerosolization performance was correlated to the in formulation particles' morphology, size, hygroscopicity and surface energy.

Particle surface properties have an influential role in the performance variation between different produced batches. In general, jet milling lead to surface heterogeneity of particles implying a non-homogenous energy distribution and morphology. Two strategies regarding the de-agglomeration behavior of the particles can be concluded from the results of this study. First, active sites with high energy have higher preference to bind strongly with the API small particles than the surface sites with lower energy. Accordingly for the high OP dose formulation evaluated, the few high energy active sites of the fine trehalose particles would be saturated easily and the majority of the OP particles are binding relatively loose to the less energetic surface sites leading to lower adhesion and easier de-agglomeration. Secondly, irregular shaped particles or rough particles with asperities may lead to strong binding between particles by mechanical interlocking or it may limit the closeness of two particles and reduce the Van der Waals forces. It can be assumed that the irregular shaped fine particles of the trehalose reduced both the mechanical

interlocking and the Van der Waals forces by being placed into the higher ratio of the fine rod shaped OP particles. This would be achieved by introducing air space in between the particles that facilitate the de-agglomeration process upon aerosolization.

The production of smooth spherical SD trehalose particles was successful in the desired particle size range. The particles produced were amorphous particles which can be considered as an inferior option in terms of physical DPI carrier stability compared to the crystalline particles of trehalose. In trial to produce more stable crystalline particles, only partial recrystallization of the smooth spherical SD trehalose particles was achieved, maintaining the produced morphology and size range. Full crystallization of spherical smooth particles could not be achieved due to the formation of sticky stones like structures instead of the required flowing powder particles under further exposure to the crystallization conditions.

Fine trehalose particles that are in similar range as the API, can be very effective as carriers to disperse the drug fines from small fluidized agglomerates of low dose drugs. However crystalline, less hygroscopic trehalose carriers are preferred for their reduced polar interactions resulting in reduced adhesion attraction for the API. Furthermore, the morphology of the API particles has two important impacts; the ease of fluidization based on its aerodynamics and the positioning for reduced mechanical interlocking. Hydrophobic API as BU with inhalable particle size of less than 5 μ m, carrying relatively intermediate dispersive surface energy, may have given best reached aerosolization performance in combination with hydrophilic irregularly shaped carrier particles of trehalose in a similar fine particle size distribution. These formulations have showed least mechanical interlocking and van der Waals interactions that lead to optimum aerosol generation. On the other hand, the SS hydrophilic API model has shown most excellent results when in crystalline rod shaped particles again with the fine hydrophilic irregularly shaped carrier particles of trehalose. Nevertheless, hydrophilic API had more affinity to agglomerate and bind to the trehalose particles. As also investigated, the amorphous spherical fine particles of trehalose have shown excellent aerosolization performance of formulations with the hydrophobic BU and was effective to reduce entrainment of highly hygroscopic DSCG. It is still slightly less performing compared to its crystalline irregular shaped

particles, but now it might have potential with highly cohesive API particles for its added adhesion counter attractions.

In conclusion, we have come to an understanding that many interconnected factors significantly influence the aerosolization performance of various API formulations in DPI. In line with the formulation development, Jet milled Trehalose dihydrate crystalline particles have been proven as a strong potential for inert DPI formulation carrier. It has the capacity to aerosolize different API types at different binary ratios attaining excellent performance using low and medium resistance inhaler devices. The emphasis on studying different DPI carriers as trehalose has set new formulation approaches and options which will definitely lead to the introduction of new drugs through the inhalation rout leading to enhanced systematic and local therapy.

7. German Abstract

Die Studie hat zum Ziel, Trehalose-Partikel als inerte, feine Träger zu nutzen, um die die Aerosolisierung in Pulvern zur Inhalation zu verbessern. Die Studie zielt auch darauf ab, die Formulierung von neuen Wirkstoffen in Trockenpulverinhalaten zu vereinfachen und die Möglichkeit zu erforschen, hohe Wirkstoffdosen auf diese Weise in die Lunge zu bringen. Feine Trehalose-Partikel wurden durch Strahlmühlen und Sprühtrocknung erzeugt, um unterschiedliche physikalisch-chemische Eigenschaften zu erreichen. Die Trehalosepartikel wurden im Weiteren mit Modellarzneistoffen in trägerbasierten Mischungen formuliert und hinsichtlich ihrer aerodynamischen Eigenschaften untersucht. Die Gabe einer hohen Dosis von Oseltamivir, einem antiviralen Medikament, wurde weiter verbessert und in Präparaten mit 25% feinen Trehalose-Teilchen konnte eine Feinpartikelfraktion von etwa 75% erreicht werden (Bestimmung mit dem Kaskadenimpaktor). Die Dispergierung von Modellarzneistoffen wurde auf Basis ihrer hydrophilen und hydrophoben Eigenschaften und dem Einfluss dieser Parameter auf das Agglomerationsverhalten mit feinen Trehalosepartikeln ausgewertet. Dementsprechend zeigen Trehalose-basierte Mischungen in Abhängigkeit von den physikochemischen Eigenschaften der Trehalosepartikel (Teilchengröße, Morphologie, Oberflächenenergie, Kristallinität und Hydratation) eine Variabilität in der Feinpartikelfraktion zwischen 1% und 80%. Zusammenfassend sind maßgeschneiderte DPI-Präparate wesentlich für jeden Wirkstoff und die Partikeltechnik, sowohl des Trägers wie des Wirkstoffs, bestimmt die Leistungsfähigkeit der Präparate. Trehalose-Teilchen zeigen Kompatibilität, Stabilität und ein gutes Dispergierverhalten mit einer Vielzahl von Wirkstoffen und Wirkstoffdosen. Es wird geschlussfolgert, dass feine Trehalose - Teilchen das Potenzial haben, hervorragende, inerte und sichere Träger für die Formulierung von neuen und bekannten Wirkstoffen in DPI- Präparaten zu sein.

Appendix

A. List of Abbreviations

API	Active pharmaceutical ingredient
BET	Brunauer–Emmett–Teller (theory)
BU	Budesonide
COPD	Chronic obstructive pulmonary diseases
DOE	Design of experiment
DPI	Dry powder inhalers
DSC	Differential scanning calorimeter
DSCG	Disodium cromoglycate
DVS	Dynamic vapor sorption
ERV	expiratory reserve volume
FID	Flame ionization detector
FPD	Fine particle dose
FPF	Fine particle fraction
IGC	Inverse gas chromatography
IRV	Inspiratory reserve volume
JM	Jet mill
MMAD	mean median aerodynamic diameter
OP	Oseltamivir phosphate
pMDI	pressurized Metered dose inhalers
PSD	Particle size distribution
RH	Relative humidity
RSD	Relative standard deviation

RV	Residual volume
SA	Surface area
SCF	Supercritical fluid technologies
SD	Spray drying
SEM	Scanning electron microscope
SFD	Spray freeze drying
SS	Salbutamol sulphate
TGA	Thermo gravimetric analysis
TLC	Total lung capacity
TR	Trehalose
VC	Vital capacity
XRPD	X-ray powder diffraction

B. List of Figures

FIGURE 1-1: RESPIRATORY ZONES WITH BRANCHING HIERARCHY SHOWING THE PARTICLE DEPOSITION MECHANISM IN DIFFERENT AREAS BASED ON AERODYNAMIC PARTICLE SIZE (ADAPTED FROM BARRETT AND GANONG 2010)	4
FIGURE 1-2: MOVEMENT OF MUSCLES, DIAPHRAGM AND RIB CAGE DURING INHALATION AND EXHALATION (DESPOPOULOS AND SILBERNAGL, 2003).....	5
FIGURE 1-3: PRINCIPLE MECHANISM OF DPI DESIGN (TELKO AND HICKEY, 2005).....	9
FIGURE 1-4: LIST OF SOME DPI DEVICES AVAILABLE IN THE MARKET; SINGLE DOSE CAPSULE DEVICES; 1) <u>AEROLIZER®</u> (LOW RESISTANCE), 2) <u>HANDIHALER®</u> (HIGH RESISTANCE), MULTI-DOSE RESERVOIR/CARTRIDGE; 3) <u>NOVOLIZER®</u> (MEDIUM RESISTANCE), 4) <u>TURBUHALER®</u> (MEDIUM RESISTANCE), 5) <u>EASYHALER®</u> (MEDIUM RESISTANCE), MULTI-DOSES ENCAPSULATED IN FOIL BLISTERS; 6) <u>DISKUS®</u> (LOW RESISTANCE).....	10
FIGURE 2-1: JET MILL SCHEMATIC DIAGRAM.....	16
FIGURE 2-2: APPLICATION SYSTEM "RACK" (STECKEL AND BOLZEN 2004).....	22
FIGURE 2-3: (A) DIFFERENT PARTS OF THE UNIHALER, (B) ASSEMBLY AND FUNCTIONAL PRINCIPLE OF THE UNIHALER.	22
FIGURE 2-4: STEPS 1 TO 4 SHOWING THE ASSEMBLY OF THE PRESEPARATOR AND THE THROAT TO THE INHALATION MODULE OF THE SYMPATEC LASER DIFFRACTION SYSTEM. (1 & 2) A PLASTIC RING AND A RUBBER RING ARE PLACED TO HAVE AN AIR TIGHT CONNECTION WITH THE PRESEPARATOR. (3) CONNECTING THE PRESEPARATOR. (4) OVERALL VIEW BEFORE PLACING THE INHALER.....	23
FIGURE 2-5: NGI CLOSED (LEFT) AND OPENED (RIGHT) SCHEMATIC DIAGRAM	24
FIGURE 3-1: BIOCONVERSION OF OSELTAMIVIR INTO OSELTAMIVIR CARBOXYLATE (EISENBERG, 2007).	28
FIGURE 3-2: DSC THERMOGRAMS AT 5°C MIN ⁻¹ (LEFT SIDE) AT 10°C MIN ⁻¹ (MIDDLE) AND 100°C MIN ⁻¹ (RIGHT SIDE) FOR DIFFERENT TREHALOSE BATCHES	33
FIGURE 3-3: ONSET OF DEHYDRATION TEMPERATURES FOR T _A CRYSTALS RELATIVE TO THE TREHALOSE GRADE (PARTICLE SIZE)	34
FIGURE 3-4: TGA OF (A) TR16400 AND (B) TR1010 SHOWING THE PERCENT WEIGHT LOSS (Y-AXIS) WITH INCREASING TEMPERATURE °C (X-AXIS).	35
FIGURE 3-5: DVS PROFILE OF DIFFERENT MICRONIZED PARTICLE GRADE TREHALOSE DIHYDRATE.....	35
FIGURE 3-6: XRPD SPECTRA OF TREHALOSE DIHYDRATE BEFORE MICRONIZATION (TR16400) AND AFTER MICRONIZATION (TR5 AND TR1010).....	36
FIGURE 3-7: PERCENT DE-AGGLOMERATION OF TESTED TREHALOSE GRADES UNDER DIFFERENT AIRFLOW RATES.....	36
FIGURE 3-8: DSC THERMOGRAMS OF OP GRADES	37
FIGURE 3-9: XRPD SPECTRA FOR OP AND OP1010	37
FIGURE 3-10: AVERAGE PERCENT DE-AGGLOMERATION OF ALL OP BLENDS PREPARED AT AIRFLOW 57L/MIN USING THE UNI-HALER (N=3).....	39
FIGURE 3-11: AVERAGE FPF% ± SD OF AEROSOLIZED OP/TR FORMULATIONS USING UNI-HALER @ 57L/MIN (N=3).....	40
FIGURE 3-12: AVERAGE FPD ± SD (MG) OF AEROSOLIZED OP/TR FORMULATIONS USING UNI-HALER @ 57L/MIN (N=3).....	40

FIGURE 3-13: AVERAGE MMAD \pm SD (μM) OF AEROSOLIZED OP/TR FORMULATIONS USING UNI-HALER @ 57L/MIN (N=3).....	40
FIGURE 3-14: AVERAGE FPF% \pm SD OF AEROSOLIZED OP/TR FORMULATIONS USING AEROLIZER @ 100L/MIN (N=3).....	41
FIGURE 3-15: AVERAGE FPD \pm SD (MG) OF AEROSOLIZED OP/TR FORMULATIONS USING AEROLIZER @ 100L/MIN (N=3).....	41
FIGURE 3-16: AVERAGE MMAD \pm SD (μM) OF AEROSOLIZED OP/TR FORMULATIONS USING AEROLIZER @ 100L/MIN (N=3).....	42
FIGURE 3-17: OP1010/TR5 - STAGE DISTRIBUTION BY UNIHALER @ 57L/MIN (N=3)	42
FIGURE 3-18: OP1010/TR5 - STAGE DISTRIBUTION BY AEROLIZER @ 100L/MIN (N=3).....	43
FIGURE 3-19: SEM IMAGES OF JET MILLED TREHALOSE QUALITIES (TR5 AND TR1010) AND IN OP1010 BLENDS UNDER MAGNIFICATION POWER 1KX (LEFT) AND 5KX (RIGHT).	44
FIGURE 4-1: SPRAY DRYING PROCESS SCHEMATIC DIAGRAM	48
FIGURE 4-2: DOE GRAPHS PRESENTING COEFFICIENTS SIGNIFICANTLY AFFECTING SD TREHALOSE PSD OUTCOME OF D10, D50 AND D90 WITH EXCELLENT MODEL FIT AND PRECISION ($R^2 > 0.9$ & $Q^2 \geq 0.75$); ON THE X-AXIS (A) CONCENTRATION, (B) GAS FLOW AND (B-B) GAS FLOW – GAS FLOW INTERACTION, WHILE THE Y-AXIS SHOWS THE CHANGE IN μM	51
FIGURE 4-3: XRPD SPECTRA OF SD TREHALOSE AND RAW TREHALOSE DIHYDRATE.....	52
FIGURE 4-4: DVS PROFILE OF SPRAY DRIED TREHALOSE BATCHES AND TREHALOSE DIHYDRATE (TR - RAW)	53
FIGURE 4-5: SEM IMAGES OF SPRAY DRIED TREHALOSE (TRSD) BATCHES.	54
FIGURE 4-6: MDSC THERMOGRAM OF TRSD (M-2914)	55
FIGURE 4-7: MDSC THERMOGRAM OF TRSD (M-2914) CONDITIONED AT 50%RH FOR 6HRS.....	56
FIGURE 4-8: SEM IMAGES OF RECRYSTALLIZED-TRSD CONDITIONED AT 50%RH FOR 6HRS (REC.M-2914).	56
FIGURE 4-9: TREHALOSE PHASE AND STATE TRANSITION UNDER THERMAL AND HUMIDITY CONDITIONS (ADAPTED FROM FURUKI ET AL., 2005)	57
FIGURE 5-1: SCHEMATIC DIAGRAM OF THE FOUR MAIN BINARY BLEND CATEGORIES PREPARED AND TESTED FOR AEROSOLIZATION PERFORMANCE; A) JET MILLED API/ JET MILLED TREHALOSE, B) SPRAY DRIED API / JET MILLED TREHALOSE, C) JET MILLED API / SPRAY DRIED TREHALOSE, D) SPRAY DRIED API / SPRAY DRIED TREHALOSE	62
FIGURE 5-2: SCHEMATIC DIAGRAM OF A) AEROLIZER® AND B) EASYHALER®, SHOWING I) PRESSING DIRECTION AND II) POWDER FLOW AND EXIT.	63
FIGURE 5-3: SEM IMAGES OF SPRAY DRIED (LEFT) AND JET MILLED (RIGHT) API PARTICLES UNDER 10000X MAGNIFICATION POWER.....	66
FIGURE 5-4: FPF% CHART FOR BUDESONIDE WITH DIFFERENT TREHALOSE BATCHES AND CARRIER FREE FORMULATIONS, AEROSOLIZED AT 100L/MIN BY AEROLIZER (N=3 \pm SD).....	69
FIGURE 5-5: FPD CHART FOR BUDESONIDE WITH DIFFERENT TREHALOSE BATCHES AND CARRIER FREE FORMULATIONS, AEROSOLIZED AT 100L/MIN BY AEROLIZER (N=3 \pm SD).....	70
FIGURE 5-6: FPF% CHART FOR BUDESONIDE FORMULATIONS WITH SPRAY DRIED TREHALOSE BATCHES, AEROSOLIZED AT 45L/MIN BY EASYHALER (N=3 \pm SD).	71

FIGURE 5-7: FPD CHART FOR BUDESONIDE FORMULATIONS WITH SPRAY DRIED TREHALOSE BATCHES, AEROSOLIZED AT 45L/MIN BY EASYHALER (N=3 ±SD).	71
FIGURE 5-8: FPF% CHART FOR SALBUTAMOL SULPHATE WITH DIFFERENT TREHALOSE BATCHES AND CARRIER FREE FORMULATIONS, AEROSOLIZED AT 100L/MIN BY AEROLIZER (N=3 ±SD).	73
FIGURE 5-9: FPD CHART FOR SALBUTAMOL SULPHATE WITH DIFFERENT TREHALOSE BATCHES AND CARRIER FREE FORMULATIONS, AEROSOLIZED AT 100L/MIN BY AEROLIZER (N=3 ±SD).	74
FIGURE 5-10: FPF% CHART FOR DISODIUM CROMOGLYCATE WITH SPRAY DRIED TREHALOSE BATCHES, AEROSOLIZED AT 100L/MIN BY AEROLIZER (N=3 ±SD).	76
FIGURE 5-11: DSCG - NGI STAGE DISTRIBUTION AT 100L/MIN BY AEROLIZER (N=3)	77
FIGURE 5-12: SEM IMAGES UNDER MAGNIFICATION POWER 1000X (LEFT) AND 5000X (RIGHT) OF 10 BLENDS AS LISTED.....	82
FIGURE 5-13: DISPERSIVE SURFACE ENERGY OF DIFFERENT JM AND SD TREHALOSE BATCHES.....	85
FIGURE 5-14: DISPERSIVE SURFACE ENERGY OF JM AND SD QUALITIES OF BU, SS AND DSCG	85

C. List of Materials

Brij 35	ICI specialty chemicals, Essen, Germany
Budesonide	Shanghai Hengtian Pharmaceutical Co. Ltd., Shanghai, China
bidistilled water	Freshly produced with the in-house Finn Aqua 75, San-Asalo – Sohlberg corp., Helsinki, Finland
Disodium Cromoglycate (Batch #: 4050/09/07)	Welding GmbH & CO. KG, Hamburg, Germany
Ethanol (96%)	Merck, KGaA, Darmstadt, Germany
Glycerol	Merck, KGaA, Darmstadt, Germany
Methanol –HPLC Grade	J.T. Baker, Deventer, The Netherlands
O-Phosphoric acid	Merck KGaA. Darmstadt, Germany
Oseltamivir phosphate (OP)	Nile Co. for Pharmaceuticals and chemical industries, Cairo, Egypt
Potassium dihydrogen phosphate Salbutamol Sulphate	FAGRON, Barsbüttel, Germany Lusochimica S.P.A. Lomagna, Italy
Triethylamine (99%)	Sigma Aldrich Chemie GmbH, Steinheim, Germany
Trehalose (TREHA™) (C ₁₂ H ₂₆ O ₁₃ ; molecular weight, 378.33g/mol; ≥98.5% purity)	Cargill, Deutschland GmbH

D. List of Equipment

Büchi B-290 Mini spray dryer	Büchi Labortechnik AG, Switzerland
Next Generation Cascade Impactor	Copley Scientific, USA
Climate controlled chamber	Developed by Imtech and operated by Siemens Simatic touch panel to control temperature and RH%.
Critical flow controller TPK	Copley Scientific, USA
Differential scanning calorimeter	Diamond DSC, Perkin Elmer, USA
Dynamic Vapor Sorption	DVS-HT, surface measurement systems Ltd., London, UK
Flow meter	Copley Scientific, USA
FT4 Powder Rheometer	Freeman Technology, UK
Gas sorption analyzer	NOVA 2200, Quantachrome Corporation, USA
Helos-Laser diffraction	Aerosol dispersing units are RODOS and INHALER modules, Sympatec GmbH "System-Partikel-Technik", Germany.
IGC column packer	Surface Measurement Systems, USA
Inverse Gas Chromatography (IGC)	Surface Measurement Systems "IGC 2000 SMS", USA
Jet-mill	Aljet mill, Fluid Energy processing and equipment company, USA.
Mass Comparator balance	AT-106 comparator, Mettler Toledo, USA
Scanning electron microscope (SEM)	Ultra Plus SEM, Carl Zeiss NTS GmbH, Oberkochen, Germany
Thermo-gravimetric analysis	TGA - TAC7/DX – Perkin Elmer, USA
Turbula mixer	Turbula T2C, Willy A Bachofen AG, Basel, Switzerland

UNI-Haler (Patent no. DE 10 2009 037 840.5)	Newly developed Inhaler at the Department of Pharmaceutics & Biopharmaceutics, Kiel, Germany.
UV/VIS-Spectrophotometer	Lambda 40, Perkin Elmer instruments, USA
Vacuum Pump HCP5	Copley Scientific, USA
X-ray diffractometer	Stoe and Cie GmbH, Darmstadt, Germany

8. References

- Andrade, F., Rafael, D., Videira, M., Ferreira, D., Sosnik, A., Sarmiento, B., 2013. Nanotechnology and pulmonary delivery to overcome resistance in infectious diseases. *Advanced drug delivery reviews* 65 (13-14), 1816–1827.
- Ashurst, I., Malton, A., Prime, D., Sumbly, B., 2000. Latest advances in the development of dry powder inhalers. *Pharmaceutical Science & Technology Today* 3 (7), 246–256.
- Aziz, S., 2011. Novel Delivery of Oseltamivir Phosphate Dry Powder Inhalation – Formulation and In-Vitro Characterization, Cairo, Egypt.
- Barrett, K.E., Ganong, W.F., 2010. *Ganong's review of medical physiology*, 23rd ed. ed. McGraw-Hill Medical, New York, 1 online resource (ix, 714).
- Beck-Broichsitter, M., Gauss, J., Packhaeuser, C.B., Lahnstein, K., Schmehl, T., Seeger, W., Kissel, T., Gessler, T., 2009. Pulmonary drug delivery with aerosolizable nanoparticles in an ex vivo lung model. *International journal of pharmaceutics* 367 (1-2), 169–178.
- Beigel, J., Bray, M., 2008. Current and future antiviral therapy of severe seasonal and avian influenza. *Antiviral Research* 78 (1), 91–102.
- Braun, M.A., Oschmann, R., Schmidt, P., 1996. Influence of excipients and storage humidity on the deposition of disodium cromoglycate (DSCG) in the Twin Impinger. *International journal of pharmaceutics* 135 (1-2), 53–62.
- Chew, Nora Y K, Tang, P., Chan, H.-K., Raper, J.A., 2005. How much particle surface corrugation is sufficient to improve aerosol performance of powders? *Pharmaceutical research* 22 (1), 148–152.
- Claus, S., Weiler, C., Schiewe, J., Friess, W., 2014. How can we bring high drug doses to the lung? *European journal of pharmaceutics and biopharmaceutics : official journal of Arbeitsgemeinschaft für Pharmazeutische Verfahrenstechnik e.V* 86 (1), 1–6.
- Clercq, E. de, 2006. Antiviral agents active against influenza A viruses. *Nature reviews. Drug discovery* 5 (12), 1015–1025.
- Cline, D., Dalby, R., 2002. Predicting the quality of powders for inhalation from surface energy and area. *Pharmaceutical research* 19 (9), 1274–1277.

- Cordts, E., Steckel, H., 2012. Capabilities and limitations of using powder rheology and permeability to predict dry powder inhaler performance. *European journal of pharmaceuticals and biopharmaceutics* 82 (2), 417–423.
- Costanzo, L.S., 2006. *Physiology*, 3rd ed ed. Saunders Elsevier, Philadelphia, PA, xi, 490.
- Das, S., Larson, I., Young, P., Stewart, P., 2009. Surface energy changes and their relationship with the dispersibility of salmeterol xinafoate powders for inhalation after storage at high RH. *European journal of pharmaceutical sciences : official journal of the European Federation for Pharmaceutical Sciences* 38 (4), 347–354.
- Despopoulos, A., Silbernagl, S., 2003. *Color atlas of physiology*, 5 // 5th ed., completely rev. and expanded ed. Georg Thieme Verlag; Thieme, Stuttgart, xiii, 436.
- Dolovich, M.B., Dhand, R., 2011. Aerosol drug delivery: developments in device design and clinical use. *The Lancet* 377 (9770), 1032–1045.
- Dreitlein, W.B., Maratos, J., Brocavich, J., 2001. Zanamivir and oseltamivir: two new options for the treatment and prevention of influenza. *Clinical Therapeutics* 23 (3), 327–355.
- Duddu, S.P., Sisk, S.A., Walter, Y.H., Tarara, T.E., Trimble, K.R., Clark, A.R., Eldon, M.A., Elton, R.C., Pickford, M., Hirst, P.H., Newman, S.P., Weers, J.G., 2002. Improved lung delivery from a passive dry powder inhaler using an Engineered PulmoSphere powder. *Pharmaceutical research* 19 (5), 689–695.
- Dutkowski, R., Smith, J.R., Davies, B.E., 2010. Safety and pharmacokinetics of oseltamivir at standard and high dosages. *International journal of antimicrobial agents* 35 (5), 461–467.
- Eisenberg, E., 2007. Case Study: Oseltamivir: An Orally Bioavailable Ester Prodrug of Oseltamivir Carboxylate, in: Stella, V., Borchardt, R., Hageman, M., Oliyai, R., Maag, H., Tilley, J. (Eds.), *Prodrugs*, V. Springer New York, pp. 1323-1334.
- Englund, J.A., 2002. Antiviral therapy of influenza. *Seminars in pediatric infectious diseases* 13 (2), 120–128.
- Florence, A.T., Siepmann, J., 2009. *Modern pharmaceuticals*, 5. ed ed. Informa Healthcare USA, New York, 2 bd.
- Forbes, B., Ehrhardt, C., 2005. Human respiratory epithelial cell culture for drug delivery applications. *European journal of pharmaceuticals and biopharmaceutics* :

- official journal of Arbeitsgemeinschaft für Pharmazeutische Verfahrenstechnik e.V
60 (2), 193–205.
- Fowkes, F.M., 1964. ATTRACTIVE FORCES AT INTERFACES. *Ind. Eng. Chem.* 56 (12), 40–52.
- Furuki, T., Kishi, A., Sakurai, M., 2005. De- and rehydration behavior of alpha,alpha-trehalose dihydrate under humidity-controlled atmospheres. *Carbohydrate Research* 340 (3), 429–438.
- Geller, D.E., 2005. Comparing clinical features of the nebulizer, metered-dose inhaler, and dry powder inhaler. *Respiratory care* 50 (10), 1313-21; discussion 1321-2.
- Gill, P., Moghadam, T.T., Ranjbar, B., 2010. Differential scanning calorimetry techniques: applications in biology and nanoscience. *Journal of biomolecular techniques : JBT* 21 (4), 167–193.
- Gillissen, A., Höffken, G., 2002. Early therapy with the neuraminidase inhibitor oseltamivir maximizes its efficacy in influenza treatment. *Medical microbiology and immunology* 191 (3-4), 165–168.
- Gradon, L., Sosnowski, T.R., 2014. Formation of particles for dry powder inhalers. *Advanced Powder Technology* 25 (1), 43–55.
- Grimsey, I.M., Feeley, J.C., York, P., 2002. Analysis of the surface energy of pharmaceutical powders by inverse gas chromatography. *Journal of pharmaceutical sciences* 91 (2), 571–583.
- Hassan, M.S., Lau, R., 2011. Inhalation performance of pollen-shape carrier in dry powder formulation: effect of size and surface morphology. *International journal of pharmaceutics* 413 (1-2), 93–102.
- Heyder, J., Gebhart, J., Rudolf, G., Schiller, C., Stahlhofen, W., 1986. Deposition of particles in the human respiratory tract in the size range 0.005–15 µm. *Journal of Aerosol Science* 17 (5), 811–825.
- Hosokawa, M., 2008. Structure and catalytic properties of carboxylesterase isozymes involved in metabolic activation of prodrugs. *Molecules (Basel, Switzerland)* 13 (2), 412–431.
- Islam, N., Cleary, M.J., 2012. Developing an efficient and reliable dry powder inhaler for pulmonary drug delivery – A review for multidisciplinary researchers. *Medical engineering & physics* 34 (4), 409–427.

- Islam, N., Gladki, E., 2008. Dry powder inhalers (DPIs)--a review of device reliability and innovation. *International journal of pharmaceutics* 360 (1-2), 1–11.
- Jain, N.K., Roy, I., 2009. Effect of trehalose on protein structure. *Protein science : a publication of the Protein Society* 18 (1), 24–36.
- Jones, M.D., Harris, H., Hooton, J.C., Shur, J., King, G.S., Mathoulin, C.A., Nichol, K., Smith, T.L., Dawson, M.L., Ferrie, A.R., Price, R., 2008. An investigation into the relationship between carrier-based dry powder inhalation performance and formulation cohesive-adhesive force balances. *European journal of pharmaceutics and biopharmaceutics : official journal of Arbeitsgemeinschaft für Pharmazeutische Verfahrenstechnik e.V* 69 (2), 496–507.
- Jones, M.D., Hooton, J.C., Dawson, M.L., Ferrie, A.R., Price, R., 2006. Dehydration of trehalose dihydrate at low relative humidity and ambient temperature. *International journal of pharmaceutics* 313 (1-2), 87–98.
- Jones, M.D., Santo, João G F, Yakub, B., Dennison, M., Master, H., Buckton, G., 2010. The relationship between drug concentration, mixing time, blending order and ternary dry powder inhalation performance. *International journal of pharmaceutics* 391 (1-2), 137–147.
- Kaialy, W., Alhalaweh, A., Velaga, S.P., Nokhodchi, A., 2012. Influence of lactose carrier particle size on the aerosol performance of budesonide from a dry powder inhaler. *Powder Technology*, 74–85.
- Kaialy, W., Momin, M.N., Ticehurst, M.D., Murphy, J., Nokhodchi, A., 2010. Engineered mannitol as an alternative carrier to enhance deep lung penetration of salbutamol sulphate from dry powder inhaler. *Colloids and surfaces. B, Biointerfaces* 79 (2), 345–356.
- Kawashima, Y., Serigano, T., Hino, T., Yamamoto, H., Takeuchi, H., 1998. Effect of surface morphology of carrier lactose on dry powder inhalation property of pranlukast hydrate. *International journal of pharmaceutics* 172 (1-2), 179–188.
- Kou, X., Chan, L.W., Steckel, H., Heng, Paul W S, 2012. Physico-chemical aspects of lactose for inhalation. *Advanced drug delivery reviews* 64 (3), 220–232.
- Lahnstein, K., Schmehl, T., Rüsç, U., Rieger, M., Seeger, W., Gessler, T., 2008. Pulmonary absorption of aerosolized fluorescent markers in the isolated rabbit lung. *International journal of pharmaceutics* 351 (1-2), 158–164.

- Larhrib, H., Martin, G.P., Marriott, C., Prime, D., 2003. The influence of carrier and drug morphology on drug delivery from dry powder formulations. *International journal of pharmaceutics* 257 (1-2), 283–296.
- Li, X., Mansour, H.M., 2011. Physicochemical characterization and water vapor sorption of organic solution advanced spray-dried inhalable trehalose microparticles and nanoparticles for targeted dry powder pulmonary inhalation delivery. *AAPS PharmSciTech* 12 (4), 1420–1430.
- Li, X., Vogt, F.G., Hayes, D., Mansour, H.M., 2014. Design, characterization, and aerosol dispersion performance modeling of advanced spray-dried microparticulate/nanoparticulate mannitol powders for targeted pulmonary delivery as dry powder inhalers. *Journal of aerosol medicine and pulmonary drug delivery* 27 (2), 81–93.
- Lindemann, L., Jacobsen, H., Schuhbauer, D., Knoflach, F., Gatti, S., Wettstein, J.G., Loetscher, H., Chu, T., Ebeling, M., Paulson, J.C., Prinssen, E., Brockhaus, M., 2010. In vitro pharmacological selectivity profile of oseltamivir prodrug (Tamiflu) and active metabolite. *European journal of pharmacology* 628 (1-3), 6–10.
- Littringer, E., Mescher, A., Schroettner, H., Achelis, L., Walzel, P., Urbanetz, N., 2012. Spray dried mannitol carrier particles with tailored surface properties – The influence of carrier surface roughness and shape. *European journal of pharmaceutics and biopharmaceutics* 82 (1), 194–204.
- Malcolmson, R.J., Embleton, J.K., 1998. Dry powder formulations for pulmonary delivery. *Pharmaceutical Science & Technology Today* 1 (9), 394–398.
- Mansour, H.M., Xu, Z., Hickey, A.J., 2010. Dry powder aerosols generated by standardized entrainment tubes from alternative sugar blends: 3. Trehalose dihydrate and D-mannitol carriers. *Journal of pharmaceutical sciences* 99 (8), 3430–3441.
- Maury, M., Murphy, K., Kumar, S., Mauerer, A., Lee, G., 2005. Spray-drying of proteins: effects of sorbitol and trehalose on aggregation and FT-IR amide I spectrum of an immunoglobulin G. *European journal of pharmaceutics and biopharmaceutics* 59 (2), 251–261.
- Minne, A., Boireau, H., Horta, M.J., Vanbever, R., 2008. Optimization of the aerosolization properties of an inhalation dry powder based on selection of excipients. *European journal of pharmaceutics and biopharmaceutics* 70 (3), 839–844.

- Nadarassan, D.K., Assi, K.H., Chrystyn, H., 2010. Aerodynamic characteristics of a dry powder inhaler at low inhalation flows using a mixing inlet with an Andersen Cascade Impactor. *European Journal of Pharmaceutical Sciences* 39 (5), 348–354.
- Nandiyanto, A.B., Okuyama, K., 2011. Progress in developing spray-drying methods for the production of controlled morphology particles: From the nanometer to submicrometer size ranges. *Advanced Powder Technology* 22 (1), 1–19.
- Nykamp, G., Carstensen, U., Müller, B., 2002. Jet milling—a new technique for microparticle preparation. *International journal of pharmaceutics* 242 (1-2), 79–86.
- Ogáin, O.N., Li, J., Tajber, L., Corrigan, O.I., Healy, A.M., 2011. Particle engineering of materials for oral inhalation by dry powder inhalers. I-Particles of sugar excipients (trehalose and raffinose) for protein delivery. *International journal of pharmaceutics* 405 (1-2), 23–35.
- Oo, C., Snell, P., Barrett, J., Dorr, A., Liu, B., Wilding, I., 2003. Pharmacokinetics and delivery of the anti-influenza prodrug oseltamivir to the small intestine and colon using site-specific delivery capsules. *International journal of pharmaceutics* 257 (1-2), 297–299.
- Oxford, J.S., Lambkin, R., 1998. Targeting influenza virus neuraminidase—a new strategy for antiviral therapy. *Drug discovery today* 3 (10), 448–456.
- Pilcer, G., Amighi, K., 2010. Formulation strategy and use of excipients in pulmonary drug delivery. *International journal of pharmaceutics* 392 (1-2), 1–19.
- Rahimpour, Y., Kouhsoltani, M., Hamishehkar, H., 2014. Alternative carriers in dry powder inhaler formulations. *Drug discovery today* 19 (5), 618–626.
- Raula, J., Lähde, A., Kauppinen, E.I., 2009. Aerosolization behavior of carrier-free l-leucine coated salbutamol sulphate powders. *International journal of pharmaceutics* 365 (1-2), 18–25.
- Sanders, M., 2007. Inhalation therapy: an historical review. *Primary care respiratory journal : journal of the General Practice Airways Group* 16 (2), 71–81.
- Schebor, C., Mazzobre, M.F., Buera, M.d., 2010. Glass transition and time-dependent crystallization behavior of dehydration bioprotectant sugars. *Carbohydrate Research* 345 (2), 303–308.
- Shi, D., Yang, J., Yang, D., LeCluyse, E.L., Black, C., You, L., Akhlaghi, F., Yan, B., 2006. Anti-influenza prodrug oseltamivir is activated by carboxylesterase human carboxylesterase 1, and the activation is inhibited by antiplatelet agent

- clopidogrel. *The Journal of pharmacology and experimental therapeutics* 319 (3), 1477–1484.
- Srichana, T., Martin, G., Marriott, C., 1998. Dry powder inhalers: The influence of device resistance and powder formulation on drug and lactose deposition in vitro. *European Journal of Pharmaceutical Sciences* 7 (1), 73–80.
- Steckel, H., Bolzen, N., 2004. Alternative sugars as potential carriers for dry powder inhalations. *International journal of pharmaceutics* 270 (1-2), 297–306.
- Steckel, H., Brandes, H.G., 2004. A novel spray-drying technique to produce low density particles for pulmonary delivery. *International journal of pharmaceutics* 278 (1), 187–195.
- Steckel, H., Müller, B.W., 1997. In vitro evaluation of dry powder inhalers II: influence of carrier particle size and concentration on in vitro deposition. *International journal of pharmaceutics* 154 (1), 31–37.
- Stegemann, S., Kopp, S., Borchard, G., Shah, V., Senel, S., Dubey, R., Urbanetz, N., Cittero, M., Schoubben, A., Hippchen, C., Cade, D., Fuglsang, A., Morais, J., Borgström, L., Farshi, F., Seyfang, K.-H., Hermann, R., van de Putte, A., Klebovich, I., Hincal, A., 2013. Developing and advancing dry powder inhalation towards enhanced therapeutics. *European Journal of Pharmaceutical Sciences* 48 (1-2), 181–194.
- Sussich, F., Cesàro, A., 2008. Trehalose amorphization and recrystallization. *Carbohydrate Research* 343 (15), 2667–2674.
- Sussich, F., Urbani, R., Princivalle, F., Cesàro, A., 1998. Polymorphic Amorphous and Crystalline Forms of Trehalose. *J. Am. Chem. Soc.* 120 (31), 7893–7899.
- Swaminathan, V., Cobb, J., Saracovan, I., 2006. Measurement of the surface energy of lubricated pharmaceutical powders by inverse gas chromatography. *International journal of pharmaceutics* 312 (1-2), 158–165.
- Tee, S.K., Marriott, C., Zeng, X.M., Martin, G.P., 2000. The use of different sugars as fine and coarse carriers for aerosolised salbutamol sulphate. *International journal of pharmaceutics* 208 (1-2), 111–123.
- Telko, M.J., Hickey, A.J., 2005. Dry powder inhaler formulation. *Respiratory care* 50 (9), 1209–1227.
- Thi, T.H., Danède, F., Descamps, M., Flament, M.-P., 2008. Comparison of physical and inhalation properties of spray-dried and micronized terbutaline sulphate. *European journal of pharmaceutics and biopharmaceutics* 70 (1), 380–388.

- Tiddens, H.A., Geller, D.E., Challoner, P., Speirs, R.J., Kesser, K.C., Overbeek, S.E., Humble, D., Shrewsbury, S.B., Standaert, T.A., 2006. Effect of dry powder inhaler resistance on the inspiratory flow rates and volumes of cystic fibrosis patients of six years and older. *Journal of aerosol medicine : the official journal of the International Society for Aerosols in Medicine* 19 (4), 456–465.
- Traini, D., Young, P.M., Jones, M., Edge, S., Price, R., 2006. Comparative study of erythritol and lactose monohydrate as carriers for inhalation: Atomic force microscopy and in vitro correlation. *European Journal of Pharmaceutical Sciences* 27 (2-3), 243–251.
- United States Pharmacopeial Convention, 2014. The United States pharmacopeia: The national formulary, USP 37 - NF 24 ed. United States Pharmacopeial Convention, Rockville, 3 v ;
- Vatsaraj, N.B., Gao, D., Kowalski, D.L., 2003. Optimization of the operating conditions of a lab scale Aljet mill using lactose and sucrose: a technical note. *AAPS PharmSciTech* 4 (2), E27.
- Vehring, R., 2008. Pharmaceutical Particle Engineering via Spray Drying. *Pharm Res* 25 (5), 999–1022.
- Vehring, R., Foss, W.R., Lechuga-Ballesteros, D., 2007. Particle formation in spray drying. *Journal of Aerosol Science* 38 (7), 728–746.
- Verhoeven, N., Neoh, T.L., Furuta, T., Yamamoto, C., Ohashi, T., Yoshii, H., 2012. Characteristics of dehydration kinetics of dihydrate trehalose to its anhydrous form in ethanol by DSC. *Food Chemistry* 132 (4), 1638–1643.
- Vicente, J., Pinto, J., Menezes, J., Gaspar, F., 2013. Fundamental analysis of particle formation in spray drying. *Powder Technology*, 1–7.
- Yang, M.Y., Chan, J.G., Chan, H.-K., 2014. Pulmonary drug delivery by powder aerosols. *Journal of Controlled Release*, 228–240.
- Young, P.M., Cocconi, D., Colombo, P., Bettini, R., Price, R., Steele, D.F., Tobyn, M.J., 2002. Characterization of a surface modified dry powder inhalation carrier prepared by "particle smoothing". *The Journal of pharmacy and pharmacology* 54 (10), 1339–1344.
- Zeng, X.M., Martin, G.P., Marriott, C., Pritchard, J., 2000a. The effects of carrier size and morphology on the dispersion of salbutamol sulphate after aerosolization at different flow rates. *The Journal of pharmacy and pharmacology* 52 (10), 1211–1221.

- Zeng, X.M., Martin, G.P., Marriott, C., Pritchard, J., 2000b. The influence of carrier morphology on drug delivery by dry powder inhalers. *International journal of pharmaceutics* 200 (1), 93–106.
- Zhu, H.-J., Markowitz, J.S., 2009. Activation of the antiviral prodrug oseltamivir is impaired by two newly identified carboxylesterase 1 variants. *Drug metabolism and disposition: the biological fate of chemicals* 37 (2), 264–267.

Acknowledgement

At first, I praise God, from whom all the blessings flow

I am heartily thankful to my supervisor, Prof. Dr. Hartwig Steckel, whose guidance and support from the initial to the final level of my PhD project enabled me to develop skills and understandings in line with my career prospective.

I owe my deepest gratitude to all the working team in the Pharmaceutics and Biopharmaceutics department in Kiel for their continuous support and invaluable assistance during my work and stay in Kiel. Special thanks to Dr. Regina Scherließ, who showed me support and care in a number of ways making life experiences in Kiel go easy and enjoyable. It was an honor for me working with Rudi, for his loving and simple attitude of doing complicated technical work support, as he was the designer for most of the schematic diagrams in this thesis. As well, I am grateful to Mathias, the one who was responsible to take the SEM images for the whole department.

Lastly, I will always be indebted to my parents whom by their love, care and support I was able to overcome all challenges and achieve my own dreams.

Curriculum Vitae

PERSONAL INFORMATION:

Surname	Aziz
Name	Shahir
Place of birth	Cairo, Egypt
Date of birth	24.12.1986
Citizenship	Egyptian

EDUCATION:

2012 – 2015	PhD candidate in Pharmaceutics and Biopharmaceutics (Institute of Pharmacy), Christian Albrecht University of Kiel, Germany.
2010 – 2011	M.Sc. in Pharmaceutical Technology – German University in Cairo Thesis: “Novel Delivery of Oseltamivir Phosphate in Dry Powder inhalation”
2003 – 2008	B.Sc. in Pharmacy and Biotechnology (Excellent with high honors) – German University in Cairo
2001 – 2003	Cambridge International general certificate of secondary education (IGCSE) with score 104% in 2 years – St. Fatima High School.

WORK EXPERIENCE

2011 – 2015	Assistant Lecturer , Pharmaceutical technology department, faculty of pharmacy and biotechnology, GUC Leading Courses: Pharmaceutics I & II
2009 – 2011	Teaching assistant , Pharmaceutical technology department, faculty of pharmacy and biotechnology, GUC

CONFERENCES

- Respiratory Drug Delivery (RDD) 2012, Phoenix Arizona, USA.
- Controlled Release Society – Germany Local chapter 2014 meeting, University of Kiel.
- International conference of photodynamic therapy and Nano medicine for cancer diagnosis and therapy 2012, German university in Cairo.

PUBLICATIONS & PRESENTATIONS

- Poster Presentation and Publication; “Oseltamivir Phosphate Dry Powder Inhalation - Formulation and In-Vitro Characterization”, Respiratory Drug Delivery (2012), Vol. 2, pp 519-524.

GRANTS AND SCHOLARSHIPS

- GUC - M.Sc. research grant 2010.
- DAAD short stay scholarship for M.Sc. practical research at the Pharmaceutics and Biopharmaceutics department in Kiel, Germany (2010).
- GUC - DAAD Conference Grant for RDD 2012.

AWARDS

- M.Sc. - Academic Excellence award by Egyptian Pharmacist Syndicate.